The Dissertation Committee for Lucas Martin Holt Certifies that this is the approved version of the following dissertation:

Admittance Derived Stroke Volume for Determination of Hemodynamic Stability during Atrial and Ventricular Arrhythmias

Committee:

Jonathan W. Valvano, Supervisor

Marc D. Feldman

John A. Pearce

Henry G. Rylander

Earl E. Swartzlander

Admittance Derived Stroke Volume for Determination of Hemodynamic Stability during Atrial and Ventricular Arrhythmias

by

Lucas Martin Holt

Dissertation

Presented to the Faculty of the Graduate School of

The University of Texas at Austin

in Partial Fulfillment

of the Requirements

for the Degree of

Doctor of Philosophy

The University of Texas at Austin

December 2017

Dedication

I dedicate this work to my family, who has always supported me.

Acknowledgements

I would like to thank the professors who have guided me throughout my research: Dr. Jonathan Valvano, for engaging me in his research and giving me the opportunities to develop the skills necessary to be successful in my research and career; Dr. Marc Feldman, for creating a research environment that has enabled invention and discovery; Dr. John Pearce, for his guidance in both academic and moral matters; Dr. Earl Swartzlander, for starting me down this path 8 years ago.

I would like to thank my research partner, Andrew Wang, for helping me stay motivated and persevere through the most difficult times.

I would like to thank the team at the University of Texas Health Science Center San Antonio including: Meagan Oglesby, Patricia Escobar, Danny Escobedo, Katie Strychalski, Clarissa Caballero, Devon Klipsic, and Sander Hacker. Together with Andrew Wang and me we conducted more than 60 experiments over the course of 2 years. This type of research was difficult for me, and the burden was even greater on them. I have a tremendous level of respect for the UTHSCSA team and the work they do on daily basis.

Admittance Derived Stroke Volume for Determination of Hemodynamic Stability during Atrial and Ventricular Arrhythmias

Lucas Martin Holt, Ph.D.

The University of Texas at Austin, 2017

Supervisor: Jonathan W. Valvano

Abstract: Implantable cardioverter defibrillators (ICDs) are medical devices proven to prevent sudden cardiac death due to ventricular arrhythmias. Their decisions are based upon intra-cardiac electrograms (IEGM). This is incomplete information since up to 5% of implantable cardioverter defibrillator (ICD) shocks are inappropriate. Receiving a shock is associated with increased mortality as well as emotional trauma. In contrast, physicians determine whether to shock a patient out of a rapid rhythm by determining if the arrhythmia is hemodynamically unstable or stable. An unstable arrhythmia is identified by decreased forward stroke volume (SV) and resultant low blood pressure (BP). It would be ideal to have beat-by-beat SV available to the ICD to assist in the delivery of therapies. A system that utilizes the right ventricular (RV) shocking lead of an ICD to measure the electrical admittance in the RV is proposed for measuring continuous SV. For this method to work, a signal processing technique to remove noise artifacts related to lead motion and respiration must be developed.

Table of Contents

List of Tables

List of Figures

1. Chapter 1: Background and Motivation

1.1. MOTIVATION

Hemodynamically unstable ventricular arrhythmias are life-threatening cardiac events and the immediate precursor to Sudden Cardiac Death (SCD). During tachycardia, physicians are taught to decide whether to shock or medically convert the patient to normal sinus rhythm based on whether the heart can still maintain adequate forward output assessed by BP and SV. This critical information is currently not available to implantable cardioverter defibrillators (ICD). The state of the art in arrhythmia detection relies on accurately interpreted intracardiac electrograms (IEGM) from the implantable cardioverter defibrillator (ICD). However, the algorithms that determine whether to shock are inaccurate since up to 5% of ICD shocks are inappropriate [1]. This raises mortality rates, and causes psychological depression in patients [2], increasing morbidity.

The problem of inappropriate shocks can be solved by adding a hemodynamic measurement to the already implanted device. I propose to accomplish this goal by utilizing existing pacemaker leads as blood volume sensors using the admittance derived stroke volume (ADSV) method, a technique developed by our group [4-16]. The ADSV method can be applied to single chamber ICDs, dual chamber ICDs, and cardiac resynchronization therapy defibrillation (CRT-D) devices [17].

1.2. BACKGROUND

1.2.1. ECG Based Arrhythmia Discrimination Algorithms

The most commonly used metric to determine the relative danger of an arrhythmia is electrocardiogram (ECG). Because all ICDs have electrical access to the leads, they have the capability to sense IEGM. The rate and morphology of the IEGM waveforms are the most commonly utilized discriminators for classifying arrhythmias. IEGM is a relatively

low-power measurement, and can be enabled with little additional instrumentation in the ICD generator.

Due to the frequency of inappropriate shocks, an improvement is needed. The reasons for these inappropriate shocks are algorithm and patient dependent, but IEGM suffers from being dissociated from hemodynamics. For example, it is possible to have an irregular rapid HR, but still have an adequate BP and SV. The addition of a SV measurement to the existing IEGM based discriminators provides a targeted solution to this problem.

1.2.2. ICD Therapies and Programming

ICDs can deliver inappropriate therapies, most often for supraventricular tachyarrhythmias, which negatively impacts patient life and increases morbidity and mortality [17A].

Programming strategies to reduce inappropriate ICD shocks have included sophisticated SVT discrimination algorithms [17B, 17C], long detection times with delayed therapies [17D, 17E], and use of anti-tachycardia pacing therapy (ATP) [17B, 17F, 17G]. Despite these advances, inappropriate therapies remain a clinical problem with reported false shock rates of 3-5% [17C, 17H, 17I].

In clinical settings, physicians evaluate hemodynamic status when deciding whether an arrhythmia requires cardioversion. However, ICDs rely solely on the intracardiac electrogram (IEGM) to discriminate arrhythmias and determine appropriate therapies.

1.2.3. Bio-impedance Measurements

Intrathoracic impedance measurements are currently used by companies such as Medtronic (Optivol, [18]) and St. Jude Medical (CorVue, [19]) to determine lung wetness.

However, their approach of extending the electric field from the ICD generator to the RV shocking lead has too many sources of noise, such as the skeletal muscle and lungs, which are also included in the resulting electric field. As a result, these approaches are much more sensitive to lung tissue wetness than heart volume.

1.2.4. Intraventricular Admittance Measurements

The ADSV method has been adapted from traditional bioimpedance measurements to more accurately monitor ventricular SV. ADSV offers significant improvements in comparison to bioimpedance by removing confounding artifacts that corrupt intraventricular bioimpedance measurements. The ADSV method can remove the following two artifacts: parallel muscle contributions and time varying respiratory artifacts. The conductance derived stroke volume (CDSV) method should also be mentioned. The CDSV method is identical to the ADSV method except for the fact that CDSV method does not remove parallel muscle contributions to the admittance signal. The calculation is performed using the magnitude of admittance |Y|.

The removal of parallel muscle contributions from the admittance signal is made possible using the admittance equation. This equation leverages unique electrical properties of blood and muscle. The amount of conductance that is removed from the signal is calculated using the phase component of the complex admittance signal. This differs from traditional bioimpedance measurements which only utilize magnitude. "Measured admittance consists of three components, $\boldsymbol{Y} = G_{\mathrm{b}} + G_{\mathrm{m}} + j\omega C_{\mathrm{m}}$, where G_{b} is the conductance of blood, Gm is the conductance of muscle and ωCm is the susceptance of muscle. Since the imaginary component arises solely from the muscle, the conductivity to permittivity ratio of muscle can be used to separate blood conductance by the conductance-capacitance analogy, $G_{\mathrm{b}} = Re\{\boldsymbol{Y}\} - (\sigma_{\mathrm{m}}/\epsilon_{\mathrm{m}})\ \mathrm{Im}\{\boldsymbol{Y}\}$" [14]. In this dissertation a $\sigma_{\mathrm{m}}/\epsilon_{\mathrm{m}}$ ratio of 800,000

is used. A diagram of the components that comprise the parallel intraventricular complex admittance signal is provided in Figure 1.

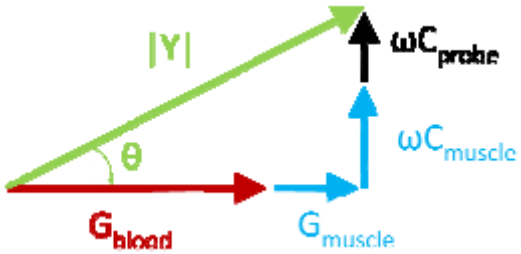

Figure 1. Parallel Complex Admittance Model
|Y| indicates magnitude of admittance, θ indicates the phase of admittance, Gblood indicates the blood conductance contribution to the real part of admittance signal, Gmuscle indicates the muscle conductance contribution to the real part of the admittance signal, ωCmuscle indicates the muscle susceptance contribution to the imaginary part of the admittance signal, ωCprobe indicates the probe susceptance contribution to the imaginary part of the admittance signal.

1.2.5. Tripolar Admittance Measurements

The admittance signal underlying the ADSV and CDSV methods is a tripolar admittance configuration using the 3 electrodes of an RV shocking lead (RV Coil, and RV Ring, RV Screw). This configuration has been experimentally validated in human patients chronically implanted with RV ICD shocking leads [20]. Typical admittance measurements are made in a tetrapolar configuration using a conductance catheter in the left ventricle (LV) of the heart [5]. The tetrapolar configuration was adapted to a tripolar configuration by using the RV shocking coil as both a voltage sensing and current stimulation electrode. Generally, it is not acceptable to use a single electrode as both a voltage sense and a current stimulation node. However, the large surface area of the RV shocking coil makes it the ideal candidate for such a configuration. A model of the RV tripolar admittance configuration is provided in Figure 2.

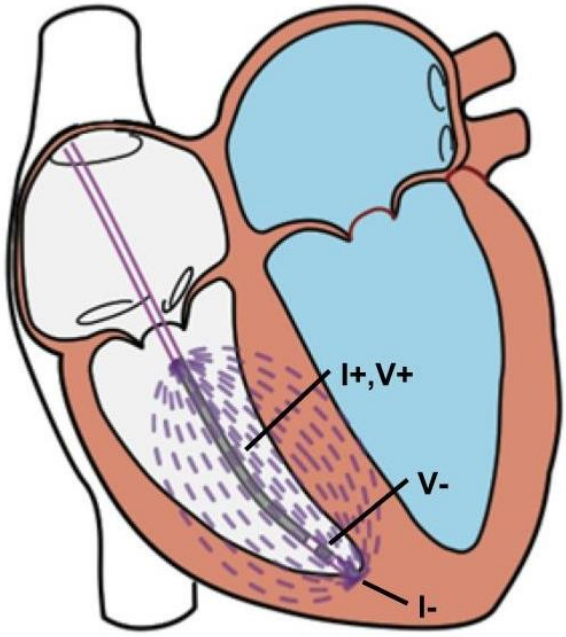

Figure 2. The RV tripolar admittance measurement configuration.
Positive current stimulation (I+) and positive voltage sense (V+) are shown on the RV Coil. Negative current stimulation (I-) is shown on the RV Screw. Negative voltage sense (V-) is shown on the RV Ring. Electric field lines, shown as dashed lines, are for illustrative purposes only.

1.3. SPECIFIC AIMS

Specific Aim 1: Develop signal processing techniques to remove respiration artifact and measure relative stroke volume changes accurately under steady state conditions in an acute pacing protocol using RV tripolar admittance.

Specific Aim 2: Develop signal processing techniques to differentiate between hemodynamically stable and hemodynamically unstable arrhythmias using RV tripolar admittance. The result of the signal processing technique will be incorporated into a shocking algorithm that could be used within an ICD. This study will be performed in a large animal (canine) model with heart failure preparation in an arrhythmia protocol.

1.4. OVERVIEW OF CHAPTERS

Chapter 1 (Background and Motivation) is meant to introduce the topic of the dissertation and make clear the specific aims. Chapter 2 (Signal Processing Methods for Admittance Signals) introduces the signal processing methods that are used to address specific aim 1. These signal processing methods are used throughout the dissertation to analyze experimental data. Chapter 3 (Preliminary Right Atrial Pacing Experiment) presents an experiment that served to validate the signal processing algorithm from specific aim 1. Chapter 4 (Congestive Heart Failure Arrhythmia Study) presents the experimental protocol that was used to address specific aim 2. Chapter 5 (Hemodynamic Based ICD Discrimination Algorithm) presents the algorithm that addresses specific aim 2. Chapter 6 (Conclusion and Future Work) concludes the dissertation and suggests areas for future research based on the findings herein.

2. Chapter 2: Signal Processing Methods for Admittance Signals

2.1. DEMODULATION TECHNIQUES

2.1.1. Analog Demodulation Techniques

The admittance measurement underlying the ADSV and CDSV methods is modulated on a 20 kHz carrier. This frequency was selected because it allows for some sensitivity to the capacitive component of the muscle and is not dramatically affected by small parasitic capacitances found in the leads. Since the signal is modulated, it is necessary to demodulate the analog signal to obtain the baseband admittance signal. A variety of analog and mixed signal approaches can be used to demodulate the signal including rectified demodulation and synchronous demodulation.

Rectified demodulation, sometimes referred to as an envelope detector, is by far the easiest way to demodulate a signal to its baseband. In this method, the amplitude modulated signal is first rectified using either a single diode for half wave rectification or a full-wave rectification circuit. The resulting signal can then be low-pass filtered, which results in the reconstructed baseband signal. A diagram outlining a diode rectified demodulation circuit is provided in Figure 3.

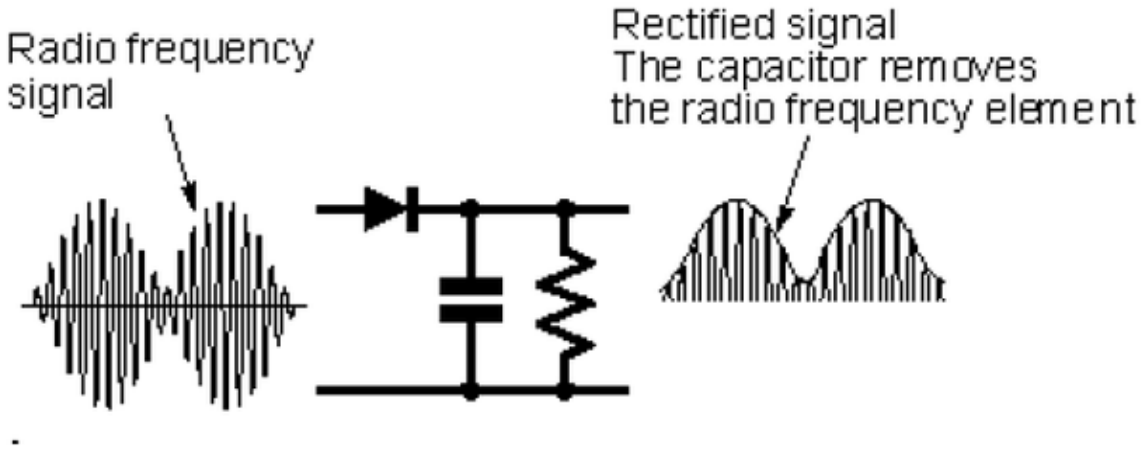

Figure 3. Diode Rectified Demodulation.

While the rectified demodulation circuit is easy to implement, it is only able to capture magnitude information in the baseband signal. If both magnitude and phase information from the baseband signal are desired more complex demodulation techniques must be used.

Synchronous demodulation is a well-known technique to measure the in-phase and out of phase components of a signal. The measurement of admittance at a carrier frequency results in a waveform that can be represented by the following equation:

$$x(t) = p(t)\cos(\omega t) + q(t)\sin(\omega t),$$

where p(t) represents the in-phase signal, and q(t) represents the out of phase signal. These are equivalent to the real and imaginary parts of the admittance signal. Synchronous demodulation is achieved by multiplying the modulated admittance signal by the in-phase and out of phase carrier frequency [21, 22]. The equations that define the demodulation of the in-phase signal are provided:

$$y(t) = \big(p(t)\cos(\omega t) + q(t)\sin(\omega t)\big) \times \cos(\omega t)$$

The signal components can then be separated using trigonometric identities.

$$y(t) = p(t)\frac{1}{2}\big(1 + \cos(2\omega t)\big) + \frac{1}{2}q(t)\sin(2\omega t)$$

After the in-phase signal has been multiplied (mixed) with the in-phase carrier the in-phase baseband signal can be extracted using a low pass filter. In practice, the generation of an ideal sine wave is difficult and a square wave implementation using D flip-flops may be used [23]. The out-of-phase component can be reconstructed using a similar equation and corresponding trigonometric identity.

2.1.2. Digital Demodulation Techniques

Digital demodulation can significantly reduce the analog complexity that is required to implement synchronous demodulation. In practice, the multiplication (mixer) operation performed in analog hardware can be moved into the digital domain. However, this is only possible if the modulated signal can be sampled at a sufficiently high sampling rate. Since the admittance measurement is modulated at a 20 kHz carrier, it is possible to sample the signal and perform the synchronous demodulation operation digitally.

In fact, in the mixed signal admittance system designed for this study (Cardiovol), the 20 kHz stimulation current underlying the admittance measurement is generated by a microcontroller that outputs to a 3-bit sine digital to analog converter (SinDAC). The microcontroller outputs to the SinDAC at a rate of approximately 160 kHz. Given that the microcontroller outputs 8 samples per cycle of the sine wave, the resulting frequency of the sine wave is 20 kHz. For every output current sample, the microcontroller also measures a corresponding input voltage sample using an on-chip analog to digital converter (ADC). Since the Cardiovol system controls both the output of current samples and the sampling of voltage samples, the admittance signal can be sampled coherently. The conditions for coherent sampling are provided:

$$\frac{f_{in}}{f_s} = \frac{M_{cycles}}{N_{samples}}.$$

where f_{in} is frequency of the input signal (20 kHz), f_s is the sampling rate (160 kHz), M_{cycles} is the number of cycles in the sampled sine wave, and $N_{samples}$ is the number of samples. $N_{samples}$ must be a power of 2 and M_{cycles} must be odd or prime. Making $N_{samples}$ a power of 2 ensures that the FFT can be calculated efficiently. Making M_{cycles} prime ensures that every value is in the sampled waveform is in a unique point in the sampled waveform. By

sampling unique points in the waveform, quantization noise and deterministic noise artifacts can be limited.

Coherent sampling ensures that the signal power for the frequency of interest (20 kHz) is contained in a single bin of the Discrete Fourier Transform (DFT). This property enables the use of the DFT to demodulate the signal. The DFT is defined as follows:

Input: N time samples

$\{a_n\} = \{a_0,a_1,a_2,\ldots,a_{N-1}\}$

Output: a set of N frequency bins

$\{A_k\} = \{A_0,A_1,A_2,\ldots,A_{N-1}\}$

$$A_k = \sum_{n=0}^{N-1} a_n W_N^{kn} \quad \text{Where } W_N = e^{-j2\pi/N}$$

$k=0,1,2,\ldots,N-1$

where k is a specific DFT bin. To calculate the entire DFT of a time domain signal with N samples the time complexity is O(N^2). However, for demodulation, only a single bin, k, needs to be calculated to demodulate the baseband information from the 20-kHz carrier. The time complexity of a single bin DFT calculation is O(N). The bin k of interest can be identified using the following equation:

$$f_r = f_s/N$$

$$f_{in} = f_s/M$$

$$f_{in}/f_r = k$$

by substitution,

$$(f_s/M)/(f_s/N) = k$$

by reduction,

$$N/M = k$$

where f_r is frequency resolution (bin resolution), f_{in} is the input signal's frequency (20 kHz), f_s is the sampling rate (160 kHz), N is the number of input samples, M is the number of samples of each cycle of the sinusoidal output waveform (8 samples/cycles), and k is the DFT bin that contains the demodulated magnitude and phase information. This demodulation method was applied by Valvano *et al* for measuring complex electrical admittance and impedance [24].

2.1.2.1. Single Bin DFT Assembly Implementation

A fixed-point implementation for calculating a single bin, k, of the DFT was implemented in assembly code on the low-power MSP430 microcontroller, providing a numerically stable and efficient way to demodulate the admittance signal and produce complex admittance measurements [24]. The fixed-point implementation is optimized using only add and shift operations, which makes it the ideal candidate for low-power implantable applications.

From reference [24]: "An example of this implementation, f_{in} = 20 kHz, M=8, and N=32. The microcontroller writes digital values to the SinDAC at a rate of fs = M* f_{in} = 160 kHz. With fs equal to 160 kHz, the time between samples is $\mathbf{\Delta t}$ = 6.25 μs. The voltage signal is sampled by the ADC at the same fs= 160 kHz rate. A total of N = 32 data points are collected with a total sample time = 200 μs. Let the sampled inputs be x0, x1, x2, …, x31. Since the sampling rate is 160 kHz, the k=4 term represents the desired 20 kHz carrier frequency. In other words, X4 represents complex impedance at f = 20 kHz. For a 32-point DFT, the complex constants can be calculated as follows:

$$\mathbf{W^k} = \exp(-2\pi i\mathbf{k}/32) = \cos(2\pi\mathbf{k}/32) - i*\sin(2\pi\mathbf{k}/32)$$

k = 4 represents **f** = 20 kHz. To calculate the **k**=4 term, we only need every fourth $\mathbf{W^k}$ term:

$$\mathrm{Re}[\mathbf{Z}_4] = x_0 - x_4 + x_8 - x_{12} + x_{16} - x_{20} + x_{24} - x_{28} + \sqrt{½}*(x_1 - x_3 - x_5 + x_7 + x_9 - x_{11} - x_{13} + x_{15} + x_{17} - x_{19} - x_{21} + x_{23} + x_{25} - x_{27} - x_{29} + x_{31})$$

$$\mathrm{Im}[\mathbf{Z}_4] = -x_2 + x_6 - x_{10} + x_{14} - x_{18} + x_{22} - x_{26} + x_{30} + \sqrt{½}*(-x_1 - x_3 + x_5 + x_7 - x_9 - x_{11} + x_{13} + x_{15} - x_{17} - x_{19} + x_{21} + x_{23} - x_{25} - x_{27} + x_{29} + x_{31})$$

$\mathbf{W^k}$ can be approximated in terms as a fixed-point numbers. Notice how close 12/17 is to the √½ (0.70588 versus 0.70711). Using fixed point saves power. Let **Z** be the complex impedance for the **k**=4 term. One possible fixed-point implementation is

$$\mathbf{ReZ} = (17*(x_0 - x_4 + x_8 - x_{12} + x_{16} - x_{20} + x_{24} - x_{28}) + 12*(x_1 - x_3 - x_5 + x_7 + x_9 - x_{11} - x_{13} + x_{15} + x_{17} - x_{19} - x_{21} + x_{23} + x_{25} - x_{27} - x_{29} + x_{31}))/32$$

$$\mathbf{ImZ} = (17*(-x_2 + x_6 - x_{10} + x_{14} - x_{18} + x_{22} - x_{26} + x_{30}) + 12*(-x_1 - x_3 + x_5 + x_7 - x_9 - x_{11} + x_{13} + x_{15} - x_{17} - x_{19} + x_{21} + x_{23} - x_{25} - x_{27} + x_{29} + x_{31}))/32$$

The divide by 32, implemented as a right shift, was added to adjust the amplitude of the calculation. Because the device will be calibrated, the "32" in these equations is arbitrary.

An important consequence of the M-to-1 ratio in both the SinDAC and the DFT is that the sampling frequency ($\mathbf{f_s}$) need not be accurate. If the input/output sampling rate is either a little too fast or too slow, the system still works. For example, if the sampling frequency moves from 160 kHz to 152 kHz, the only consequence is that now the electrical measurements are being made at 19 kHz instead of 20 kHz. Luckily, the change in electrical properties of blood and muscle tissue do not significantly vary for frequencies 19 to 21 kHz. It requires a significant amount of electrical power to create a precise sampling clock.

Conversely, this device can derive its timing from a low-power voltage-controlled oscillator (VCO).” [24]. Additionally, the sampled waveform need not be windowed because the output current waveform and corresponding voltage input samples are collected coherently.

2.1.2.2. Goertzel Filter Implementation

The Goertzel filter algorithm is a well-known method for calculating a single bin of the DFT. It has been used extensively for tone detection [25] and has also been used for digital demodulation [26]. The Goertzel filter algorithm can be used as an alternative to the single bin DFT assembly implementation. The Goertzel filter is implemented using an infinite impulse response (IIR) filter with the following form:

$$\omega_0 = 2\pi\frac{k}{N}.$$

$$s[n] = x[n] + 2\cos(\omega_0)s[n-1] - s[n-2].$$

The above filter is run for input samples x[0], x[1], …., x[n-1] and terminates when the x[n-1] sample is processed. The samples are then passed into a second stage that produces the final complex value for the k^{th} bin of the DFT. The second stage is defined as follows:

$$c_r = \cos(2\pi\tfrac{k}{N}),$$
$$c_i = \sin(2\pi\tfrac{k}{N}),$$
$$y[N] = c_r s[N-1] - s[N-2] + jc_i s[N-1].$$

where C_r represents the coefficient for the real part for the kth bin of the DFT and C_i represents the coefficient for the imaginary part for the kth bin of the DFT. The value y[N] represents the complex value for the kth bin of the DFT.

The Goertzel filter can be realized using fixed point computations like the single bin DFT implementation discussed previously. The coefficients C_r, C_i, and ω_o can be

efficiently implemented using a series of add and shift operations. However, since the Goertzel filter is in fact an IIR filter with one of the poles for the filter's Z transform on the unit circle, it is considered a marginally stable filter and is vulnerable to numerical error accumulation. Any inaccuracies in the coefficient ω_o are scaled to the N^{th} power, where N is the number of samples. This polynomial error scaling requires that the estimate of ω_o using add and shift be significantly more precise than the estimate used in the single bin DFT implementation discussed previously. In practice, it was found that the number of add and shift operations required for numerical stability was approximately 13. This implies that the Goertzel filter requires approximately 13 times the number of machine operations when compared to the single bin DFT implementation if it is implemented on a fixed-point processor that does not have a divide unit. While a fixed-point processor that does have a divide unit would reduce the computational complexity of the Goertzel filter significantly, the numerical stability issues that arise from the feedback properties of the underlying IIR filter remain. In practice, the Goertzel filter (as with all IIR filters) should be implemented on a processor where a floating-point unit is available.

2.1.3. Numerical Accuracy and Stability Simulations

The single bin DFT implementation and the Goertzel filter algorithm were simulated to evaluate the accuracy and numerical stability of each algorithm. In the simulation, the methods were evaluated for their ability to measure impedance in ohms. The Cardiovol instrument is designed to measure electrical impedance and values are converted to admittance in mS post processing. The instrument outputs a constant current at 20 kHz on two leads and measures the resulting voltage on two other leads. Since the instrument is designed to measure impedance, the simulations are presented in terms of impedance. The simulation swept impedance measurements with a magnitude from [0-

100] ohms in increments of 2 ohms. For each impedance magnitude the phase was swept from [-90, 90] degrees in increments of 5 degrees. The single bin DFT implementation had a percent of full-scale error for the real part of 0.027% ± 0.023% (max = 0.087%) and for the imaginary part 0.027% ± 0.023% (max = 0.087%). The errors for the single bin DFT implementation were deterministic. For the single bin DFT implementation, the results for the real part are provided in Figure 4 and the imaginary part is provided in Figure 5. The Goertzel Filter algorithm had a percent of full-scale error for the real part of 0.047% ± 0.036% (max = 0.2%) and for the imaginary part 0.052% ± 0.042% (max = 0.23%). The errors for the Goertzel filter algorithm were not deterministic. For the Goertzel filter algorithm, the results for the real part are provided in Figure 6 and the imaginary part are provided in Figure 7.

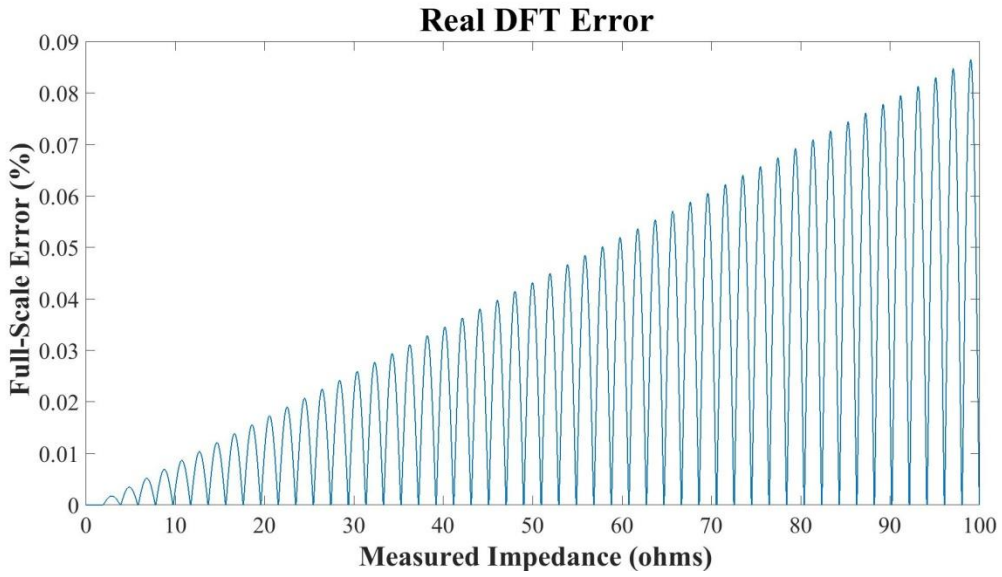

Figure 4. Single Bin DFT Real Error Simulation Results

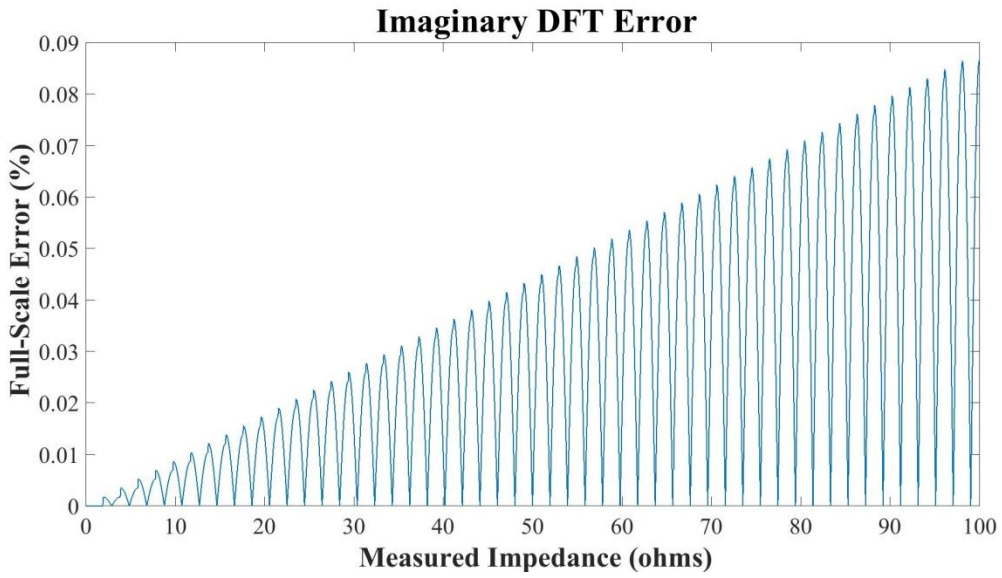

Figure 5. Single Bin DFT Imaginary Error Simulation Results

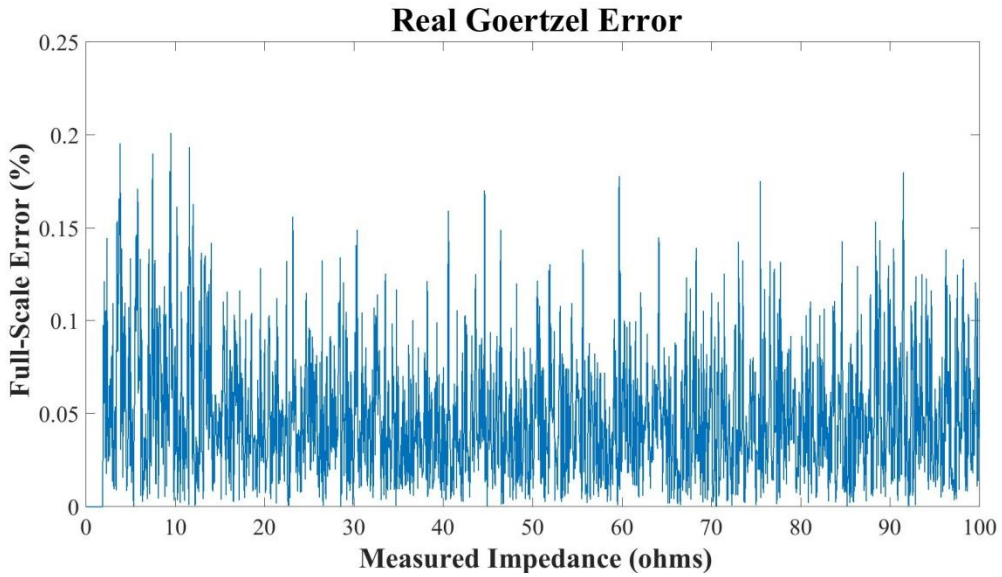

Figure 6. Goertzel Filter Algorithm Real Error Simulation Results

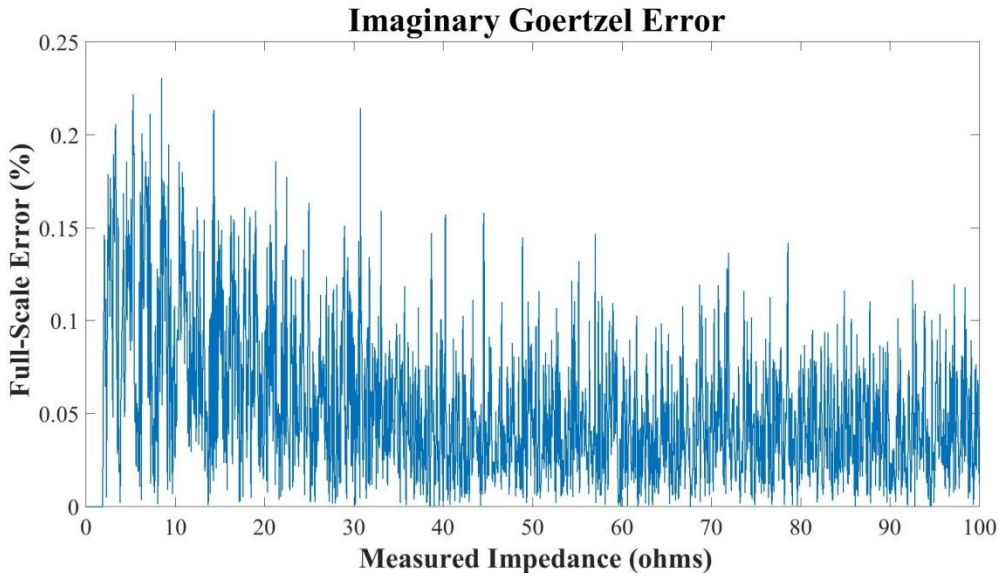

Figure 7. Goertzel Filter Algorithm Imaginary Error Simulation Results

The single bin DFT implementation was found to be the clear winner when compared to the Goertzel filter algorithm. It is 13 times more computationally efficient, has better numeric stability, and has 2.5 times less maximum full-scale error.

The accuracy of the single-bin FFT could be improved by increasing the precision of the fixed-point math. The size of the frequency bin could be tightened by increasing the sampling rate. The sampling rate of 160 kHz and numerical precision of 16-bits were chosen to allow for implementation of a battery-powered implant.

2.2. ADMITTANCE BASED STROKE VOLUME METHODS

The admittance derived stroke volume (ADSV) and conductance derived stroke volume (CDSV) methods are designed to estimate stroke volume (SV) from an intraventricular admittance signal in the presence of respiratory artifact. The ADSV method uses both the phase and magnitude information from the admittance signal. The CDSV method only uses the magnitude information from the admittance signal. Both methods go through the same signal processing algorithm. The signal processing algorithm

involves both time and frequency domain analysis. The time domain admittance signal is first windowed using a Tukey window that is approximately 25 seconds long. Next, the signal is transformed into the frequency domain using the discrete Fourier transform (DFT). In the frequency domain, either a narrow band or wide band Fourier filter is applied to remove non-cardiac signal components. The inverse discrete Fourier transform (IDFT) is then applied to transform the signal back into the time domain. Finally, the amplitude of the Fourier filtered admittance signal is determined using either a peak detection algorithm or a root mean squared (RMS) calculation. Detailed explanations of these signal processing blocks are provided in the subsequent sections. A visual representation of signal processing chain for the ADSV/CDSV method can be found in Figure 8.

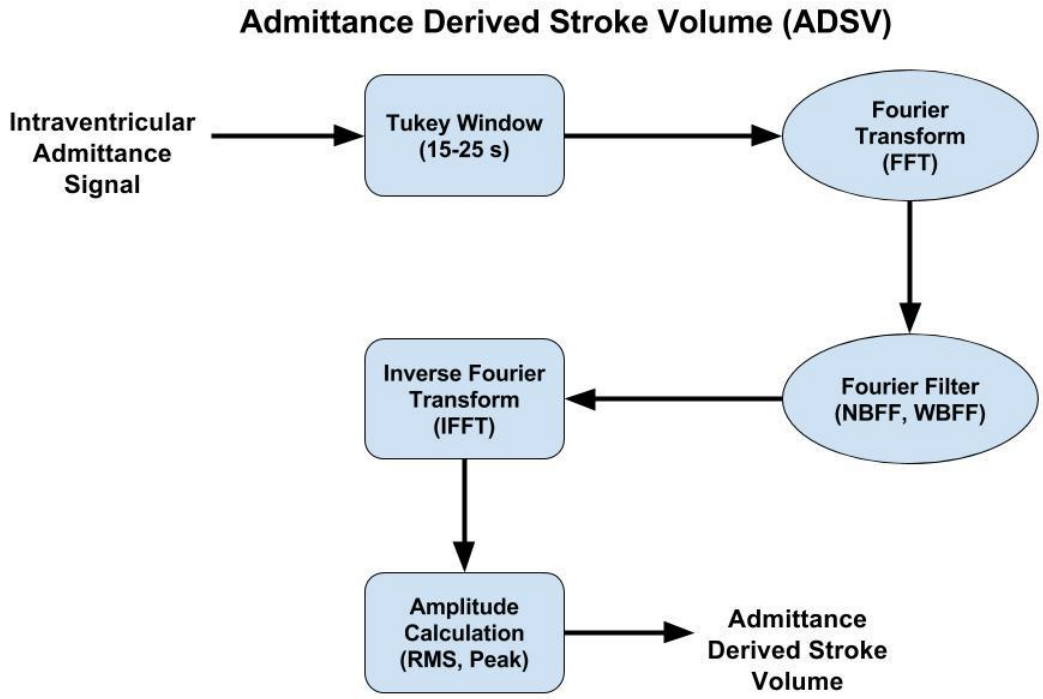

Figure 8. ADSV and CDSV Signal Processing Chain

Time domain operations are indicated using rectangles, frequency domain operations are indicated using ovals, FFT indicates a fast Fourier Transform operation, NBFF indicates a Narrow Band Fourier Filter operation, WBFF indicates a Wide Band Fourier Filter operation, IFFT indicates an inverse fast Fourier transform, RMS indicates root mean squared, Peak indicates peak detection, and ADSV indicates admittance derived stroke volume.

2.2.1. Fourier Filtering of Admittance Signals

Fourier analysis is used extensively in science and engineering using the Fourier transform. The Fourier transform decomposes a time domain signal into a combination of sinusoids that when combined form the original time domain signal. The information provided by the Fourier transform is referred to as the frequency domain and provides a set of orthogonal information to the time domain. It can be used to isolate signals with specific frequency characteristics. The Fourier methods discussed herein are implemented using The Fast Fourier Transform (FFT), which is an efficient implementation of the DFT. The DFT has a time complexity of O(N^2). The FFT has a time complexity of O(N*log(N)). For large data sets, the processing time for the FFT is significantly faster when compared to the DFT. The computational efficiency of the FFT is achieved through a divide and conquer methodology. In this way, a single DFT operation is broken down into several smaller DFT operations whose numerical outputs can be combined systematically to recreate the larger parent DFT operation. The FFT leverages reuse of the numerical operations of the smaller DFTs that may be recalculated in the standard DFT implementation. One of the original and most common FFT algorithms is the Cooley-Tukey algorithm [27].

Fourier analysis is particularly useful for removing unwanted noise artifacts from a signal of interest. This action is referred to as Fourier filtering. Fourier filtering has been used extensively for the processing biological signals that are often distorted by unwanted

noise artifacts [28]. Some researchers have applied the technique to impedance/admittance spectroscopy [29].

Using Fourier filtering, the cardiac and respiratory components of an admittance signal can be isolated. This is possible because of a frequency separation between the two components. The respiratory rate of an adult is typically between 12 - 20 breaths per minute (< 0.33 Hz). The heart rate of an adult is typically between 60 - 100 beats per minute (> 1.0 Hz). During both tachycardia and fibrillation rhythms both heart rate and respiration rate can increase, but the frequency separation between the two components is generally maintained. In the case of bradyarrhythmias, the method is not as effective as the cardiac rate and respiratory rate may converge.

When using a Fourier filter, it is important to consider the frequency resolution of the filter. The frequency resolution is the minimum resolvable frequency distinction that can be made by the filter. The frequency resolution is determined by the window size that is used for the Fourier filter. The following equations define the relationship between frequency resolution ($f_{r)}$ and window size ($T_{w)}$:

$$f_r = f_s/N$$

$$N=fs*T_w$$

by substitution,

$$f_r = f_s /(fs*T_{w)}$$

by reduction,

$$f_s = 1/T_w$$

where f_r is frequency resolution (bin resolution) in Hz, f_s is the sampling rate in Hz, N is the number of samples, and T_w is the amount of time the sampling window covers in seconds. For the Fourier filter to have a 0.05 Hz $f_{r,}$ the window size must be 20 seconds long.

2.2.2. Window Selection

Before the Fourier transform can be applied, the time domain signal must be properly windowed. Window type and size are both important considerations. If the window type and size are not selected properly, the Fourier transform will cause undesired spectral leakage that results in the frequency components within a bin to spread into neighboring bins. Spectral leakage is an important consideration for the ADSV/CDSV method since leakage from the respiratory frequencies into the cardiac frequencies prevents the removal of respiratory artifacts from the intraventricular admittance signal.

The reason spectral leakage occurs in this application of the Fourier transform and not in the demodulation application discussed above is because the signals are not sampled coherently. Without coherent sampling a signal will be sampled without regard for its period. Non-coherent sampling results in the sampled signal containing incomplete cycles of a waveform. Since, the DFT assumes that the sampled time domain signal is repeated infinitely, the partial cycles in the waveform create discontinuities which result in spectral leakage [30]. Take for example the input signal provided in Figure 9A; when the signal is repeated as shown in Figure 9B a discontinuity can be seen at T=5 seconds.

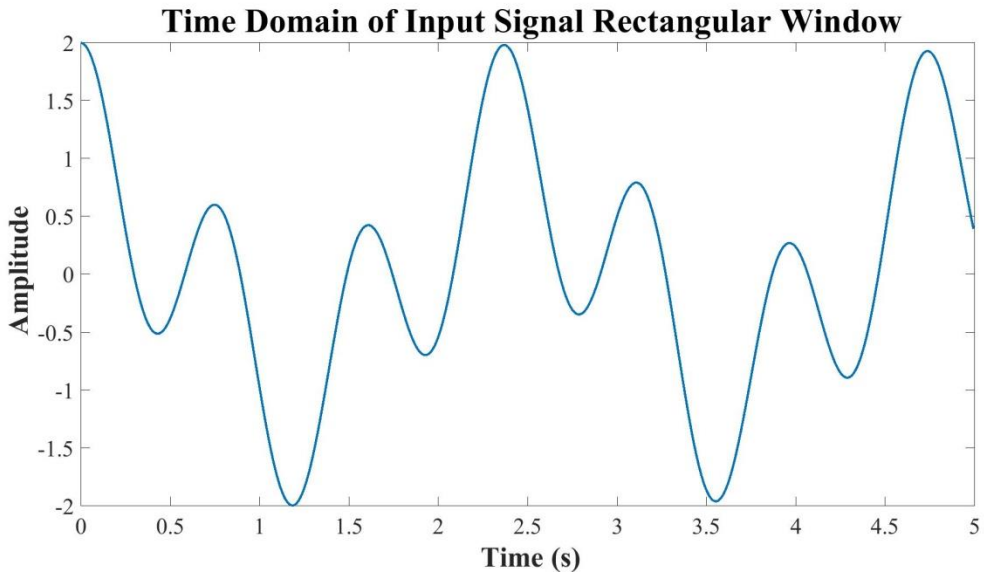

Figure 9A. Time Domain Input Signal (Rectangular Window)

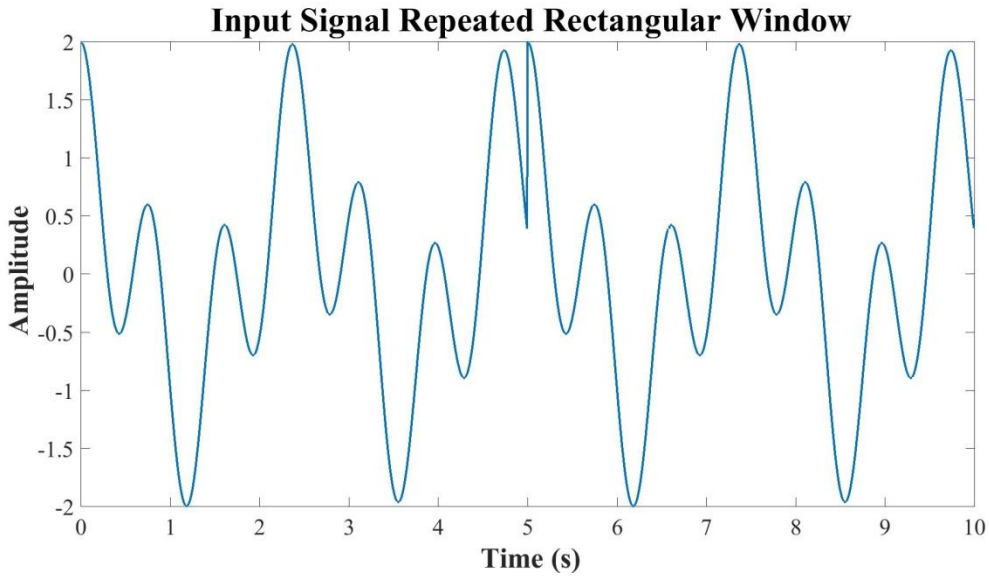

Figure 9B. Repeated Time Domain Input Signal (Rectangular Window)

The signals shown in Figures 9A and 9B are windowed using a rectangular window. A rectangular window is effectively no window. Typically, a window function acts to smooth the time domain signal at the beginning and end of the window. This is achieved

using a sequence of coefficients that form a window function, which are multiplied with the samples of the time domain input signal. In the case of the rectangular window, the window coefficients are all of value 1 and the original time domain samples are unchanged. This type of window is acceptable for coherently sampled signals, but for signals that are not coherently sampled other window functions must be used to prevent spectral leakage. The undesirable effects of the rectangular window have been demonstrated in the time domain, but they can also be observed in the frequency domain, as Figure 10 shows.

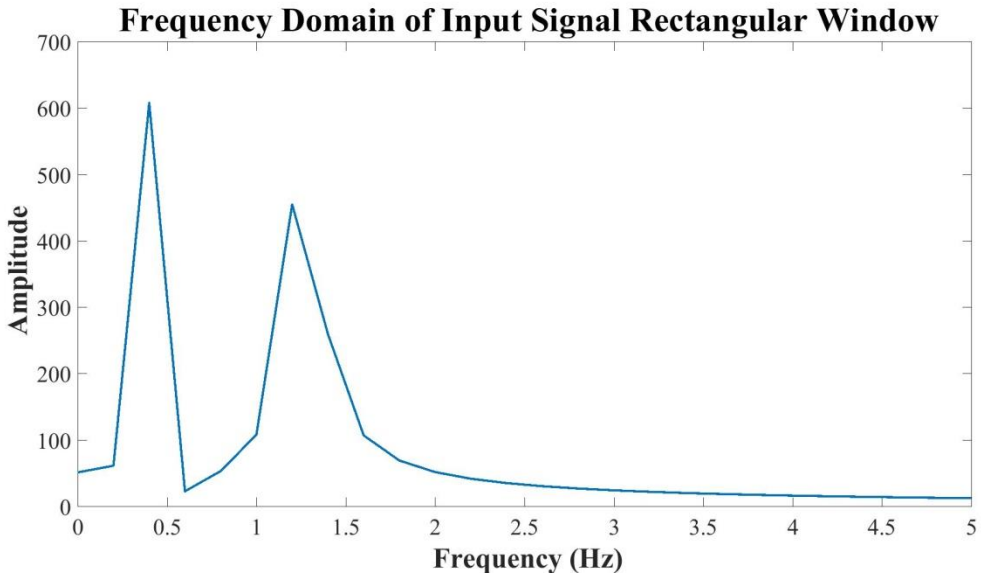

Figure 10. Frequency Domain Input Signal with Rectangular Window

This input signal was composed of sinusoids, one at 1.27 Hz and another at 0.41 Hz. While the frequency domain of the signal provided in Figure 10 does show the presence of the intended frequencies, it also shows significant leakage of these frequencies into adjacent bins. It can be observed that all bins shown in the range of 0-5 Hz are non-zero. This indicates that the discontinuity observed in the time domain of Figure 9B has caused high frequency distortion that appears in most bins.

To reduce this undesired spectral leakage, a more effective window can be used. The Hann window is one of the most commonly used windows for spectral analysis [30]. The equation for the Hann window is as follows:

Hann Window:

$$w(n) = \frac{1}{2}\left(1 - \cos\left(\frac{2\pi n}{N-1}\right)\right)$$

The time domain representation of a standard Hann window is provided in Figure 11.

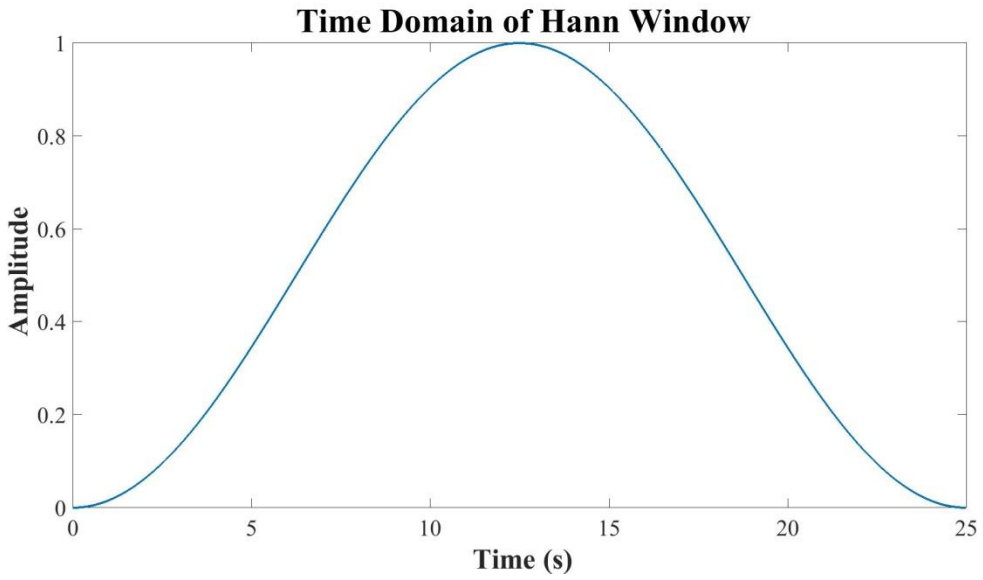

Figure 11. Time Domain of Hann Window

The Hann window was applied to the input signal forming the signal provided in Figure 12. A repeated representation of the windowed signal is provided in Figure 13.

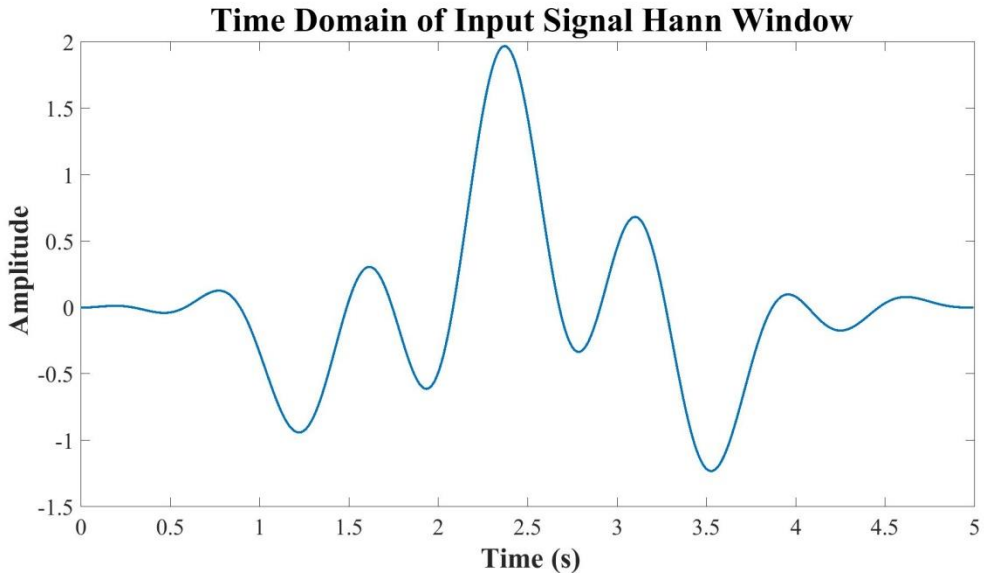

Figure 12. Time Domain Input Signal with Hann Window

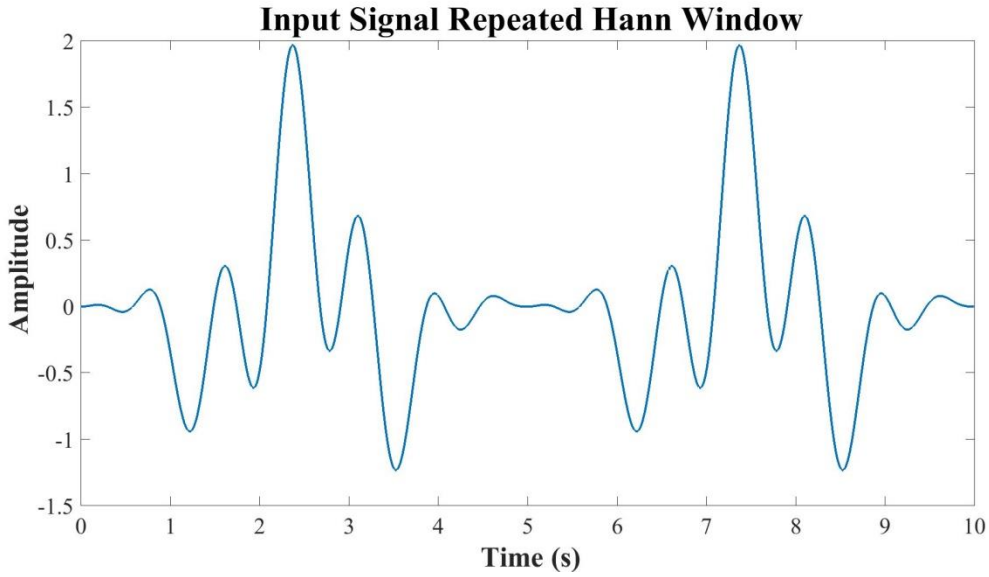

Figure 13. Repeated Time Domain Input Signal with Hann Window

Figure 13 shows that the discontinuity observed with the rectangular window was eliminated by the Hann window. The resulting Fourier transform of the signal in Figure 12 is provided in Figure 14.

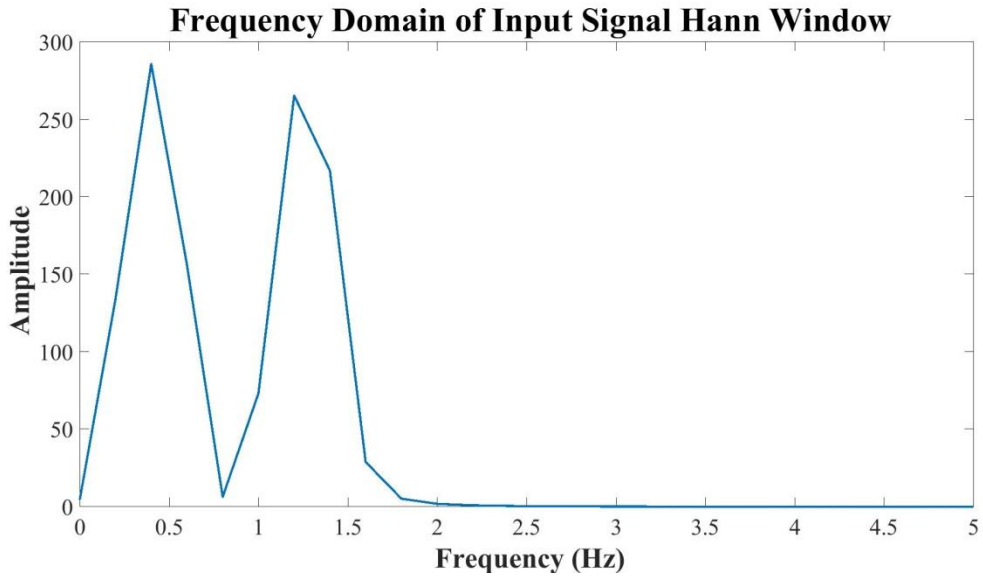

Figure 14. Frequency Domain Input Signal with Hann Window

It can be observed that the signal frequencies of 1.27 Hz and 0.41 Hz are still spreading into adjacent bins. However, all the bins after 2 Hz are zero valued. Hence, the Hann window was effective at reducing the amount of spectral leakage into the bins that correspond with higher frequencies.

Generally, the only way to completely remove spectral leakage is to sample a signal coherently and use a rectangular window (No Window). However, if a signal cannot be sampled coherently, the amount of spectral leakage can be managed using window type and window size. The two subsequent sections will provide insight about the selection of the windows used for the ADSV/CDSV method.

2.2.2.1. Window Type Simulations

When selecting the window type, it important to consider both the amount of spectral leakage that the window causes as well as the amount of coherent gain the window has. Window functions typically attenuate the power of time domain signals. The amount

of attenuation that a window function causes is referred to as the coherent gain of the window [30].

In practice, hundreds of window functions exist. The Hann window is perhaps the most commonly used window function. The Hann windows spectral leakage characteristics are ideal. However, it has a coherent gain of 0.5 and due to the non-stationary nature of intraventricular admittance signals it is not the best option for the ADSV/CDSV method. By design, the Hann window causes an amplitude bias in the admittance signal at the middle of the window. By focusing more heavily on the signal in the middle of the window, the amplitude measurement of the ADSV/CDSV method will be biased towards the amplitudes observed in the middle of the window. Since the ADSV/CDSV amplitudes are constantly changing in the sampled window this behavior is not desired. For this reason, a window with a larger and more uniform coherent gain is desired. After a detailed search, the Tukey window was identified [31]. The equations representing the Hann window and Tukey window are provided below.

Hann Window:

$$w(n) = \frac{1}{2}\left(1 - \cos\left(\frac{2\pi n}{N-1}\right)\right)$$

Tukey Window:

$$w(n) = \begin{cases} \frac{1}{2}\left[1 + \cos\left(\pi\left(\frac{2n}{\alpha(N-1)} - 1\right)\right)\right] & 0 \leqslant n < \frac{\alpha(N-1)}{2} \\ 1 & \frac{\alpha(N-1)}{2} \leqslant n \leqslant (N-1)(1-\frac{\alpha}{2}) \\ \frac{1}{2}\left[1 + \cos\left(\pi\left(\frac{2n}{\alpha(N-1)} - \frac{2}{\alpha} + 1\right)\right)\right] & (N-1)(1-\frac{\alpha}{2}) < n \leqslant (N-1) \end{cases}$$

A time domain representation of the Hann window was provided previously in Figure 11 A time domain representation of the Tukey window with an α coefficient of 0.2

(Tukey α= 0.2) is provided in Figure 15. The coherent gain of the Tukey α = 0.2 window is 0.9.

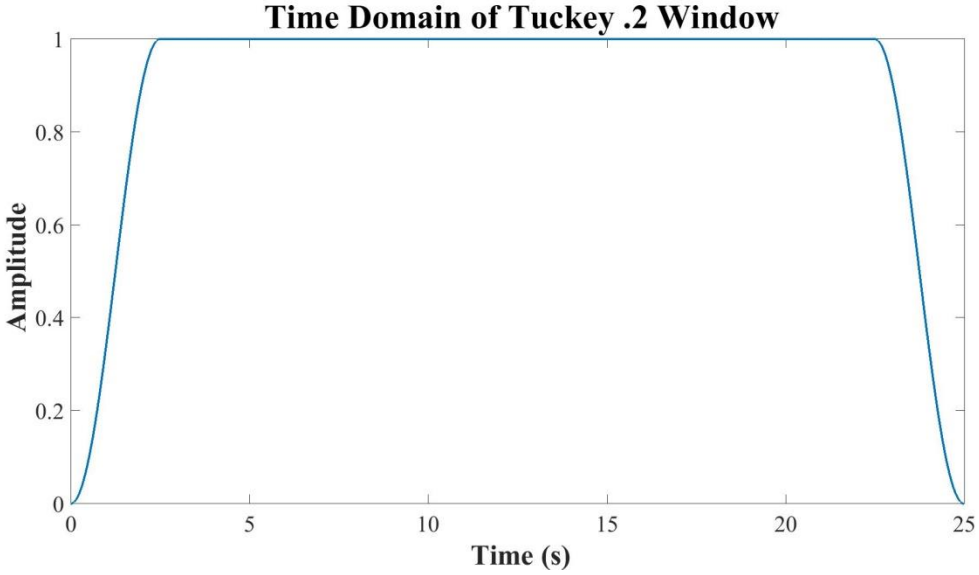

Figure 15. Time Domain of Tukey Window (α = 0.2)

The Fourier transform of a time domain window function provides insight into how the window will cause spectral leakage. Window functions are applied in the time domain using multiplication. The convolution theorem states that convolution in the time domain is equivalent multiplication in the frequency domain. The theorem also works the other way around.

$$\mathcal{F}\{f * g\} = \mathcal{F}\{f\} \cdot \mathcal{F}\{g\}$$

$$\mathcal{F}\{f \cdot g\} = \mathcal{F}\{f\} * \mathcal{F}\{g\}$$

Hence, convolution in the frequency domain by the window function is what causes the spectral leakage. The wider the bandwidth of the Fourier transform for the window function, the more spectral leakage it will cause. The Fourier transform of the Hann

window is provided in Figure 16. The Fourier transform of the Tukey α = 0.2 window is provided in Figure 17.

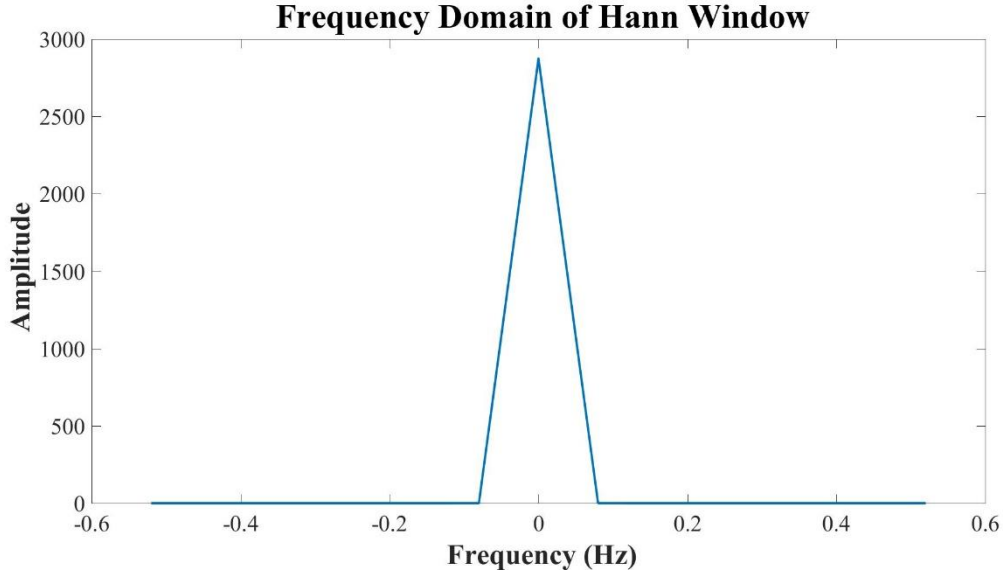

Figure 16. Frequency Domain of Hann Window (25 s)

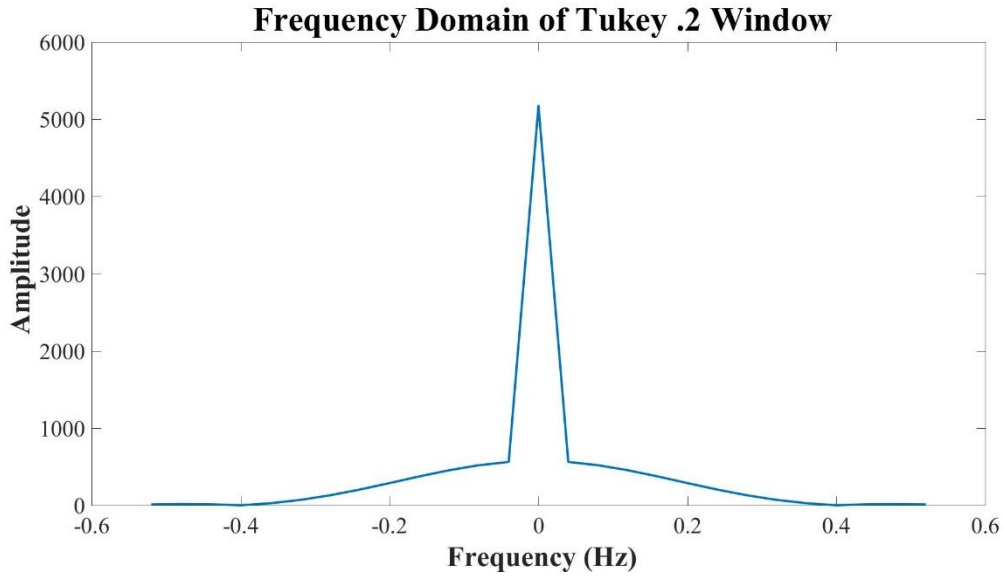

Figure 17. Frequency Domain of Tukey Window (α = 0.2, 25 s)

The Hann window will result in spectral leakage of approximately 0.1 Hz forwards and backwards. The Tukey $\alpha = 0.2$ window will result in approximately 0.3 Hz forwards and backwards. However, for the Tukey $\alpha = 0.2$ window, the leakage after .05 Hz is approximately 10% of the maximum. Additionally, the resting respiratory rate of 0.33 Hz and heart rate of 1 Hz discussed previously have a frequency separation of approximately 0.65 Hz. Therefore, a spectral leakage of 0.3 Hz is tolerable. To summarize, The Tukey $\alpha = 0.2$ window allows for a tolerable amount of spectral leakage with a coherent gain of 0.9.

For this simulation, a waveform was generated with 2 sinusoids at distinct frequencies. The first frequency (1.01 Hz) was representative of a cardiac admittance signal (fo_c). The second frequency (0.33 Hz) was representative of a respiratory admittance signal (fo_r). The amplitude of fo_c ($amplitude_c$) was configured to 1. The amplitude of fo_r ($amplitude_r$) was configured to 0.5. The analysis time of the window T_w was configured to 25 seconds. The Hann windowed time domain signal is provided in Figure 18 and the Tukey $\alpha = 0.2$ windowed time domain signal is provided in Figure 19. The Hann windowed frequency domain signal is provided in Figure 20 and the Tukey $\alpha = 0.2$ windowed frequency domain signal is provided in Figure 21.

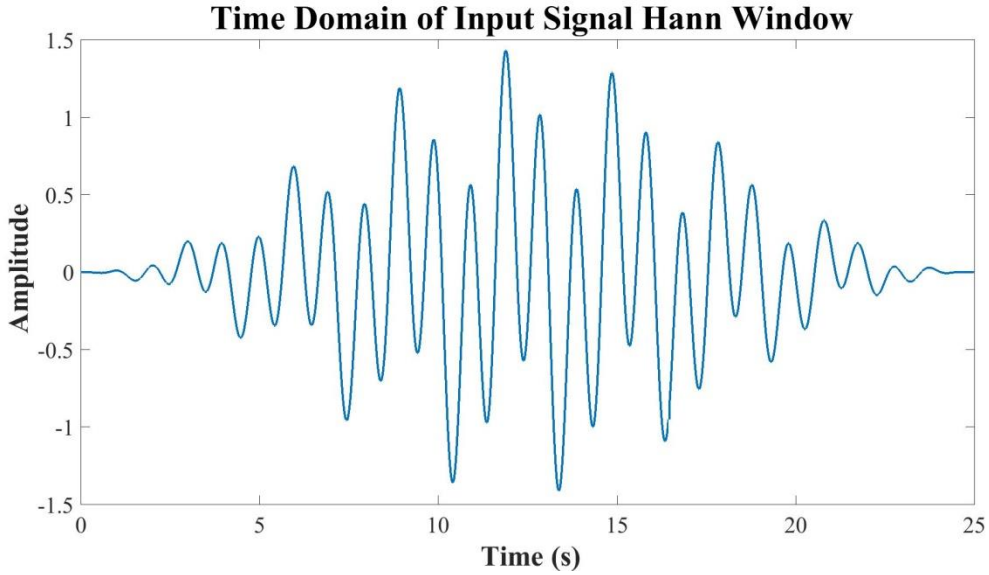

Figure 18. Time Domain Hann Windowed Input Signal

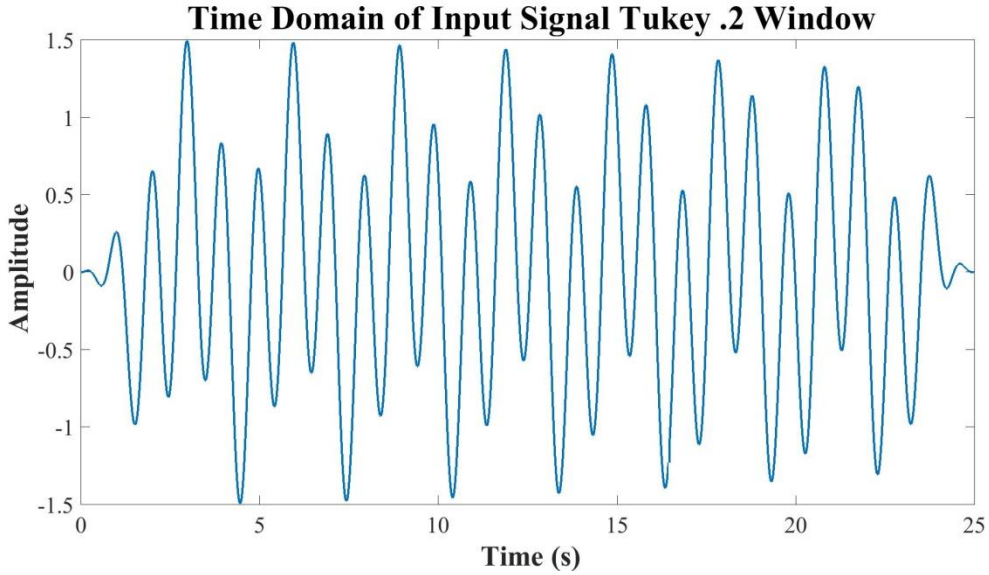

Figure 19. Time Domain Tukey $\alpha = 0.2$ Windowed Input Signal

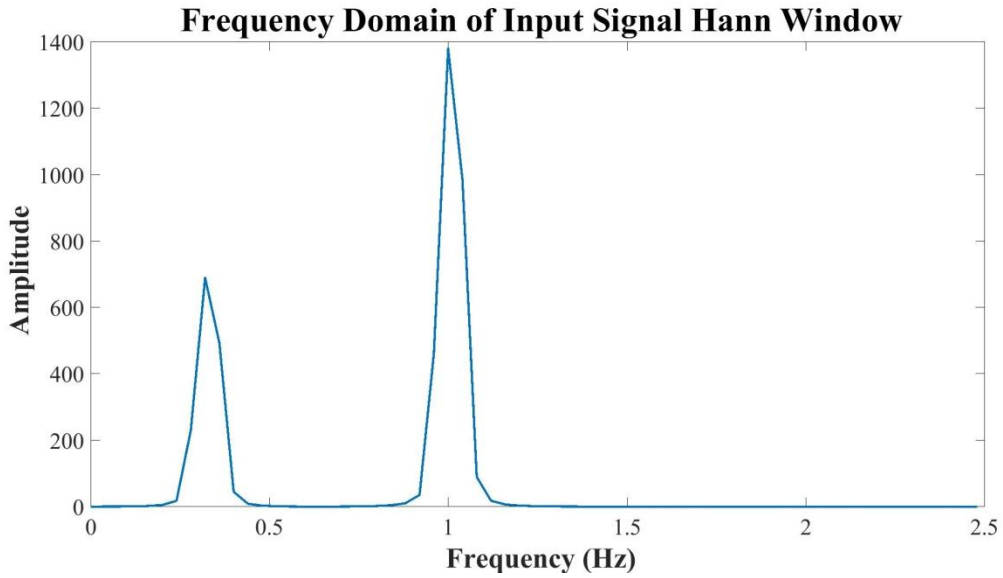

Figure 20. Frequency Domain Hann Windowed Input Signal (25 s)

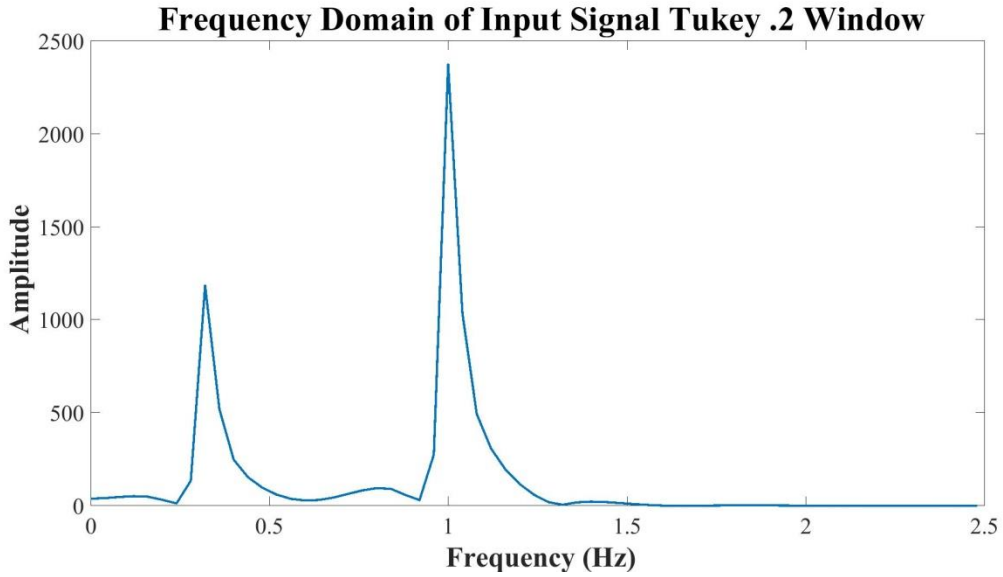

Figure 21. Frequency Domain Tukey α = 0.2 Windowed Input Signal (25 s)

2.2.2.2. Window Size Simulations

The amount of spectral leakage induced by a window is inversely proportional to the window size. Therefore, if the windows analyzed in the previous section were

reproduced for T_w=5 seconds instead of T_w=25 seconds it is expected that the bandwidth of the window in the frequency domain will increase by a factor 5. The frequency domain for the Hann window at T_w=5 is provided in Figure 22 and the frequency domain for the Tukey α = 0.2 window at T_w=5 is provided in Figure 23.

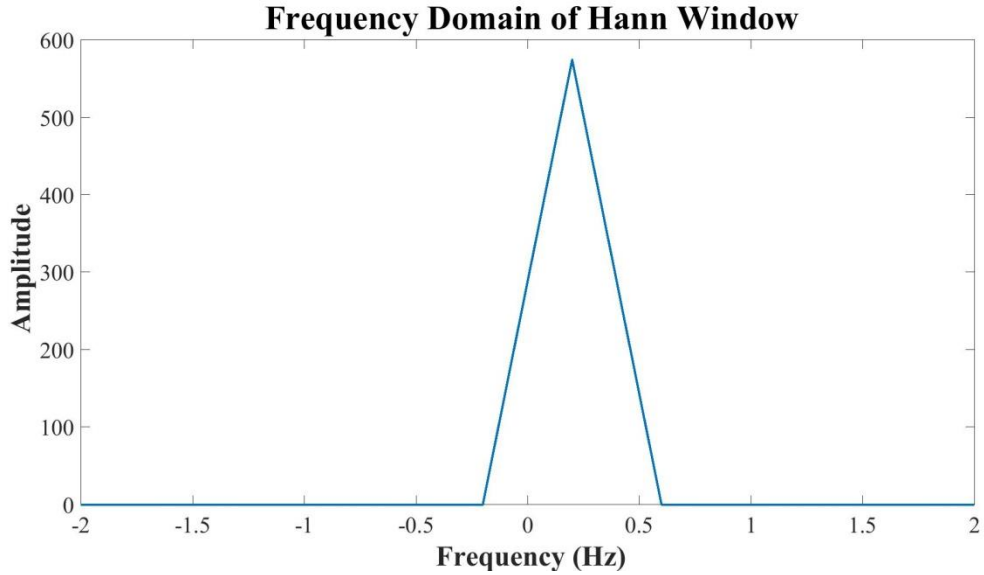

Figure 22. Frequency Domain of Hann Window (5 s)

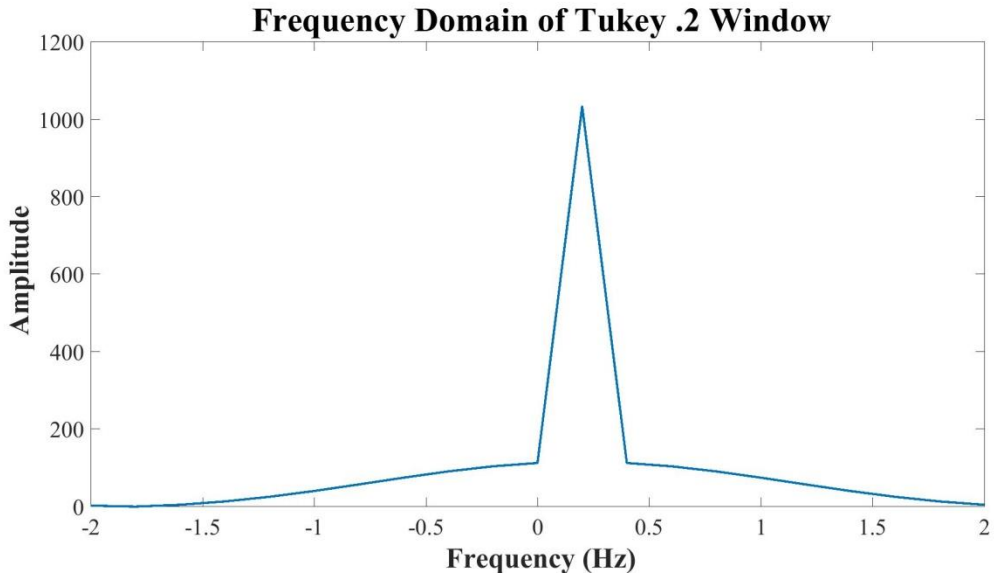

Figure 23. Frequency Domain of Tukey α = 0.2 Window (5 s)

As expected, the bandwidths of the windows increased inversely proportional to window size. Based on this, the Tukey $\alpha = 0.2$ window should not be used for analysis windows less than 15 seconds. For analysis windows less than 15 seconds the α parameter may be adjusted or a different window should be utilized.

2.2.3. Fourier Filtering Bin Selection

After the time domain signal is properly windowed, the signal is transformed into the frequency domain using the FFT. Fourier filtering is performed by altering the values of specific bins in the Fourier transformed data. Frequency bins that contain respiratory and noise artifacts are set to zero. Two methods were used for identifying which bins should be set to zero: wide band and narrow band. Both methods set bins that correspond to non-cardiac frequencies to zero. The relationship between bin number and frequency is defined as follows:

$$f_r = 1/T_w$$

$$K_n = f_n/f_r$$

$$K_n(\text{mirror}) = (N-1) - (K_n-1)$$

$$\text{by reduction,}$$

$$K_n(\text{mirror}) = N-K_n$$

where f_r is the frequency resolution (bin resolution), T_w is the amount of time in the sampling window, K_n is bin within the Fourier transform that contains the noise artifact, f_n is the frequency containing the noise, N is the number of samples, and K_n(mirror) is the mirrored bin in the Fourier transform containing the noise artifact.

When identifying K_n and K_n(mirror) it is important to understand the mirrored symmetry of the DFT. For an odd number of samples (N) the DFT bins (K) are defined as follows:

General Solution:

K=0 ; The DC bin with no corresponding mirrored bin

K=1 through K=(N-1)/2; frequency bins with corresponding mirrored bins

K=(N+1)/2 through K=(N-1); frequency bins with corresponding mirrored bins

Example: N = 5 samples:

K = 0; The DC bin with no corresponding mirrored bin

K=1 through K=2; K=1 mirrors to K=4 & K=2 mirrors to K=3

K=3 through K=4; K=3 mirrors to K=2 & K=4 mirrors to K=1

For an even number of samples (N) the DFT bins (K) are defined as follows:

General Solution:

K=0 ; The DC bin with no corresponding mirrored bin

K=1 through K=(N/2)-1; frequency bins with corresponding mirrored bins

K=N/2; The $f_s/2$ bin with no corresponding mirrored bin

K=(N/2)+1 through K=(N-1); frequency bins with corresponding mirrored bins

Example: N = 6 samples:

K = 0; The DC bin with no corresponding mirrored bin

K=1 through K=2; K=1 mirrors to K=5 & K=2 mirrors to K=4

K=3; The $f_s/2$ bin with no corresponding mirrored bin

K=4 through K=5; K=4 mirrors to K=2 & K=5 mirrors to K=1

2.2.3.1. Cardiac Harmonic Narrow Band Fourier Filter

The cardiac harmonic Narrow Band Fourier Filter (NBFF) is designed to preserve the fundamental cardiac component and N cardiac harmonic components. The filter acts as a composite filter that is the summation of N High Q bandpass filters, where the center frequency for each filter is placed at the fundamental cardiac frequency and its N harmonics. The filter is implemented in the frequency domain by selecting specific frequency bins within the DFT that should be preserved.

To identify the bins that should be preserved, the fundamental cardiac bin is first identified. This is done using the max function, which returns the index of the DFT bin with the highest value. This is referred to as index fundamental (I_f). Next, the N harmonics of I_f are calculated (I_2, I_3, …, I_N). Typically, the first 5 harmonics are sufficient to capture a majority of the cardiac signal power. The indexes (I_f, I_2, I_3, …, I_N) correspond to the centers of the pass band for the N High Q bandpass filters. The bandwidth for each filter can be configured. Typically, a bandwidth (f_{bw}) of 0.5 Hz effectively preserves the cardiac signal power.

This filtering method is effective for intraventricular admittance signals collected during stable heart rate conditions. If the heart rate becomes variable (HRV), the cardiac signal power will no longer be contained in a narrow bandwidth, and the filters will no longer preserve a majority of the cardiac signal power. To account for HRV f_{bw} may be increased. An example admittance signal with stable heart rate conditions collected during atrial pacing at 120 beats per minute (BPM) is provided in Figure 24.

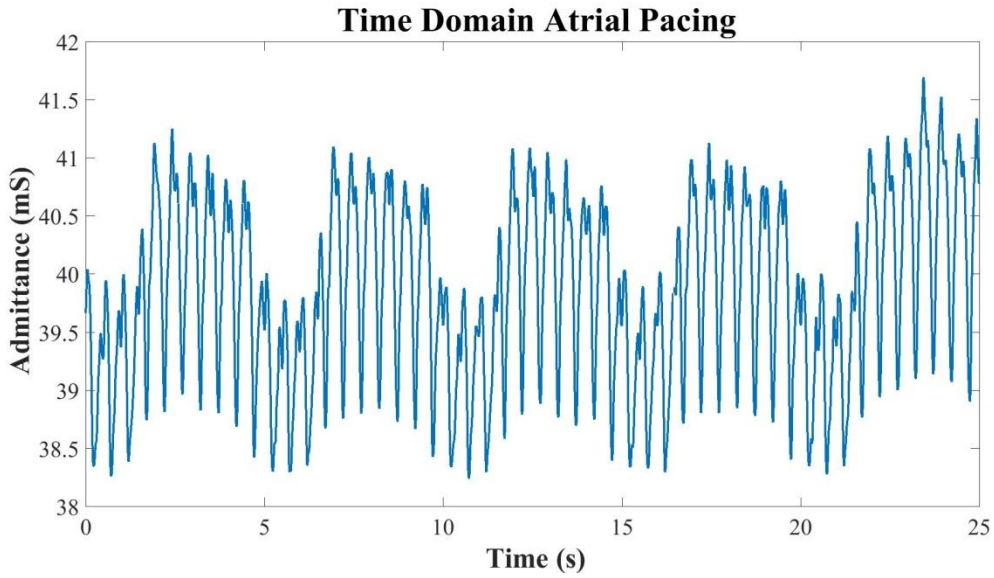

Figure 24. Time Domain Atrial Pacing Signal (120 BPM)

In the time domain admittance signal provided in Figure 24, both cardiac and respiratory components of the admittance signal can be identified. The frequency domain representation of this signal is provided in Figure 25.

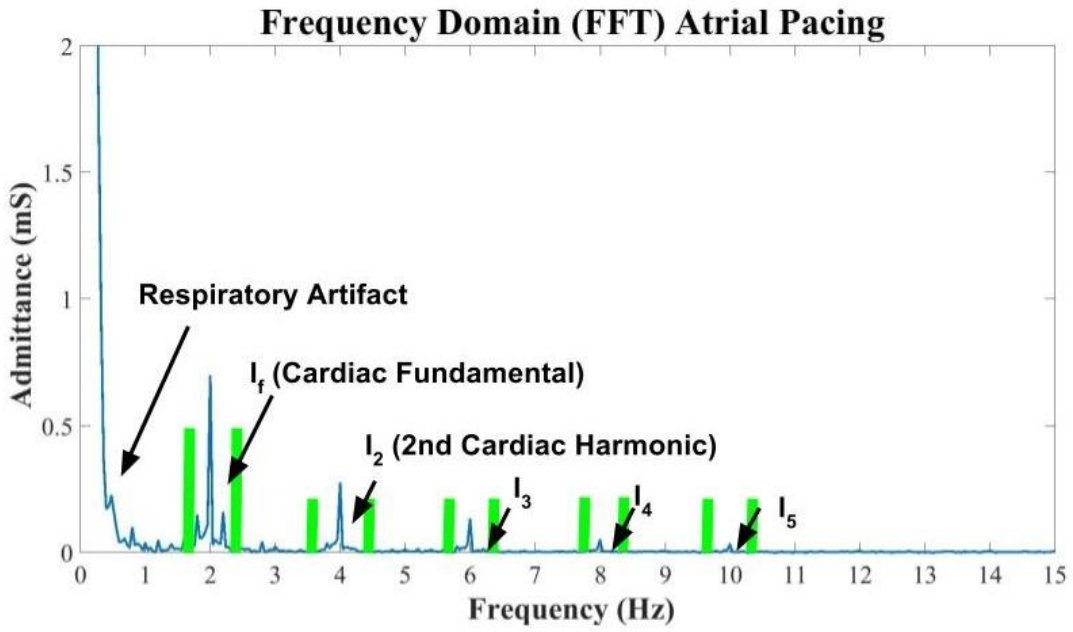

Figure 25. Frequency Domain Atrial Pacing Signal (120 BPM)

In Figure 25, the frequency domain representation of the signal shows the fundamental cardiac signal and 4 of its harmonics. The green bars around each of the cardiac signal components represent f_{bw}. The fundamental cardiac frequency is centered at 2 Hz, corresponding to a heart rate of 120 BPM. The large signal component bellow 1 Hz is a combination respiratory artifact and spectral leakage from the DC bin. It is important to note that Figure 25 does not show the mirrored bins that also need to be maintained to ensure symmetry within the DFT. If the corresponding mirrored bins are not preserved the inverse Fourier transform used later will not correctly reconstruct the time domain signal.

2.2.3.2. Cardiac Wide Band Fourier Filter

The cardiac Wide Band Fourier Filter (WBFF) is simply a bandpass filter that is designed to remove respiratory frequencies and preserve cardiac frequencies. This filter is useful when the heart rate is variable. During arrhythmias, heart rate can be variable making the WBFF a better choice when compared to the NBFF. The defining characteristics of a traditional bandpass filter are provided in Figure 26.

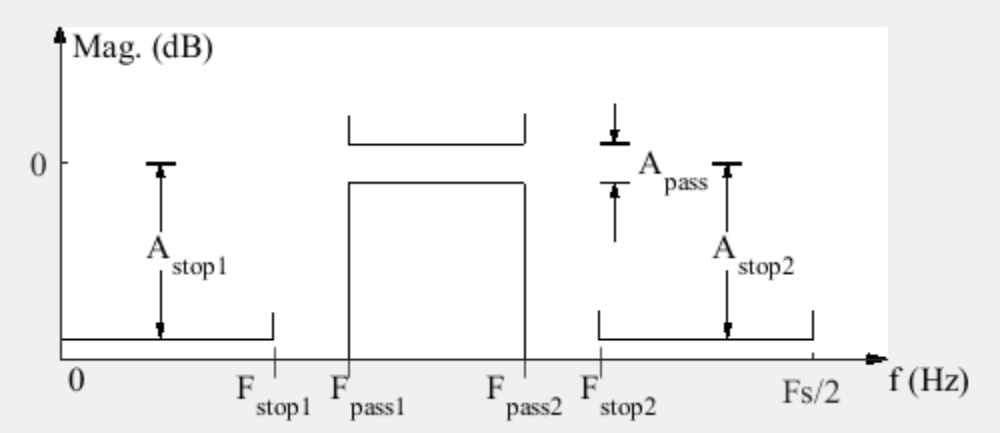

Figure 26. Bandpass Filter Characteristics

Traditional bandpass filters can be implemented as either a finite impulse response (FIR) of infinite impulse response (IIR) filter. The Fourier filter method has several benefits when compared to FIR and IIR filter implementations. One of the most important benefits of the Fourier filter is that it can be used to create very quick transitions between the pass band (F_{pass}) and the stop band (F_{stop}). To removing respiratory admittance signals (0.33 Hz) from cardiac admittance signals (1 Hz), this property is required. An example admittance signal collected during atrial fibrillation is provided in Figure 28.

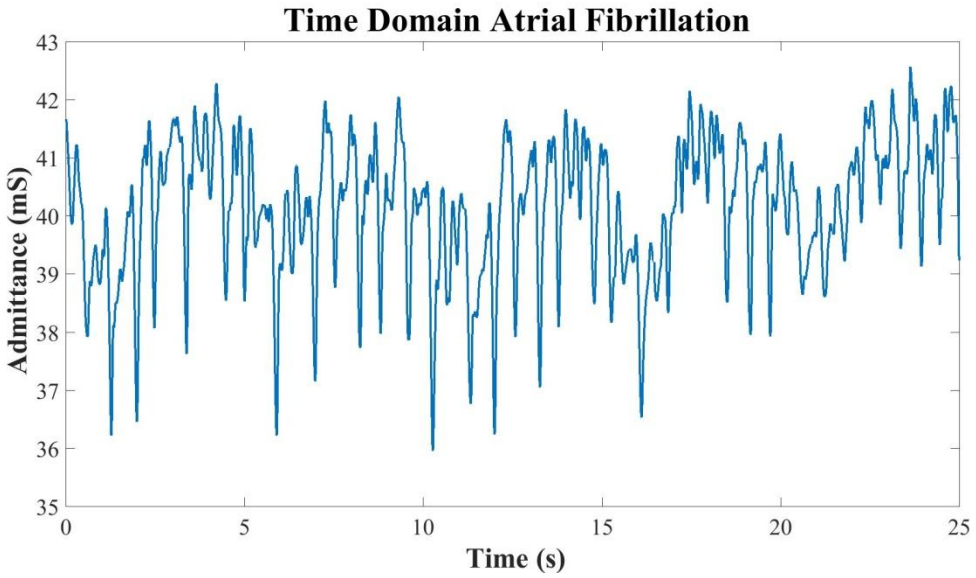

Figure 28. Time Domain Atrial Fibrillation Signal

In the atrial fibrillation signal provided in Figure 28 a variable heart rate can be observed in the presence of a significant respiratory component. The frequency domain of the atrial fibrillation signal is provided in Figure 29.

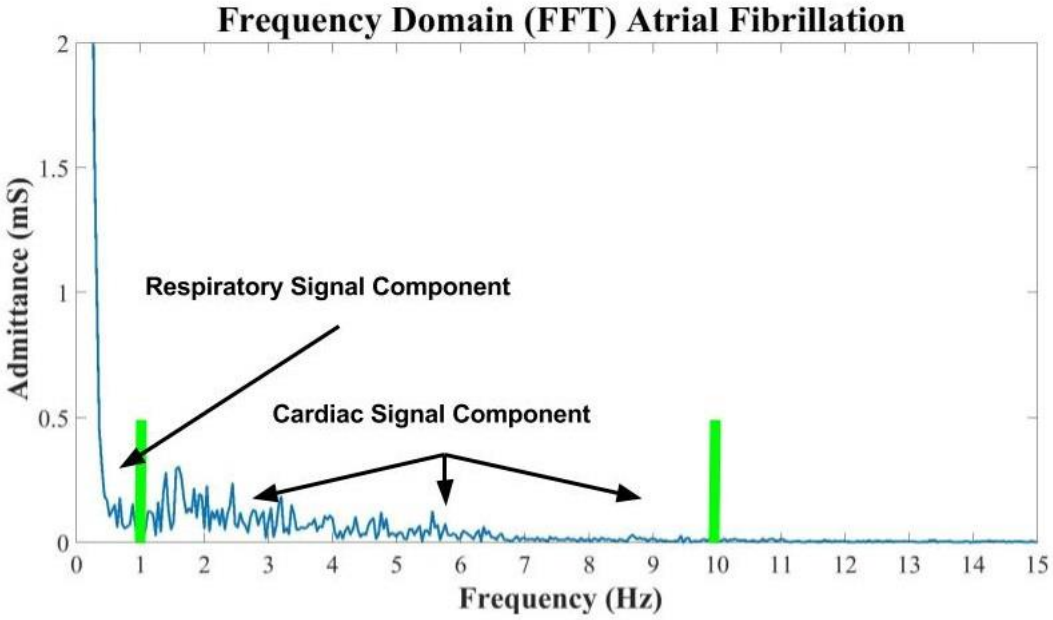

Figure 29. Frequency Domain Atrial Fibrillation Signal

From the frequency domain signal provided in Figure 29, it can be observed that the cardiac signal component is composed of a wide band of frequencies. The NBFF described in the previous section would not be effective at preserving the cardiac components of this signal. However, the WBFF which was configured to pass cardiac frequencies between 1 Hz and 10 Hz and preserves a majority of the cardiac signal power while removing respiratory artifacts. It is important to note that Figure 29 does not show the mirrored bins that also need to be preserved to ensure symmetry within the DFT. If the corresponding mirrored bins are not properly preserved, the inverse Fourier transform used later will not correctly reconstruct the time domain signal.

2.2.4. Inverse Discrete Fourier Transform (IDFT)

After the admittance signal is filtered in the Fourier domain, it is helpful to transform the signal back into the time domain for further analysis. The inverse discrete Fourier transform (IDFT) is applied to transform the signal back to the time domain. The definition of the IDFT is provided bellow:

$$x_n = \frac{1}{N} \sum_{k=0}^{N-1} X_k \cdot e^{i2\pi kn/N}$$

Where x_n ($0<n<N-1$) represent the N time domain samples, X_k ($0<k<N-1$) represent the N complex bins of the DFT. Like the DFT, the IDFT can be calculated efficiently using a divide and conquer method. Efficient implementations of the IDFT are referred to as inverse fast Fourier transforms (IFFT).

2.2.4.1. Stroke Volume Estimation

Admittance measurements have units of Siemens (S) and for intraventricular measurements are typically presented in milliSiemens (mS). Intraventricular admittance measurements are a surrogate for blood volume [9]. To estimate SV, the amplitude of the

intraventricular admittance signal must be calculated. Typically, this is done by subtracting an end-diastolic admittance measurement from a corresponding end-systolic admittance measurement. In general, RV tripolar admittance measurements are correlated with blood volume i.e., larger admittance values correspond to larger volumes. Therefore, the highest admittance measurement corresponds to end-diastole and the lowest admittance measurement corresponds to end-systole. An example of an unfiltered admittance signal is provided in Figure 30.

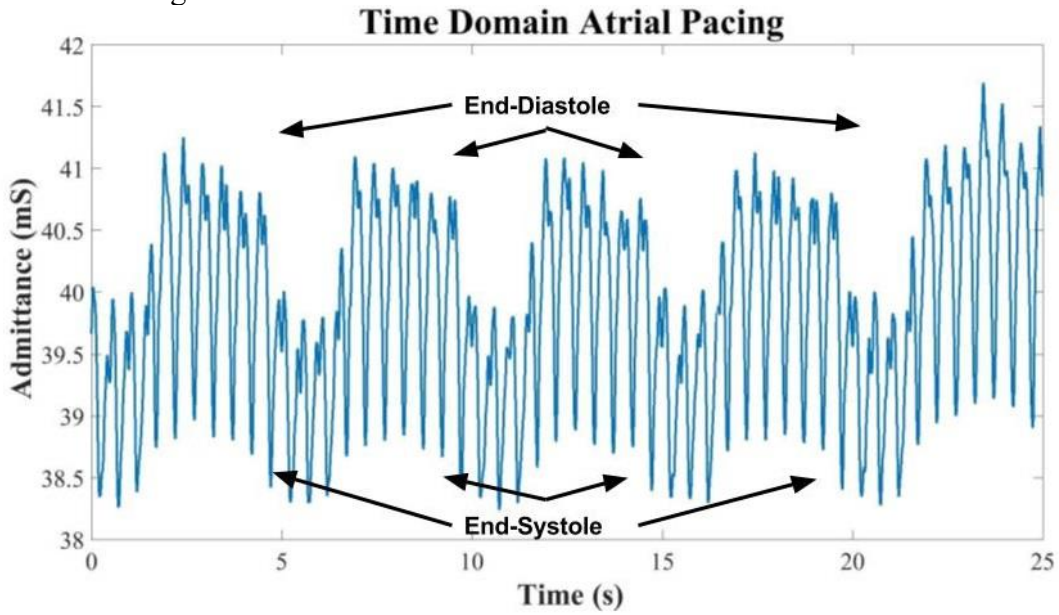

Figure 30. Admittance Signal End-diastole & End-Systole

In the admittance signal provided in Figure 30, it can be observed that the amplitude of the admittance signal changes through the respiratory cycle. The NBFF can be applied in the frequency domain to reduce the amount of respiratory artifact in the signal. After the NBFF is applied in the frequency domain the signal is transformed back into the time domain using the IFFT. The resulting time domain signal is provided in Figure 31.

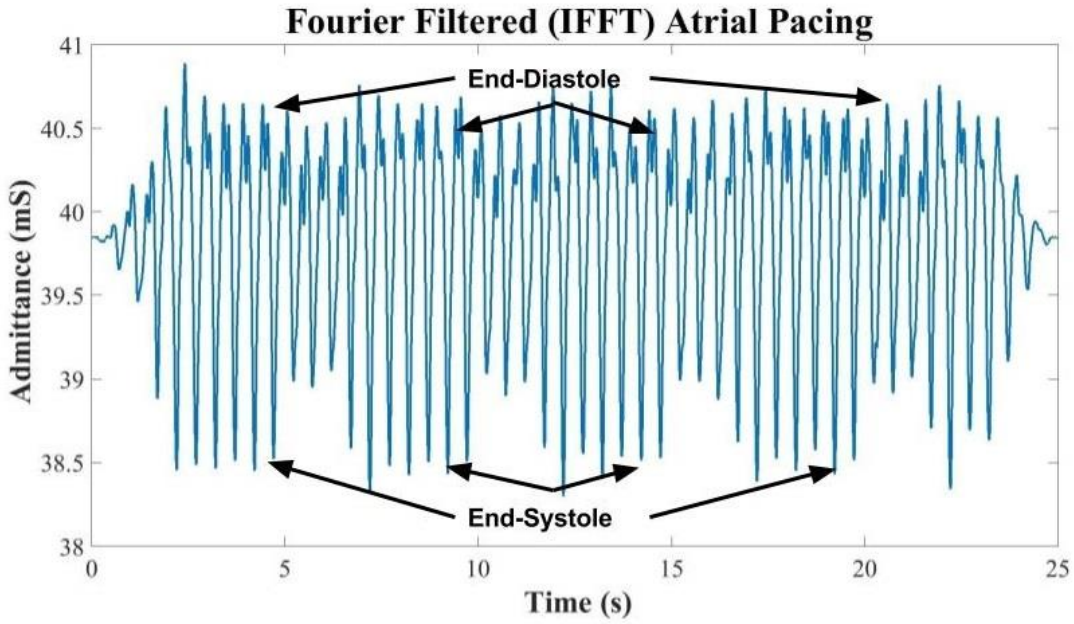

Figure 31. IFFT of Fourier Filtered Admittance Signal

While most of the respiratory artifact has been removed, Figure 31 shows that some respiratory artifact remains in the admittance signal even after the Fourier filter has been applied. The remaining respiratory artifact was not removed by the NBFF because this respiratory artifact is modulated on the cardiac admittance signal. The frequency of the modulated respiratory artifact is defined below:

$$fo_{r\text{-}MOD} = fo_c \pm fo_r$$

The respiratory rate (fo_r) can be as low as 0.1 Hz meaning the modulated respiratory artifact ($fo_{r\text{-}MOD}$) may end up very close to the frequency of the cardiac signal frequency (fo_c). Assuming a HR of 120 BPM and a respiratory rate of 6 breaths per minutes, the $fo_{r\text{-}MOD}$ artifact would be at 2 ± 0.1 Hz. The modulated artifact cannot be filtered due to spectral leakage and heart rate variability. To minimize the effect that the respiratory modulation has on the SV amplitude calculation, the amplitude of the admittance signal is calculated

over several respiratory cycles. Assuming a respiration rate of 12 breaths per minute, a 25 second analysis window will contain approximately 5 respiration cycles.

Traditionally, the amplitude of the admittance signal is calculated by subtracting an end-systolic admittance measurement from an end–diastolic admittance measurement. This calculation is generally done for a single cardiac cycle. Due the significant amplitude variability in the admittance signal, taking an amplitude measurement for a single cardiac cycle is an inaccurate method for measuring admittance stroke volume. To perform this operation over 25 seconds (50 cardiac cycles at 120 BPM), a peak detection algorithm was used to identify all the end-diastolic and end-systolic admittance measurements in the 25 second window. The end-systolic measurements were subtracted from the end-diastolic measurements. The resulting amplitude measurements were then averaged over the entire 25 second window.

The amplitude can also be calculated using root mean squared (RMS) approach. RMS is much simpler to implement when compared to peak detection and yields comparable results. Additionally, RMS uses every data point in the sampling window in the amplitude calculation. The peak detection algorithm calculates amplitude using only 2 data points for each cardiac cycle and as a result may be more susceptible to inaccuracies in the presence of noise artifacts.

2.2.4.2. End-diastolic and End-systolic Calculation

The NBFF and WBFF remove the DC component of the admittance signal. For SV calculations the DC component is not needed. However, for end-diastolic and end-systolic admittance calculations the DC component of the admittance signal is needed. The DC component of the admittance signal can be added back in the time domain. The DC bin value in the frequency domain must be divided by N to obtain the DC signal amplitude in

the time domain. This operation follows from Parceval's theorem, which states that signal energy in the frequency domain and time domain must be equivalent:

$$\sum_{n=0}^{N-1} |x[n]|^2 = \frac{1}{N} \sum_{k=0}^{N-1} |X[k]|^2$$

Additionally, the coherent gain caused by the window function must be reversed. The complete operation to calculate the DC signal amplitude is as follows:

$$DC_{Amplitude} = (K_0/N)/(W_g)$$

where $DC_{Amplitude}$ is the DC signal amplitude in the time domain, K_0 is the DC bin of the Fourier transform, N is the number of samples, and W_g is the coherent gain of the window function.

The $DC_{Amplitude}$ can be used to calculate the end-diastolic and end-systolic admittance values in the time domain. If the peak detection algorithm is used to measure ADSV/CDSV, the $DC_{Amplitude}$ should be added back to the time domain signal before the peak detection algorithm is run. This will ensure that end-diastolic and end-systolic values returned by the peak detection algorithm include the DC signal component.

If the RMS calculation is used to determine ADSV/CDSV, the $DC_{Amplitude}$ should not be added back to the time domain signal before the calculation. After the RMS calculation is performed without the $DC_{Amplitude,}$ the following equations can be applied to obtain end-diastolic and end-systolic admittance measurements:

$$\text{End-Diastolic} = DC_{Amplitude} + (A_{rms}/W_g * \sqrt{2})$$

$$\text{End-Systolic} = DC_{Amplitude} - (A_{rms}/W_g * \sqrt{2})$$

where A_{rms} is the RMS value of the Fourier filtered admittance signal.

The multiplication by $\sqrt{2}$ is used to convert from RMS measurement to a Peak measurement. This conversion from RMS to Peak is only applicable to single frequency sinusoids; however, it is a fair estimate in this case since a majority of the signal energy is

captured in the fundamental frequency. Additionally, this estimate of end-diastolic and end-systolic admittance assumes that the wave form is balanced around the DC signal component. The end-diastolic and end-systolic measurements do not necessarily need to be the same distance away from the DC signal component.

2.2.4.3. Heart Rate Calculation

The heart rate can be calculated directly from the Fourier transform of the admittance signal. In fact, I_f, the index of the fundamental cardiac signal can be used to directly calculate the heart rate in BPM:

$$HR\ (BPM) = (I_f * f_r) * 60$$

where I_F is the bin of the Fourier transform that contains the fundamental cardiac signal component, and f_r is the frequency resolution in Hz.

2.3. DISCUSSION

2.3.1. Window Size Limitations

A too-short sampling window results in an inadequate number of respiratory cycles to properly isolate the cardiac and respiratory components of the admittance signal. However, it should also be noted that a too-large window is also not acceptable. For an ICD arrhythmia discrimination algorithm, the system must be able to provide a hemodynamic classification in a clinically relevant amount of time. It is acceptable to delay ICD therapies for 100-150 beats [17D, 17E]. At a rate of 250 BPM, 100 beats correspond to approximately 24 seconds. Therefore, a 25 second processing window may be acceptable. A multi-time scale analysis window may be considered to provide classification in a shorter amount of time. For example, very large changes in ADSV/CDSV could be detected using a shorter processing window (10 seconds) that would not remove respiratory artifacts as effectively. Smaller changes in ADSV/CDSV

could be detected using the standard 25 second processing window to more accurately remove respiratory artifacts.

2.3.2. Low-power Computation Considerations

The amplitude of the admittance signal can be calculated in the Fourier domain without transforming the signal back into the time domain using the IFFT. This calculation can be performed by adding the bins of the Fourier transform and calculating the magnitude as shown below:

$$X_{total} = \frac{1}{N}\sum_{k=0}^{N-1}(\mathrm{X_k})\text{^}2\sum_{k=0}^{N-1}\mathrm{X_k}$$

where X_{total} is complex and of the form Z = X + jY

$$X_{magnitude} = \sqrt{X^2 + Y^2}$$

where X_k are the K bins of the DFT, and N is the number of bins in the DFT. This calculation produces an equivalent result to the RMS time domain calculation. By performing this operation in the frequency domain the IFFT operation can be eliminated. The calculation must also include mirrored bins.

Additionally, it is not necessary to calculate the entire DFT. In fact, for the WBFF only the bins between 1 Hz and 10 Hz need to be calculated since all other bins in the Fourier transform will be set to zero. A similar optimization can be made for the NBFF. Since the mirrored bins for the DFT are simply the complex conjugates of the positive bins (for real valued time domain inputs), those bins can simply be calculated by changing the sign of the imaginary component of the positive bins. Assuming an admittance sampling rate of 250 Hz (fs), an analysis time of 25 seconds (T_w), a minimum cardiac frequency of

1 Hz (fc_{min}), and a maximum cardiac frequency of 10 Hz (fc_{max}), the number of DFT bins that need to be calculated are as follows:

$$fr = 1/ T_w = 1/25 = .04$$

$$K_{min} = fc_{min}/fr = 1/.04 = 25$$

$$K_{max} = fc_{max}/fr = 10/.04 = 250$$

$$K_{total} = K_{max} - K_{min} + 1 = 226 \text{ (bins)}$$

$$N_{total} = fs * T_w = 250 * 25 = 6{,}250 \text{ (Samples)}$$

$$C_{total} = N_{total} * K_{total} = 6{,}250 * 226 = 1{,}412{,}500 \text{ (Calculations)}$$

$$OP_{total} = C_{total} * OP_{cnt} = 1{,}412{,}500 * 10 = 14{,}125{,}000 \text{ (Operations)}$$

where fr is the frequency resolution in Hz, K_{min} is the minimum cardiac frequency bin, K_{max} is the maximum cardiac frequency bin, K_{total} is the total number of DFT bins that need to be calculated, N_{total} is the total number of samples for each bin calculation, C_{total} is the total number of calculations required for all of the bin calculations, OP_{cnt} is the number of machine operations per calculation, and OP_{total} is the total number of machine operations to calculate all of the bins required for the ADSV/CDSV method.

To run at low power, the microcontrollers in many pacemakers run with bus speeds as slow as 1 MHz for an embedded processor running at 1 MHz, this would consume over 14 seconds of computation time. To reduce the computation time, several optimizations were considered

Since the maximum cardiac frequency of interest is 10 Hz, the admittance signal could be sampled at 250 Hz and low pass filtered to the Nyquist rate of 20 Hz, and then down sampled by 10, making the effective sampling rate 25 Hz. Additionally, the divide and conquer methodology of the FFT could be applied to further reduce the effect of the number of samples to log(N):

$$N_{total} = fs * T_w = 25 * 25 = 625 \text{ (Samples)}$$

$$C_{total} = \log(N_{total}) * K_{total} = \sim 10 * 226 = 2{,}260 \text{ (Calculations)}$$

$$OP_{total} = C_{total} * OP_{cnt} = 2{,}260 * 10 = 22{,}600 \text{ (Operations)}$$

The divide and conquer methodology of the FFT can only be applied when the entire DFT is being calculated and to optimize a partial bin calculation further investigation is required.

An alternative approach to the DFT would be to use finite impulse response (FIR) filter banks. FIR filters have a time complexity of O(N) and are well suited for embedded applications. A simple bandpass FIR filter can be designed using two low pass filters (LPF). The first LPF could be designed to pass frequencies between 0 Hz and 10 Hz (respiration + cardiac). The second LPF could be designed to pass frequencies between 0 Hz and 1 Hz (respiration). Subtraction of the second LPF from the first LPF would yield a bandpass filter which passes frequencies between 1 Hz and 10 Hz (cardiac). It is critically important that the second LPF has a sharp transition from the pass-band to the stop-band or else the resulting bandpass filter will not properly remove the respiratory component from the admittance signal. This FIR filter bank implementation also requires further investigation.

The use of customized FIR filter banks as an alternative to the FFT is sometimes referred to as a wavelet transform. Each “filter bank” in the wavelet transform can be thought of as an independent wavelet “bin”. Rather than having a signal composed of sines and cosines (FFT bins) a signal can be represented as a combination of the coefficients from the distinct filters that compose the wavelet transform. The filters of the wavelet transform can be customized to the specific application. The creation of a set of customized filters for the NBFF and WBFF and the grouping the filters into a wavelet transform should be considered as a potential method to optimize the ADSV/CDSV algorithm.

2.3.3. Energy Consumption Considerations

The ADSV/CDSV measurement cannot be performed without increasing the power consumption of ICDs. However, if used appropriately the amount of energy consumed by the system negligible. The analog power consumption of the ADSV/CDSV measurement is around 2 mA in the lowest power configuration. With a 200 Hz sampling rate, the analog measurement can be performed at a 20% duty cycle. Hence, the continuous power consumption with a 200 Hz sampling rate is approximately 400 μA. In the arrhythmia discrimination algorithm presented in Chapter 5, it is only necessary for the measurement to be made after the ICD has detected an arrhythmia event. Assuming the ADSV/CDSV measurement is made for 20 seconds after the detection of an arrhythmia event, approximately 2.2 μAh of battery life would be consumed by ADSV/CDSV during a single arrhythmia event. ICD's generally have around 1000 mAh of battery capacity. Assuming 0.1% (1 mAh) of the power budget could be allocated for ADSV/CDSV measurements, approximately 450 arrhythmia episodes could be monitored by ADSV/CDSV.

3. Chapter 3: Preliminary Right Atrial Pacing Experiment

3.1. MOTIVATION

The purpose of the right atrial pacing experiment was to validate that the Cardiovol admittance measurement can track changes in SV. An acute pacing protocol was used to cause changes in SV. The changes were tracked with 2D-TTE (trans-thoracic echo ultrasound) and RV tripolar admittance. This study was designed and carried out by the Chief Scientific Officer of Admittance Technologies, John Porterfield PhD. I attended the experiments, assisted in data collection, and analyzed the data set.

3.2. METHODS

In an acute study, N=5 canine subjects were implanted with an RV ICD shocking lead and an RA pacing lead. The pacing protocol was carried out by pacing the RA lead using an external pacemaker. In each part of the protocol, 10 seconds of 2D-TEE and RV tripolar admittance measurements (end-systolic volume (ESV), end-diastolic volume (EDV), and SV) were recorded.

The 2D-TTE SV measurements were calculated using Simpson's method, which is used to approximate the end-diastolic and end-systolic chamber volumes from a 2-dimensional image of the LV chamber [34]. The end-diastolic and end-systolic chamber volumes can then be subtracted to measure SV.

RV tripolar admittance measurements were analyzed using the NBFF described in Chapter 2. Since only 10 seconds of data were collected during each protocol part, the data was windowed with a Tukey window ($\alpha = 0.5$) to limit the amount of spectral leakage that occurs with a reduced window size. The RV tripolar admittance measurements were then calibrated from mS to mL using 2D-TTE measurements collected as baseline.

3.2.1. Protocol Overview

First, baseline measurements were taken without pacing. The pacing protocol consists of 6 parts listed chronologically as follows:

1) paced-baseline (PBL) paced at a rate slightly above baseline

2) paced-baseline+40 (PBL+40), paced at 40 BPM higher than step 1

3) paced-baseline (PBL), paced at same rate as step 1

4) paced-baseline+40 (PBL+40), paced at 40 BPM higher than step 1

5) paced-baseline (PBL), paced at same rate as step 1

6) paced-baseline+40 (PBL+40), paced at 40 BPM higher than step 1.

3.3. RESULTS

In the acute atrial pacing protocol, it was expected that the stroke volume would fall from PBL to PBL+40. Physiology anticipates that a fall in stroke volume will be observed with an increased atrial pacing rate due to a drop in end-diastolic volume. The drop in end-diastolic volume occurs because of a decrease in ventricular filling time.

For each of the 5 canine subjects, the admittance and 2D-TTE results were analyzed for repeatability and conformation of the hypothesis: SV will fall with increased atrial pacing rate. Results are presented for 2D-TTE, admittance derived stroke volume (ADSV σ_m/ϵ_m = 800,000), and conductance derived stroke volume (CDSV). CDSV is calculated using the same signal processing methods as the ADSV analysis technique. However, the CDSV method does not use the admittance equation, which leverages the phase information from the admittance signal to remove muscle contributions from the admittance signal. The CDSV results are provided to evaluate whether the admittance equation provides any tangible benefits to the RV tripolar configuration on canine subjects.

3.3.1. 2D-TTE Echo Results

The 2D-TTE EDV, ESV, and SV measurements were calculated using Simpson's method. The 2D-TTE measurements were highly variable and provided little to no insight about the true physiologic function of the subjects. 2D-TTE Echo SV results are provided in Figure 32.

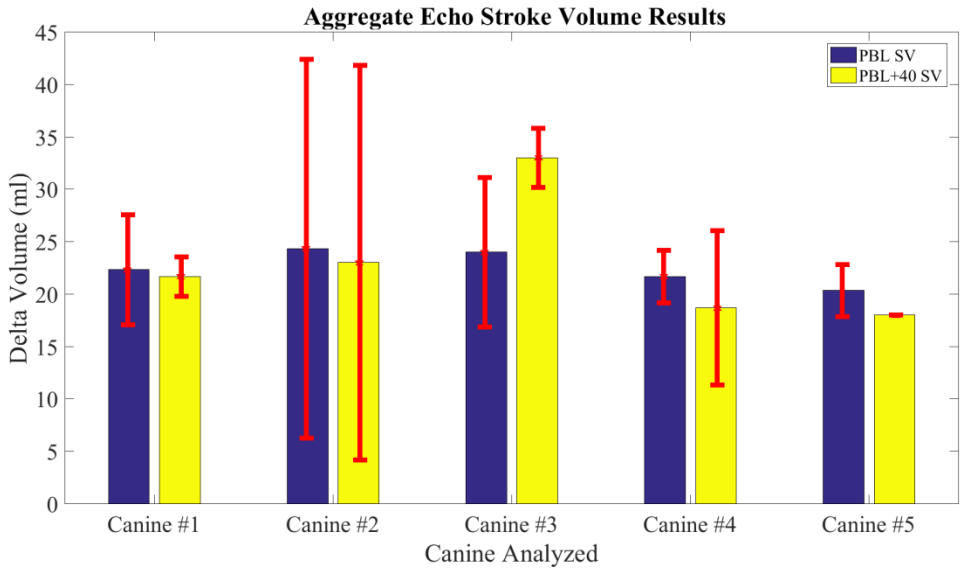

Figure 32. Acute 2D-TTE Echo SV Results

In Figure 32, the 2D-TTE Echo SV results for 5 canine subjects are presented. For each subject, PBL SV values and PBL+40 SV values are an average of the 3 measurements collected. Error bars are provided with ± 1 standard deviation of error. From the graph, no significant determination about physiologic function can be made from the 2D-TTE data.

2D-TTE EDV and ESV measurements were also not very useful for determining physiologic function. The 2D-TTE EDV and ESV results are provided in Figure 33.

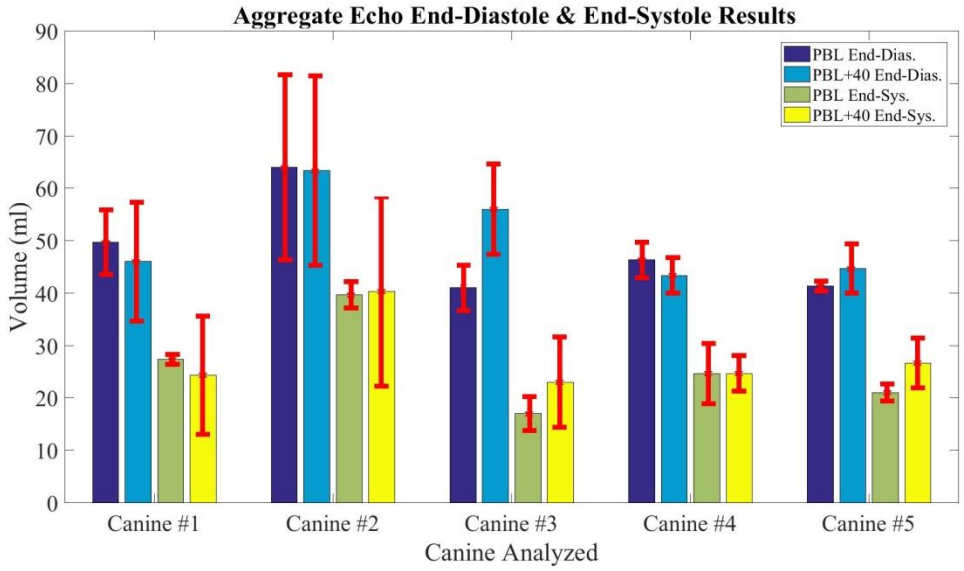

Figure 33. Acute 2D-TTE Echo EDV & ESV Results

In Figure 33 the 2D-TTE Echo EDV & ESV results for 5 canine subjects are presented. For each subject, PBL EDV/ESV values and PBL+40 EDV/ESV values are an average of the 3 measurements collected. Error bars are provided with ± 1 standard deviation of error. From the graph no significant determination about physiologic function can be made from the 2D-TTE data.

3.3.2. Admittance Derived Stroke Volume (ADSV) Results

The ADSV results were much more repeatable when compared to the 2D-TTE measurements. In fact, the ADSV measurements followed the hypothesis of the experiment: SV will fall with increased atrial pacing rate. The ADSV results for the 5 canine subjects are provided in Figure 34.

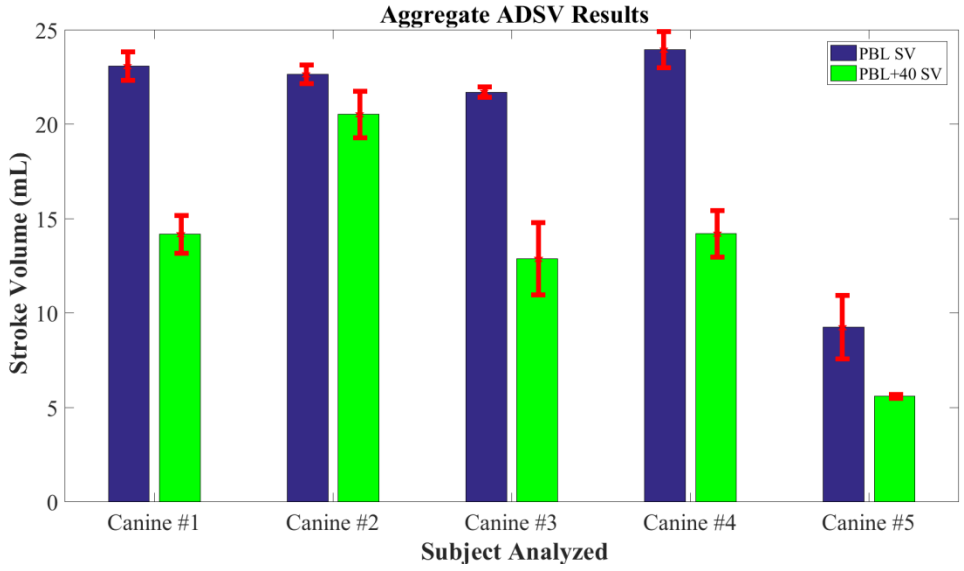

Figure 34. Acute ADSV Results

In Figure 34 the ADSV results for 5 canine subjects are presented. For each subject, PBL SV values and PBL+40 SV values are an average of the 3 measurements collected. Error bars are provided with ± 1 standard deviation of error. From the graph most subjects displayed a significant drop in SV with increased right atrial pacing rate.

The ADSV method was also used to measure EDV and ESV. The ADSV EDV/ESV results are provided in Figure 35.

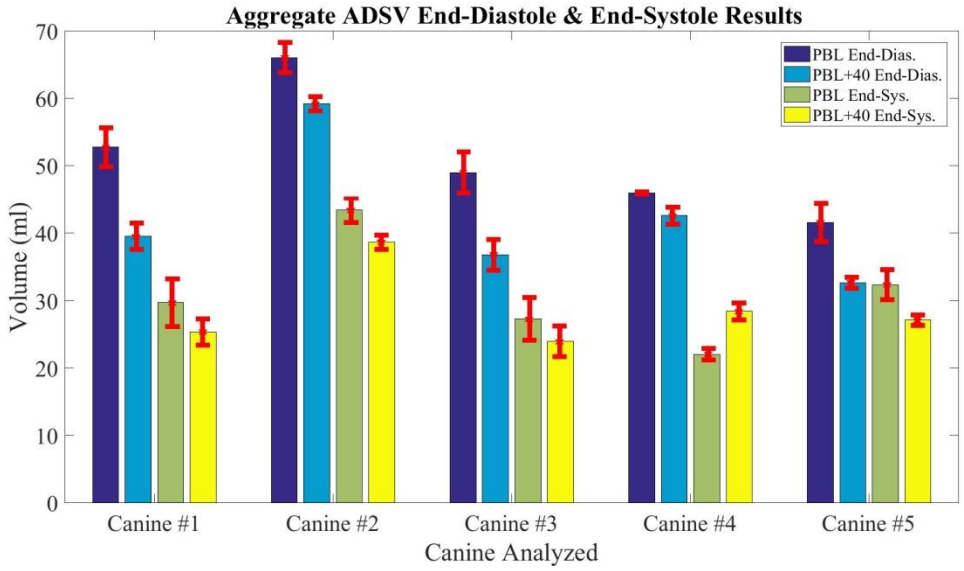

Figure 35. Acute ADSV EDV & ESV Results

In Figure 35 all 5 subjects exhibit a drop in EDV from PBL to PBL+40. This result is consistent with the expected physiologic response to increase right atrial pacing: EDV will fall with increased right atrial pacing rate due a decrease in ventricular filling time.

3.3.3. Conductance Derived Stroke Volume (CDSV) Results

The conductance derived stroke volume method is processed using the same signal processing methods as ADSV. However, the admittance equation, which removes the muscle contribution from the admittance signal, is not used. The CDSV SV measurements are provided in Figure 36 and the CDSV EDV & ESV results are provided in Figure 37.

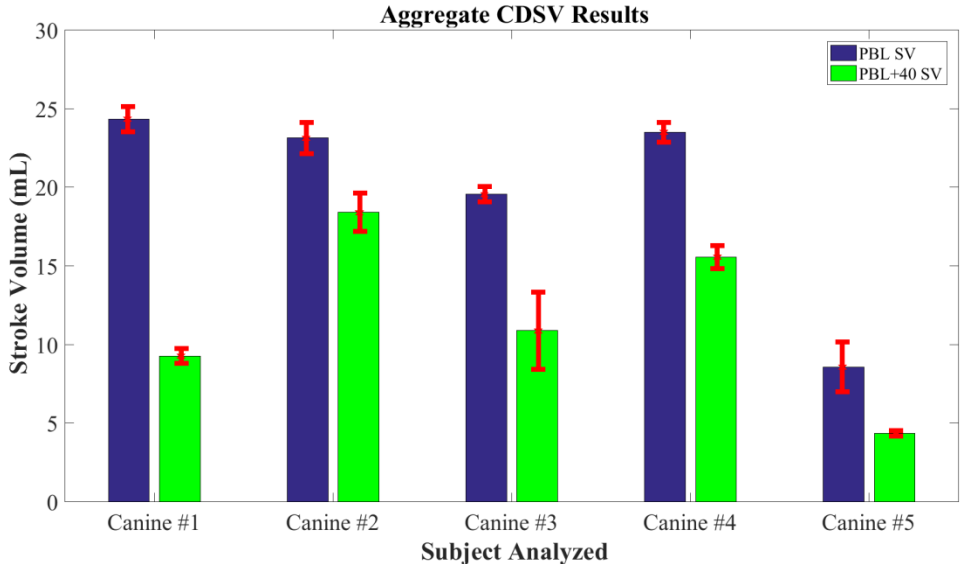

Figure 36. Acute CDSV SV Results

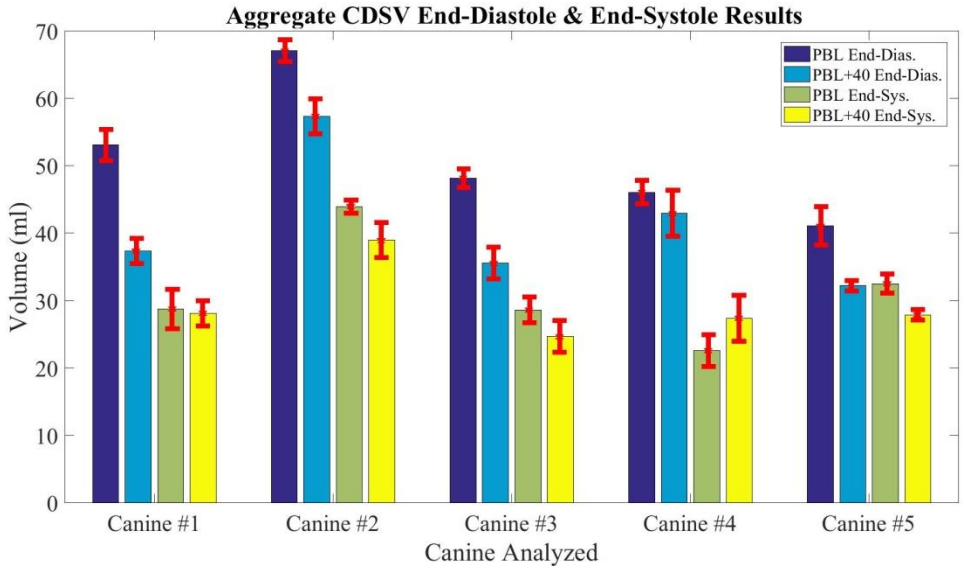

Figure 37. Acute CDSV EDV & ESV Results

The CDSV results provided in Figure 36 and Figure 37 are comparable to the ADSV results provided in Figure 34 and Figure 35. The data appears to show that the

admittance equation does not significantly improve the results of intraventricular admittance measurements captured using the RV tripolar configuration in canine subjects.

3.3.4. Statistical Analysis

The 3 SV measurements (ADSV, CDSV, and 2D-TTE Echo) were evaluated against the hypothesis using a paired T-Test. Since, the ground truth for the study was not found to be accurate, T-Test hypothesis testing was the best option for statistical evaluation. A paired T-Test was selected because the evaluation was performed on paired data collected for each subject individually. ADSV and CDSV rejected the null hypothesis ($p < 0.05$) in all 5 of the subjects. The echo results accepted the null hypothesis ($p > 0.05$) did not show significance for any subject; further supporting the need for an improved ground truth in subsequent studies. The p-values of the paired T-Tests for each of the subjects are provided in Table 1.

Table 1. ADSV, CDSV, and 2D-TTE SV Paired T-Test p-values

Subject	ADSV (Paired T-Test)	CDSV (Paired T-Test)	ECHO (Paired T-Test)
Canine 1	0.0024	0.0005	0.6349
Canine 2	0.0200	0.0131	0.9113
Canine 3	0.0065	0.0142	0.0985
Canine 4	0.0062	0.0037	0.3555
Canine 5	0.0278	0.0147	0.1181
Average	0.0126	0.0092	0.4236
Std. Dev.	0.0108	0.0066	0.3486

It is assumed that the null hypothesis should have been rejected in all 5 of the canine subjects. However, without an adequate ground truth indicator this assumption cannot be confirmed. The results from Table 1 show that CDSV had the highest statistical performance. However, overall the statistical results for CDSV were only marginally better than those of ADSV.

3.4. DISCUSSION

The acute right atrial pacing experiment lacked an adequate ground truth and did not record an adequate amount of data during each part of the protocol.

2D-TTE data analyzed using Simpson's method is not an effective way to measure LV SV in canine subjects. After collaboration with 2D-TTE canine imaging specialist, Sonya Gordon DVM, 2D-TTE left ventricular outflow tract (LVOT) aortic velocity time integral (VTI) was identified as a more effective measure of LV SV. Unlike Simpson's method for estimating ventricular SV from 2D-TTE images, LVOT VTI measures the instantaneous velocity of blood moving through the aortic outflow tract rather than calculating volumes from end-diastolic and end-systolic 2D-TTE chamber images. To make the measurement, the cross-sectional area of the aorta is first measured with a standard 2D-TTE image. Pulsed wave Doppler is then used throughout the experiment to measure the instantaneous velocity of blood flowing through the aortic outflow tract. The blood velocity is then multiplied by the cross-sectional area of the aorta to obtain a flow estimate. SV is then calculated by integrating the flow over a single cardiac cycle.

In addition to LVOT VTI, a second ground truth for arterial pressure should be added to better monitor cardiac hemodynamics. An arterial pressure catheter is a reliable way to measure instantaneous arterial pressure. The arterial pressure signal can be used to track important hemodynamic markers such as pulse pressure (PP) and mean arterial pressure (MAP). PP is a peak to peak measurement of an arterial pressure signal. MAP is the mean value of an arterial pressure signal.

The amount of data recorded during each part of the protocol (10s) was insufficient to properly assess the effects of respiration on the admittance signal. A 10 second recording is only long enough to capture approximately 2 respiratory cycles. The Fourier filtering methods presented in Chapter 2 can be used effectively with 10 seconds of data provided

the correct windowing function is used. However, it would be ideal to have a larger data window. A 30 second recording allows for the flexibility to analyze admittance signals with a range of window sizes (10 s -25 s).

4. Chapter 4: Congestive Heart Failure Arrhythmia Study

4.1. SUMMARY

Methods and Results: N=8 canine subjects were implanted with a pacemaker lead in the right atrium (RA) and an ICD shocking lead in the right ventricle (RV). Congestive heart failure (CHF) was induced by rapid RV pacing for 3 ± 1 weeks and monitored by weekly 2-dimensional transthoracic echocardiography (2D-TTE). After the induction of CHF, an arrhythmia protocol was performed. For each subject, atrial tachycardia (AT), atrial fibrillation (AF), ventricular tachycardia (VT), and ventricular fibrillation (VF) were induced. During each arrhythmia, the following measurements were recorded: arterial pressure, 2D-TTE left ventricular outflow tract (LVOT) velocity time integral (VTI), RA IEGM, RV IEGM, and ADSV/CDSV. Arterial pulse pressure (PP) and LVOT VTI were used to assess changes in SV during the arrhythmias. IEGM was recorded to evaluate commercial ICD arrhythmia discrimination algorithms using an arrhythmia playback system post hoc.

4.2. METHODS

4.2.1. Study Overview

The study was designed to evaluate the ADSV/CDSV method in a large animal CHF model during atrial and ventricular arrhythmias. The study was performed using N=8 canine subjects. Subjects were first implanted with a RA pacing lead and a RV ICD shocking lead. The leads were given 4 ± 1 weeks to scar-in. After the scar-in period, subjects were implanted with a single chamber pacemaker that interfaced to the RV lead. CHF was induced by rapid ventricular pacing at 220 beats per minute (BPM) for 3 ± 1

weeks and monitored by weekly 2D-TTE. After sufficient levels of CHF were observed an arrhythmia protocol was performed. For each subject, atrial tachycardia (AT), atrial fibrillation (AF), ventricular tachycardia (VT), fast ventricular tachycardia (FVT), and ventricular fibrillation (VF) were induced or simulated. During each arrhythmia, the following measurements were recorded: arterial pressure, 2D-TTE left ventricular outflow tract (LVOT) velocity time integral (VTI), RA intracardiac electrogram (IEGM), RV IEGM, and intraventricular admittance (ADSV/CDSV). Arterial pressure and LVOT VTI were used to assess changes in stroke volume (SV). IEGM was recorded to evaluate commercial ICD arrhythmia discrimination algorithms using an arrhythmia playback system post hoc. The ADSV/CDSV method was evaluated against SV calculated from LVOT VTI (LVOT VTI SV) and arterial pulse pressure (PP). CDSV was found to outperform ADSV. CDSV was then evaluated for its ability to determine the hemodynamic stability of subjects during the induced arrhythmias.

4.2.2. Species Selection & HF Model

Most patients implanted with an ICD as a prevention for sudden cardiac death have heart failure with reduced ejection fraction (HFrEF) with a left ventricular ejection fraction (LVEF) < 35% [32]. There are several large animal HF models. For this study, a dilated cardiomyopathy (DCM) model was sought. DCM is defined by cardiac remodeling wherein dilation and wall thinning of the LV are observed in addition to a reduction in LVEF. Chronic rapid ventricular pacing is a well-studied model for inducing DCM [33] and has been used successfully in a canine model. The canine subjects used in the study were mongrel adult females with an age of 2.5 ± 0.9 years and a weight of 24.2 ± 3.8 kg. The characteristics for the subjects used in this study are provided in Table 2.

Table 2. Subject Characteristics

Subject	Age (Years)	Weight (kg)
Canine 1	1.80	18.60
Canine 2	2.00	28.12
Canine 3	1.80	27.67
Canine 4	4.50	27.67
Canine 5	1.80	26.76
Canine 6	2.60	20.86
Canine 7	2.70	20.40
Canine 8	2.60	23.59
Average	2.48	24.21
Std. Dev.	0.85	3.84

4.2.3. 2D-TTE Echo Views

All 2D-TTE measurements were acquired using a Philips iE33 ultrasound machine with a medium frequency transducer (Philips S5-1). To track the progression of CHF, weekly exams were performed with animals fully awake and standing with pacemakers programmed temporarily off. The weekly US exam protocol included short axis, long axis, and apical views that were analyzed to determine LV internal diameter (LVID), LV wall thickness, and fractional shortening (FS). All reported values for individual subjects are the mean of at least 3 measurements.

To measure LV SV during all surgical procedures, a pulsed wave Doppler measurement of the left ventricular outflow tract (LVOT) velocity time integral (VTI) was taken from an apical five-chamber view. This view was acquired with the animal lying left-side-down on the surgical table.

Transducer position, angle, and orientation plane for all 2D-TTE views were executed as per recommended canine echocardiography procedures [34].

4.2.4. Study Protocols

The study protocol included the following 3 surgical procedures: lead implant, pacemaker implant, and CHF arrhythmia protocol. The first two surgeries were sterile recovery procedures. Between surgeries 1 and 2, the leads were given 4 ± 1 weeks to scar-in. Between surgeries 2 and 3, subjects were induced into CHF by rapid right ventricular pacing.

All experiments were approved by the Institute for Animal Care and Use Committee at the University of Texas Health Science Center at San Antonio. The following preparation was performed for all surgical procedures. A percutaneous catheter was placed in a peripheral vein (cephalic) for anesthesia induction and fluid administration. Anesthesia was induced with 2-6 mg/kg Propofol IV (given to effect) followed by placement of an appropriately sized endotracheal tube. Anesthesia was then maintained on 1-4% Isoflurane in 100% Oxygen at 1-3 liters/min. The animal was placed on top of a warming pad on a surgical table followed by placement of temperature, heart rate, respiratory rate, EtCO2 (spell this one out the first time it is used) and ECG monitors. Lactated Ringer's solution (LRS) fluids were infused through the cephalic catheter at 10ml/kg/hr for the first hour then decreased to 3-5ml/kg/hr for the continuation of the surgery. A urinary catheter was placed to ensure the animal could relieve itself. A percutaneous pressure catheter was introduced into the left femoral artery and advanced into the descending aorta under fluoroscopy. A pacing catheter was introduced into the right femoral vein and advanced into the RA under fluoroscopy.

In the lead implant surgery canines were outfitted with a St. Jude Medical (SJM) active fixation bipolar RA pacing lead (Model 2088TC) and a SJM single coil RV ICD shocking lead (Model 7122). Leads were introduced into the heart through sheaths in the right jugular vein and placed into the heart under fluoroscopic guidance. At the time of

implant, an abridged RA pacing protocol was executed to confirm that ADSV/CDSV was sensitive to changes in SV.

After the lead implant surgery, leads were given 4 ± 1 weeks to scar-in. During the scar-in period, fibrotic tissue forms around the leads which reduces lead motion and results in an improved ADSV/CDSV measurement.

In the pacemaker implant surgery, a SJM single chamber pacemaker was placed in a subcutaneous pocket on the right side of the neck and attached to the IS-1 bifurcation of the RV lead. During the pacemaker implant procedure, an RV pacing protocol was executed to further validate the accuracy of ADSV/CDSV in healthy canine subjects with scarred-in leads.

After the pacemaker implant surgery, CHF was induced by rapid RV pacing. Subjects were monitored by weekly 2D-TTE during CHF induction. The LV dilation endpoint was defined as an increase from baseline for LV internal diameter (LVID) of approximately 30% [35]. The LV cardiac function endpoint was defined as a decrease from baseline for LV fractional shortening (FS) of 60% of baseline [36]. To acclimate the subjects, rapid RV pacing was started at a rate of 150 BPM for 2 days, then increased to 170 BPM for 5 days, and finally increased to 220 BPM and sustained. All 2D-TTE measurements were acquired with the animal awake and standing with pacemakers programmed off for the duration of the exam. The CHF endpoints for each subject are provided in Table 3.

Table 3. CHF Endpoints Table

	LVID			FS			LV Wall Thickness		
Subject	**PRE HF (cm)**	**POST HF (cm)**	**Change (%)**	**PRE HF (%)**	**POST HF (%)**	**Change (%)**	**PRE HF (cm)**	**POST HF (cm)**	**Change (%)**
Canine 1	3.76	4.26	13.30	46.37	17.77	-61.68	1.03	0.69	-33.01
Canine 2	3.60	5.13	42.50	40.00	13.47	-66.33	0.98	0.92	-6.12
Canine 3	4.31	5.53	28.31	31.00	18.27	-41.06	0.93	0.88	-5.38
Canine 4	4.46	5.05	13.23	39.70	10.73	-72.97	1.05	1.00	-4.76
Canine 5	3.70	4.22	14.05	30.20	17.57	-41.82	0.90	0.92	2.22
Canine 6	3.37	4.18	24.04	47.40	16.23	-65.76	1.06	0.77	-27.36
Canine 7	3.54	4.45	25.71	33.10	11.37	-65.65	1.00	0.79	-21.00
Canine 8	4.15	4.57	10.12	31.83	10.64	-66.57	0.93	0.75	-19.35
Average	3.86	4.67	21.41	37.45	14.51	-60.23	0.99	0.84	-14.35
Std. Dev.	0.40	0.50	10.90	6.92	3.32	12.00	0.06	0.11	12.54

In the CHF arrhythmia protocol, AT, AF, VT, FVT, and VF were induced or simulated. Baseline measurements were collected for arterial pressure, 2D-TTE LVOT VTI, ADSV/CDSV, and IEGM. These measurements were also collected during each arrhythmia.

A pacing catheter was placed in the RA to simulate atrial arrhythmias. AT was simulated by rapidly pacing the RA. Inter-subject variations in atrioventricular (AV) node block prevented the same pacing rate from being used across all subjects. For each subject, the maximal RA pacing rate with 1:1 conduction was used. This resulted in a rate of 167 ± 33 BPM across subjects. AF was simulated by pacing the RA with a semi-randomized pulse train comprised of the following 5 simultaneous pulse trains: 80 BPM, 125 BPM, 160 BPM, 95 BPM, and 170 BPM. The simultaneous pulse trains cause randomized intermittent RA conduction and randomized intermittent AV node conduction. The result is a variable RV contraction rate near the rate identified during AT with rapid and

randomized RA contractions. IEGM and arterial pressure signals collected during the simulation were consistent with signals observed during natural and sustained AF.

After the completion of the atrial arrhythmia simulations, the pacing catheter was advanced into the RV under fluoroscopic guidance and baseline measurements were recollected. VT was simulated by rapidly pacing the RV at 200 BPM. FVT was simulated by rapidly pacing the RV at 250 BPM. Lastly, VF was induced using the SJM ICD DC Fibber™ function. The DC Fibber™ function stimulates the heart with a long duration DC pulse.

4.2.4.1. Lead Implant Protocol

See Appendix A. for complete Lead Implant protocol.

4.2.4.2. Pacemaker Implant Protocol

See Appendix B. for complete Pacemaker Implant protocol.

4.2.4.3. Overdrive Pacing Protocol

See Appendix C. for complete Overdrive Pacing protocol.

4.2.4.4. CHF Arrhythmia Protocol

See Appendix D. for complete CHF Arrhythmia protocol.

4.2.5. Data Analysis and Assumptions

ADSV/CDSV data was correlated with both LVOT VTI SV and PP to evaluate SV accuracy, and was compared with MAP to assess performance in classifying hemodynamic stability.

The results from the ADSV/CDSV method are then calibrated into mL, which is performed using a single point calibration to a baseline LVOT VTI SV measurement.

LVOT VTI SV and PP were used to assess the accuracy of the ADSV/CDSV method. LVOT VTI SV serves as a direct measure of LV SV. Despite the nonlinear relationship between SV and arterial PP, arterial PP can be used to assess general trends in SV [37]. For this study, LVOT VTI SV was the primary measurement for which the ADSV/CDSV method was evaluated against. PP was used as an additional point of comparison to detect irregularities in LVOT VTI SV measurements.

4.3. RESULTS

4.3.1. ADSV, CDSV, PP, and LVOT VTI SV

The ADSV and CDSV results were evaluated against LVOT VTI SV and arterial PP for each subject. CDSV, on average, had a strong positive correlation between LVOT VTI SV ($R^2 = 0.73 \pm 0.21$) and arterial PP ($R^2 = 0.84 \pm 0.15$). ADSV, on average, had a lower positive correlation between LVOT VTI SV ($R^2 = 0.62 \pm 0.19$) and arterial PP ($R^2 = 0.71 \pm 0.19$) when compared to CDSV. The CDSV correlation results for individual subjects are provided in Table 4. The ADSV correlation results for individual subjects are provided in Table 5.

Table 4. CDSV Statics for Individual Subjects

Subject	LVOT VTI SV (R^2)	Arterial PP (R^2)
Canine 1	0.90	0.95
Canine 2	0.76	0.92
Canine 3	0.91	0.92
Canine 4	0.38	0.67
Canine 5	0.61	0.58
Canine 6	0.50	0.77
Canine 7	0.91	1.00
Canine 8	0.87	0.94
Average	0.73	0.84
Std. Dev.	0.21	0.15

Table 5. ADSV Statics for Individual Subjects

Subject	LVOT VTI SV (R^2)	Arterial PP (R^2)
Canine 1	0.78	0.84
Canine 2	0.79	0.91
Canine 3	0.52	0.45
Canine 4	0.28	0.54
Canine 5	0.55	0.66
Canine 6	0.56	0.76
Canine 7	0.88	0.96
Canine 8	0.60	0.53
Average	0.62	0.71
Std. Dev.	0.19	0.19

The lower correlation values obtained using the ADSV method were the results of large offsets between ADSV and LVOT VTI SV/PP collected during the VT and FVT arrhythmia simulations. In the Acute Atrial Pacing study presented in Chapter 3, CDSV marginally out performed ADSV. In the CHF arrhythmia study CDSV dramatically

outperformed ADSV. This difference may be due the addition of a pacing catheter in the RV of the heart, which was used to simulate ventricular arrhythmias. The pacing catheter influences the electric field induced by the RV shocking lead. Additionally, it can alter the motion of the RV shocking lead, which can influence the admittance measurement. It is equally probable that the rapid turbulent motion induced in the ventricle during the VT and FVT simulations causes a motion artifact in the admittance phase measurement. Regardless of these possible explanations, CDSV was found to outperform ADSV. For this reason, all further results will be presented in regard to CDSV. ADSV will not be used for arrhythmia discrimination.

The complete CDSV, PP, and LVOT VTI results for canines 1-8 are provided in Figures 38-45, respectively. For all of the subjects the results for BL, AT, AF, VT, FVT, and VF are provided. BL indicates baseline, AT indicates atrial tachycardia, AF indicates atrial fibrillation, VT indicates ventricular tachycardia, FVT indicates fast ventricular tachycardia, and VF indicates ventricular fibrillation. VTI SV indicates stroke volume calculated from left ventricular outflow tract velocity time integral. PP indicates pulse pressure. CDSV indicates conductance derived stroke volume. BPM indicates heart rate in beats per minute calculated from the PP signal. PP results are associated with the y-axis on the right. CDSV and VTI SV results are associated with the y-axis on the left.

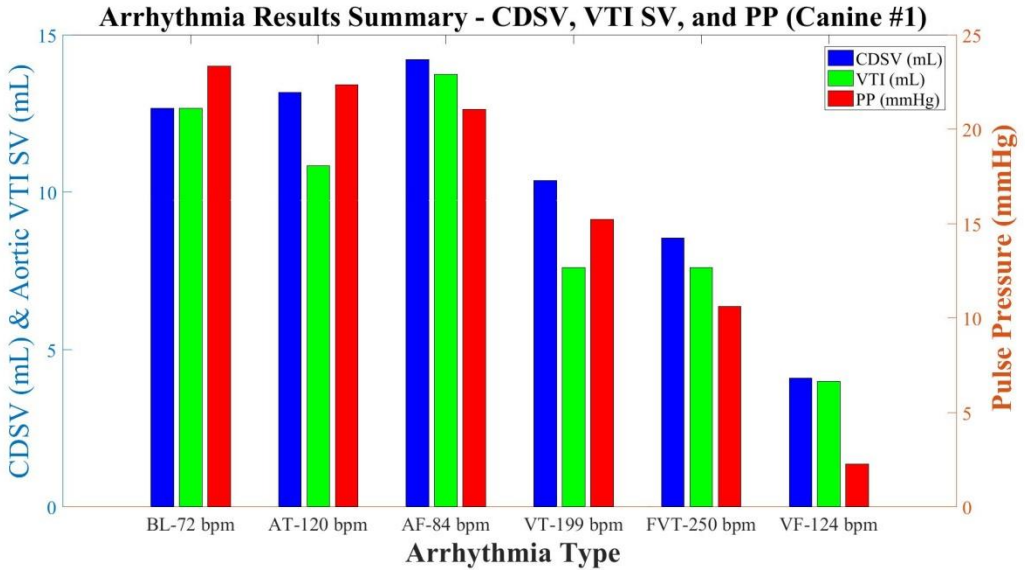

Figure 38. Canine #1 CHF Arrhythmia CDSV, PP, and LVOT VTI Results

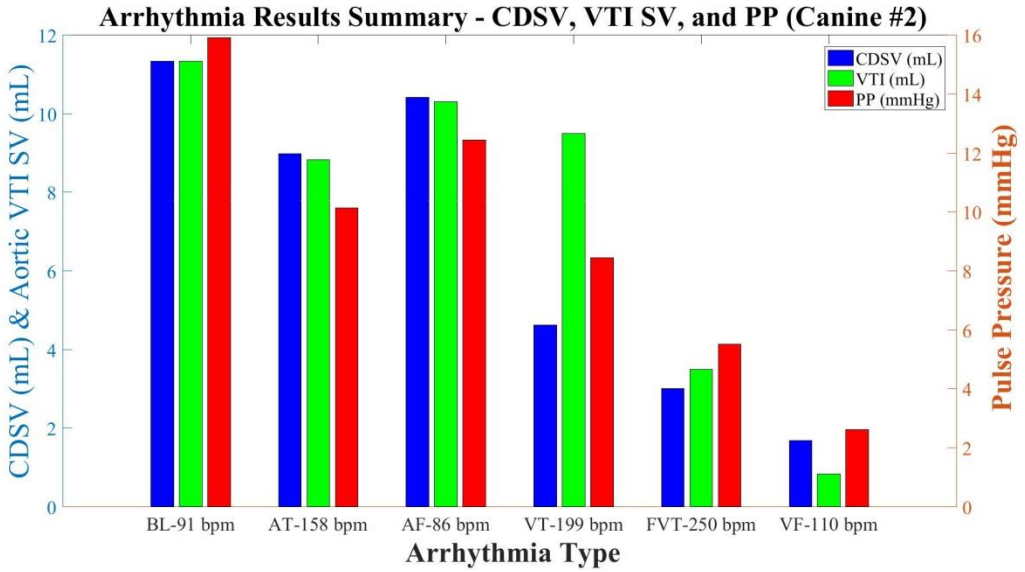

Figure 39. Canine #2 CHF Arrhythmia CDSV, PP, and LVOT VTI Results

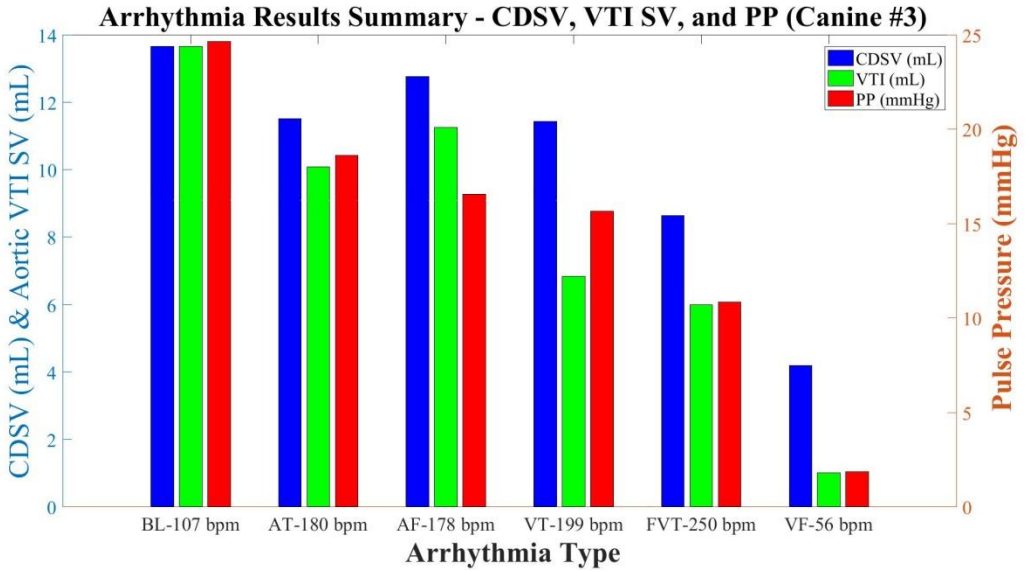

Figure 40. Canine #3 CHF Arrhythmia CDSV, PP, and LVOT VTI Results

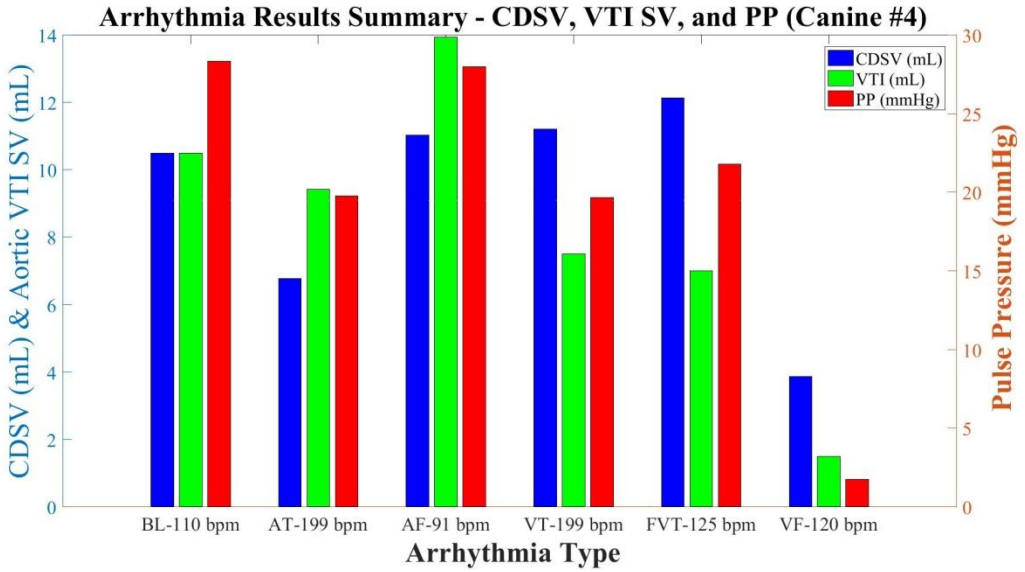

Figure 41. Canine #4 CHF Arrhythmia CDSV, PP, and LVOT VTI Results

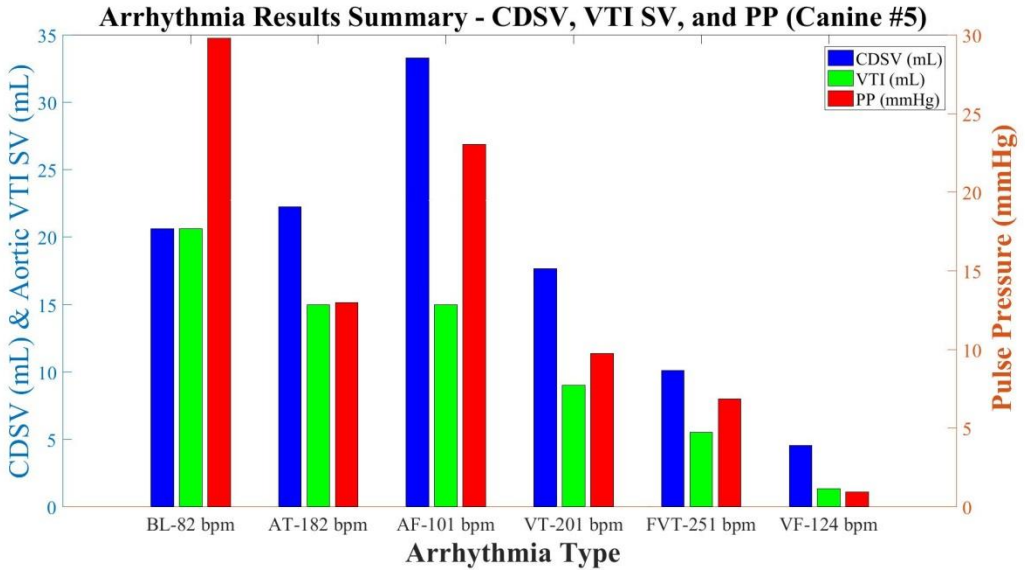

Figure 42. Canine #5 CHF Arrhythmia CDSV, PP, and LVOT VTI Results

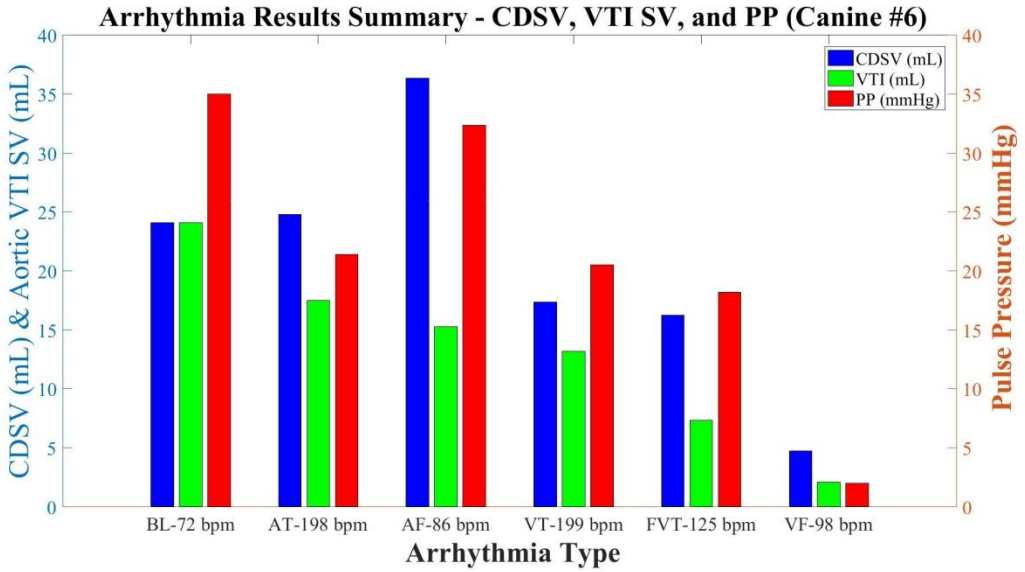

Figure 43. Canine #6 CHF Arrhythmia CDSV, PP, and LVOT VTI Results

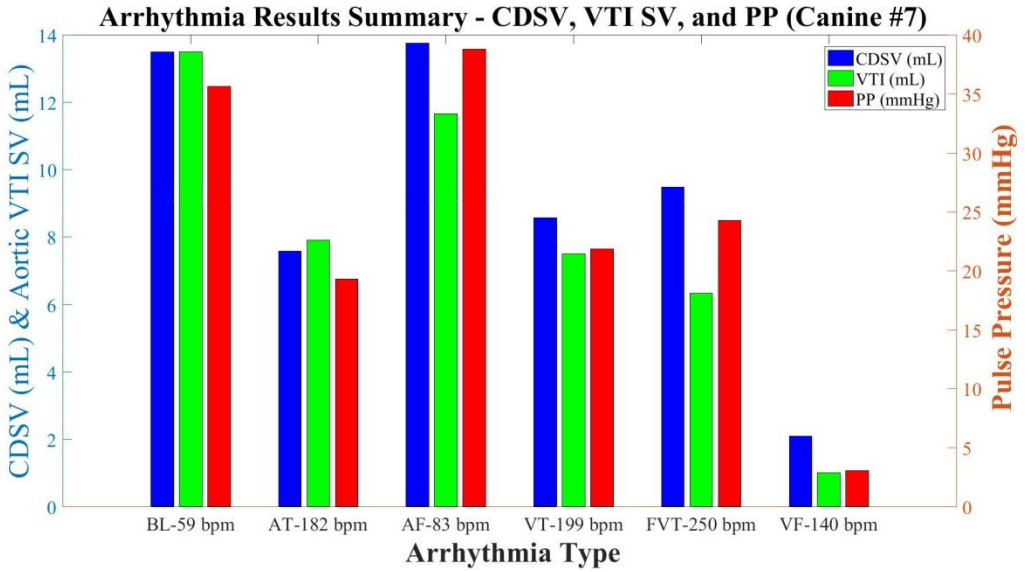

Figure 44. Canine #7 CHF Arrhythmia CDSV, PP, and LVOT VTI Results

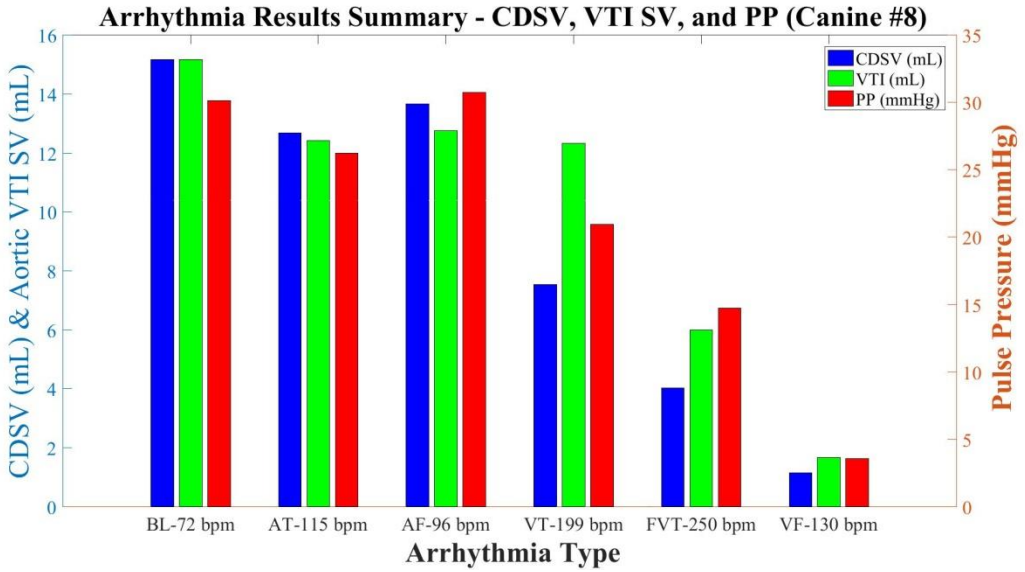

Figure 45. Canine #8 CHF Arrhythmia CDSV, PP, and LVOT VTI Results

In order to evaluate trends in the data across subjects, each subject's data was normalized to a percentage of baseline. The normalization was necessary because of inter-subject variations in baseline measurements for CDSV, LVOT VTI, and PP. CDSV, LVOT

VTI, and PP are presented in separate figure. In each figure, the data for N=8 canine subjects during BL, AT, AF, VT, FVT, and VF is provided. BL indicates baseline, AT indicates atrial tachycardia, AF indicates atrial fibrillation, VT indicates ventricular tachycardia, FVT indicates fast ventricular tachycardia, VF indicates ventricular fibrillation, and LVOT VTI SV indicates stroke volume calculated from left ventricular outflow tract velocity time integral. Each subject is presented as a separate line in the graph. The data is expressed as percent change from baseline. The LVOT VTI SV results are provided in Figure 46, the PP results are provided in Figure 47, and the CDSV results are provided in Figure 48.

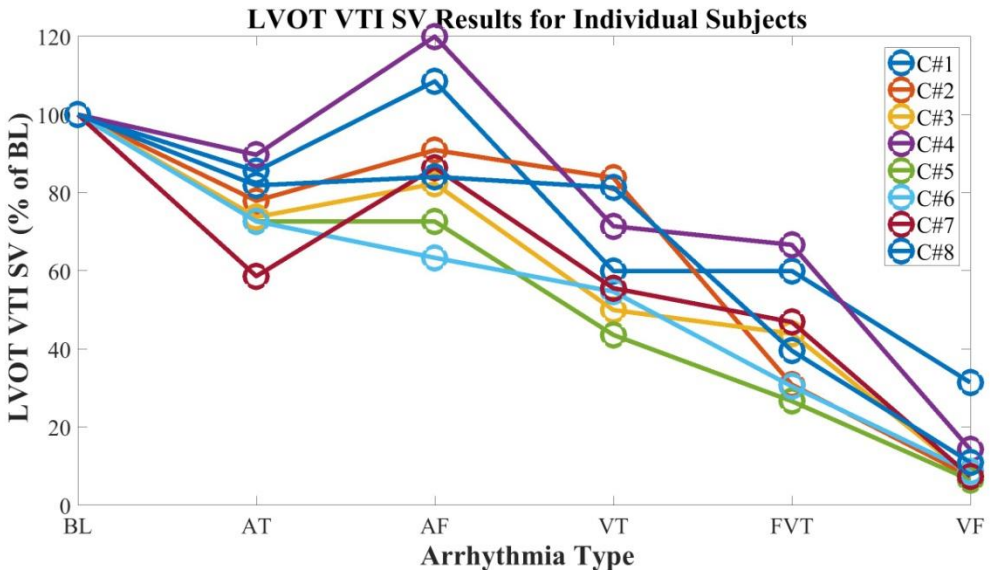

Figure 46. Baseline Normalized CHF Arrhythmia LVOT VTI Results

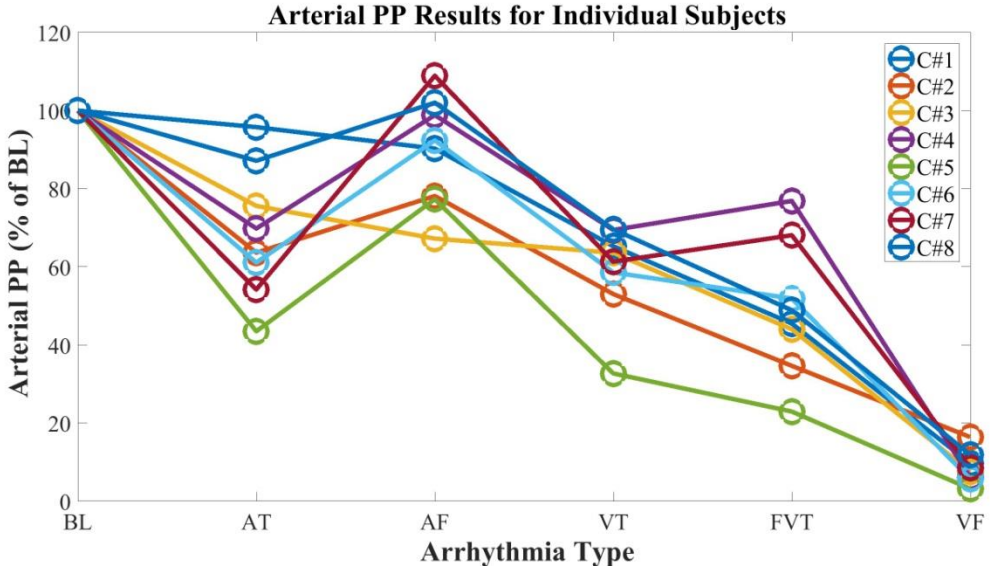

Figure 47. Baseline Normalized CHF Arrhythmia LVOT VTI Results

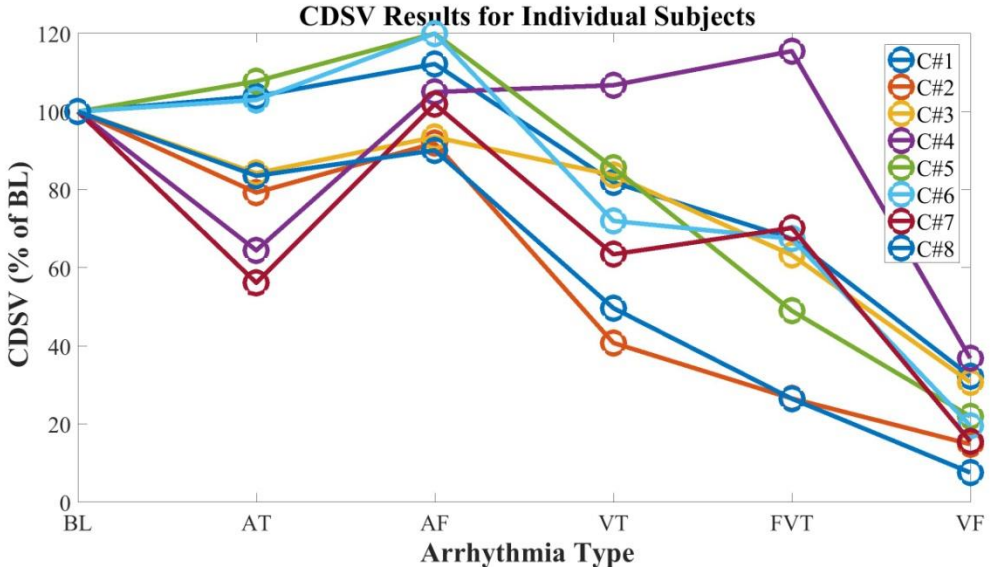

Figure 48. Baseline Normalized CHF Arrhythmia LVOT VTI Results

The CDSV data for canine #4 contained two outliers during VT and FVT. This behavior is reflected in the low R^2 values for canine #4 provided in Table 4. After review of the experimental records, it was identified that the subject's dobutamine drip was

changed from 12 mL/hr to 7 mL/hr 10 minutes before the VT and FVT arrhythmias were collected. The regular use of dobutamine in the CHF arrhythmia experiment started with canine #4. Prior to canine #4's experiment the mortality rate for subjects was >30 % during the CHF arrhythmia experiment. It was identified that the reduced cardiac function resulting from the DCM CHF model in combination with sedation was causing cardiogenic shock. The use of dobutamine for subjects with a systolic blood pressure <70 mmHg was added to the protocol immediately preceding the experiment for Canine #4. At that time, titration of the dobutamine drip was not fully developed. Going forward, the use of dobutamine was better controlled and there were no additional unintended mortalities or outlier datasets. It should be noted that canine #4 was hemodynamically stable during VT and FVT and exhibited an increase in MAP. Hence, the outliers in the CDSV measurement did not result in the hemodynamic misclassifications that will be presented in the following chapter.

The aggregate results for the subjects were analyzed as a percentage of baseline. The aggregate results were then calculated by averaging the percentage of baseline measurements for all 8 subjects. In the aggregate results, CDSV had a strong positive correlation with LVOT VTI SV (R^2 = 0.95) and arterial PP (R^2 = 0.96). The aggregate results are provided in Figure 49. Error bars are provided for ± 1 standard deviation.

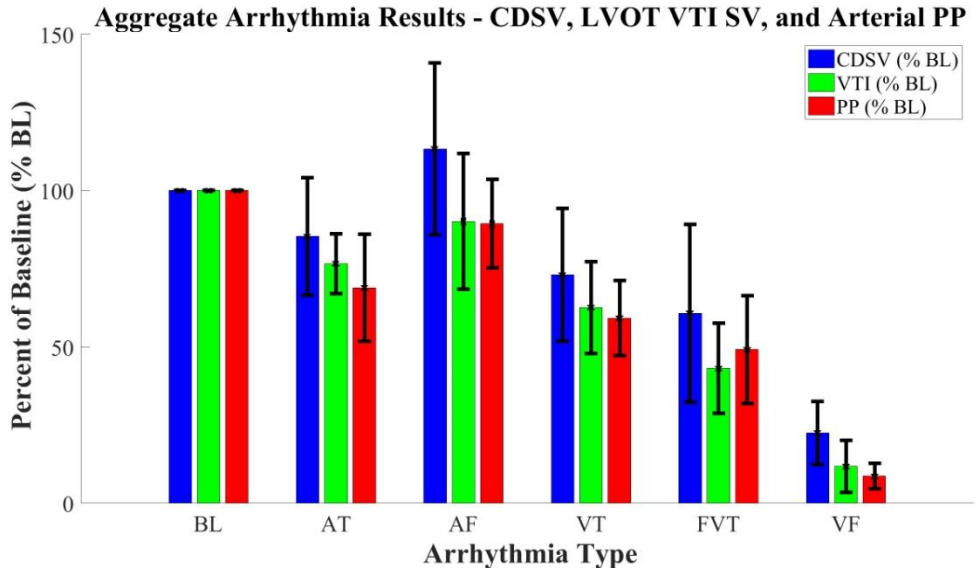

Figure 49. Aggregate CHF Arrhythmia CDSV, LVOT VTI Results

4.3.2. CDSV and MAP

Since MAP is used to directly determine hemodynamic stability, the CDSV results were also evaluated against MAP for each subject. CDSV, on average, had a strong positive correlation between MAP ($R^2 = 0.74 \pm 0.13$). The CDSV correlation results for individual subjects are provided in Table 6.

Table 6. CDSV & MAP Statics for Individual Subjects

Subject	MAP (R^2)
Canine 1	0.86
Canine 2	0.77
Canine 3	0.90
Canine 4	0.80
Canine 5	0.71
Canine 6	0.74
Canine 7	0.49
Canine 8	0.64
Average	0.74
Std. Dev.	0.13

The complete CDSV and MAP results for canines 1-8 are provided in Figures 50-57, respectively. For all of the subjects the results for BL, AT, AF, VT, FVT, and VF are provided. BL indicates baseline, AT indicates atrial tachycardia, AF indicates atrial fibrillation, VT indicates ventricular tachycardia, FVT indicates fast ventricular tachycardia, and VF indicates ventricular fibrillation. MAP indicates mean arterial pressure. CDSV indicates conductance derived stroke volume. BPM indicates heart rate in beats per minute calculated from the arterial pressure signal. MAP results are associated with the y-axis on the right. CDSV results are associated with the y-axis on the left.

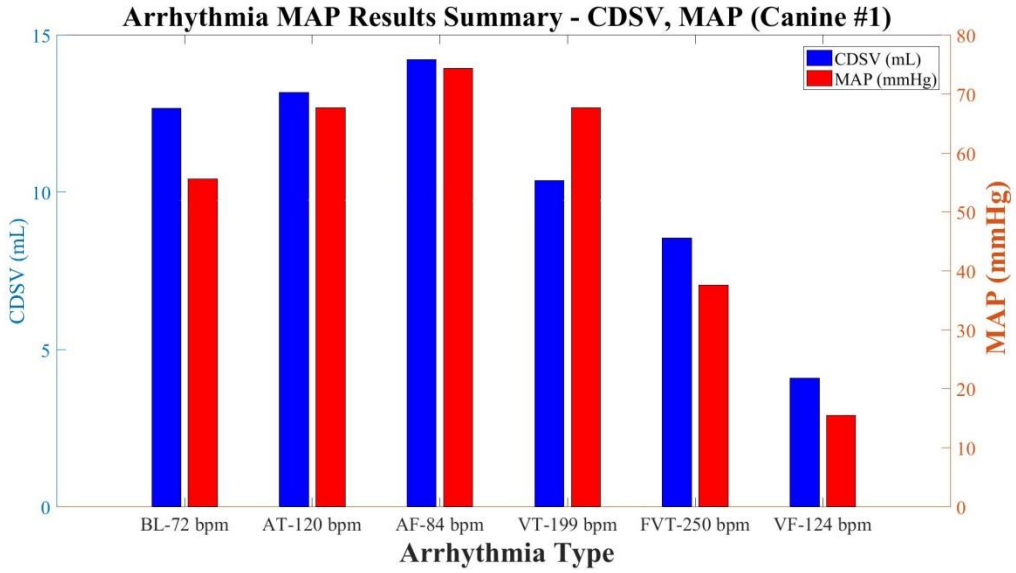

Figure 50. Canine #1 CHF Arrhythmia CDSV and MAP Results

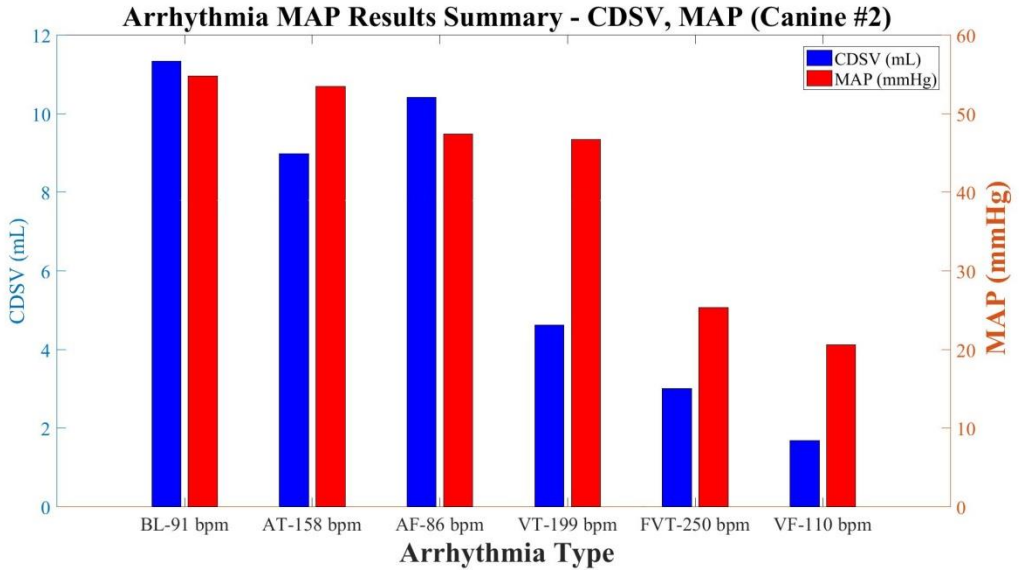

Figure 51. Canine #2 CHF Arrhythmia CDSV and MAP Results

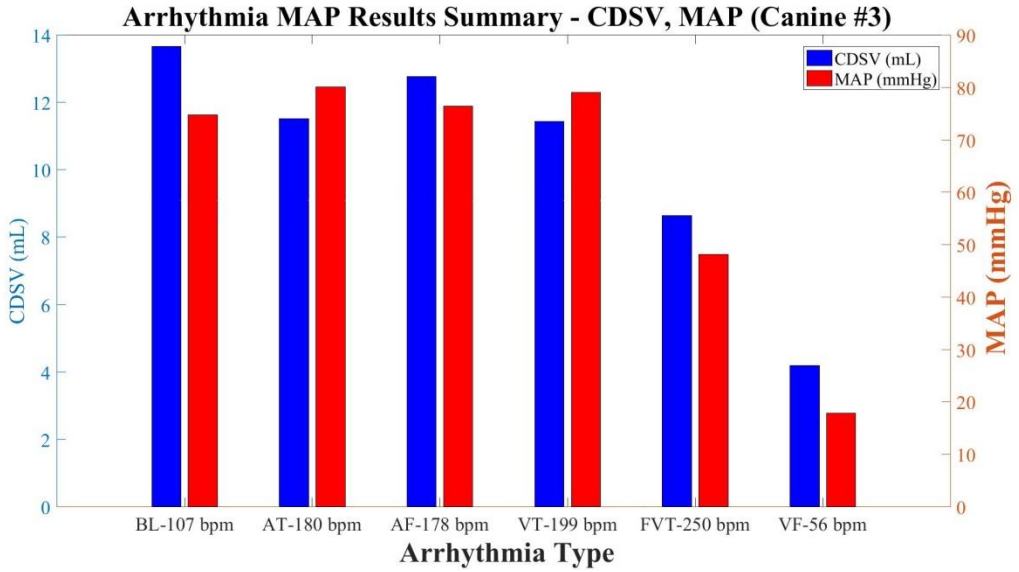

Figure 52. Canine #3 CHF Arrhythmia CDSV and MAP Results

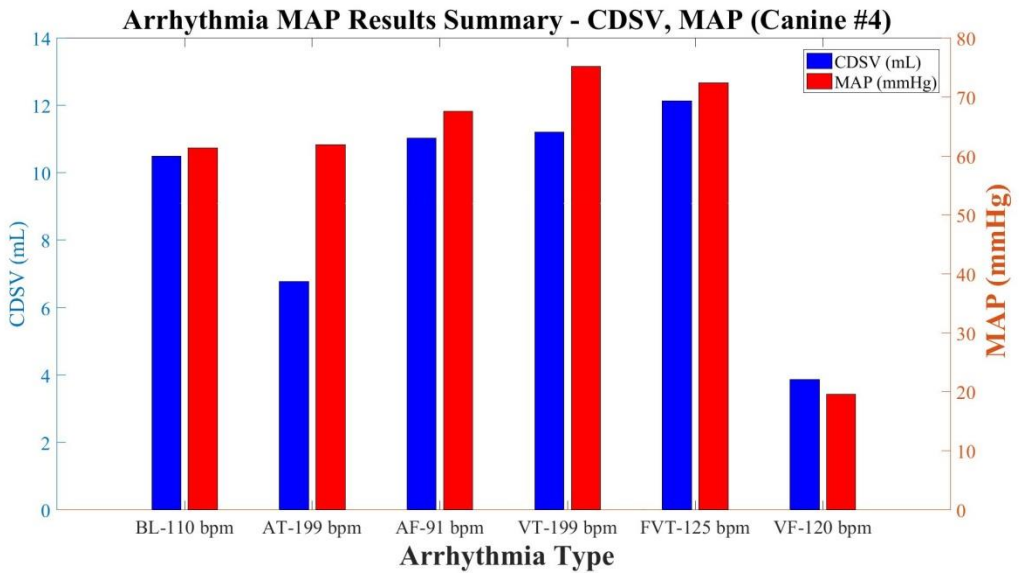

Figure 53. Canine #4 CHF Arrhythmia CDSV and MAP Results

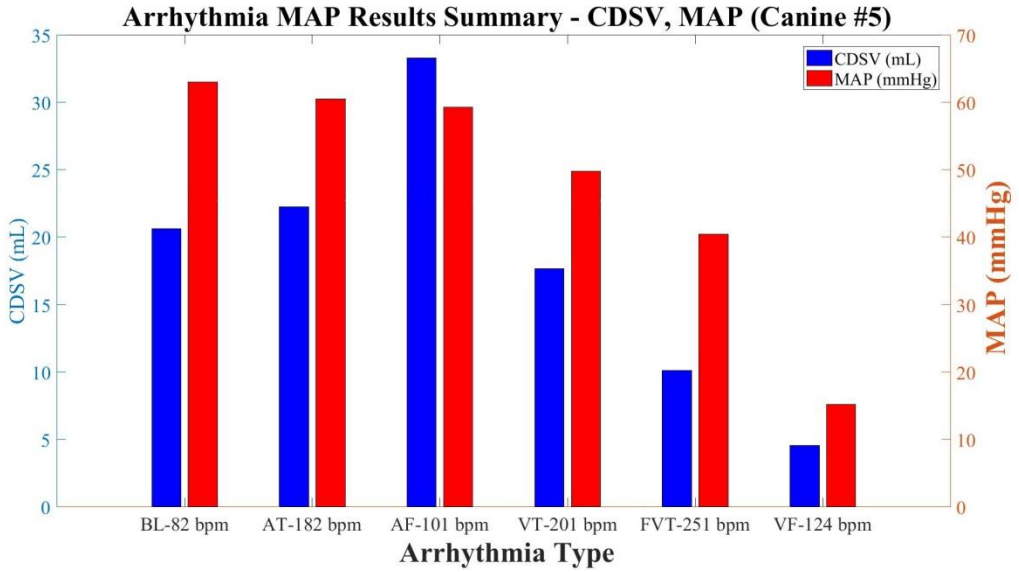

Figure 54. Canine #5 CHF Arrhythmia CDSV and MAP Results

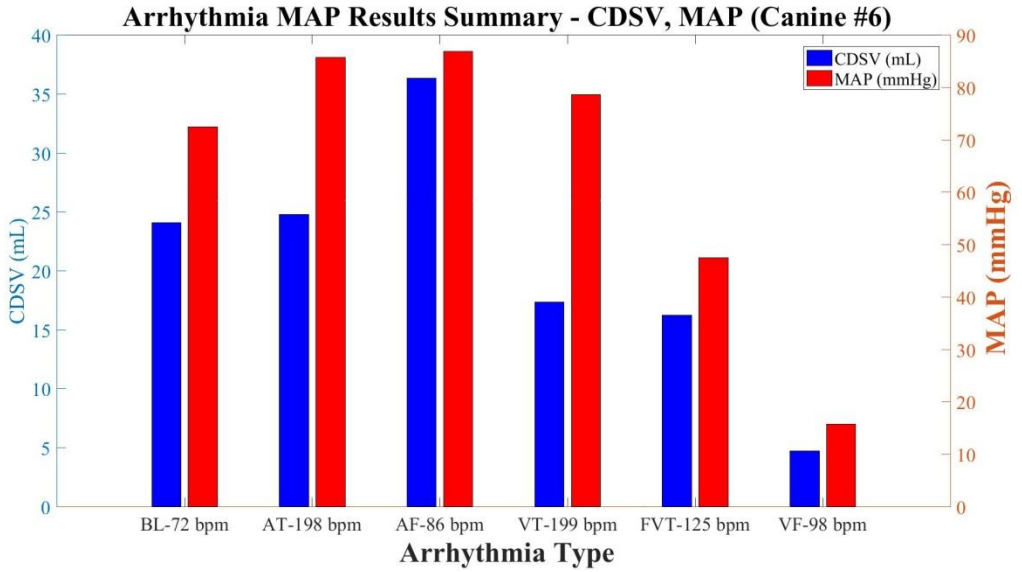

Figure 55. Canine #6 CHF Arrhythmia CDSV and MAP Results

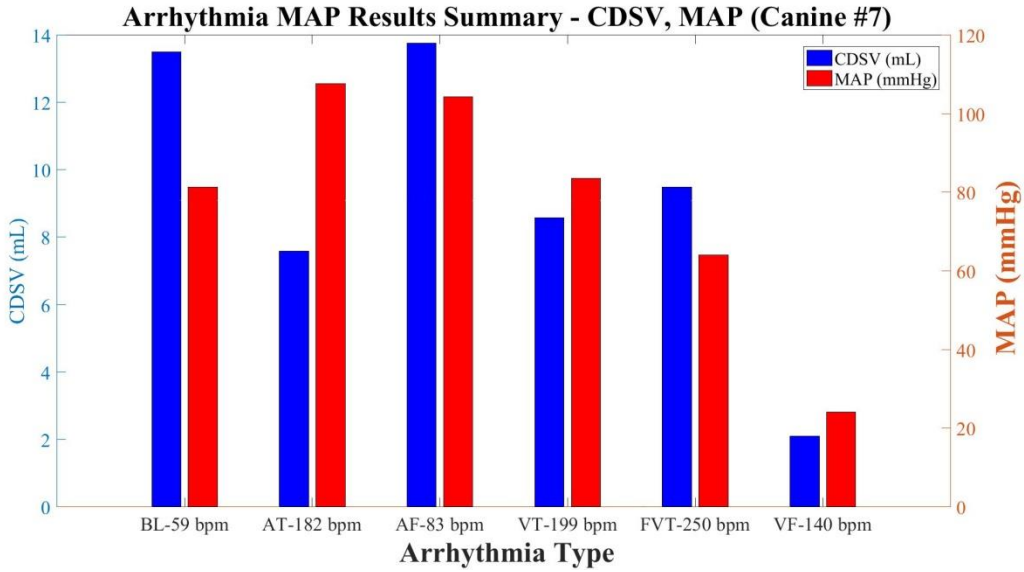

Figure 56. Canine #7 CHF Arrhythmia CDSV and MAP Results

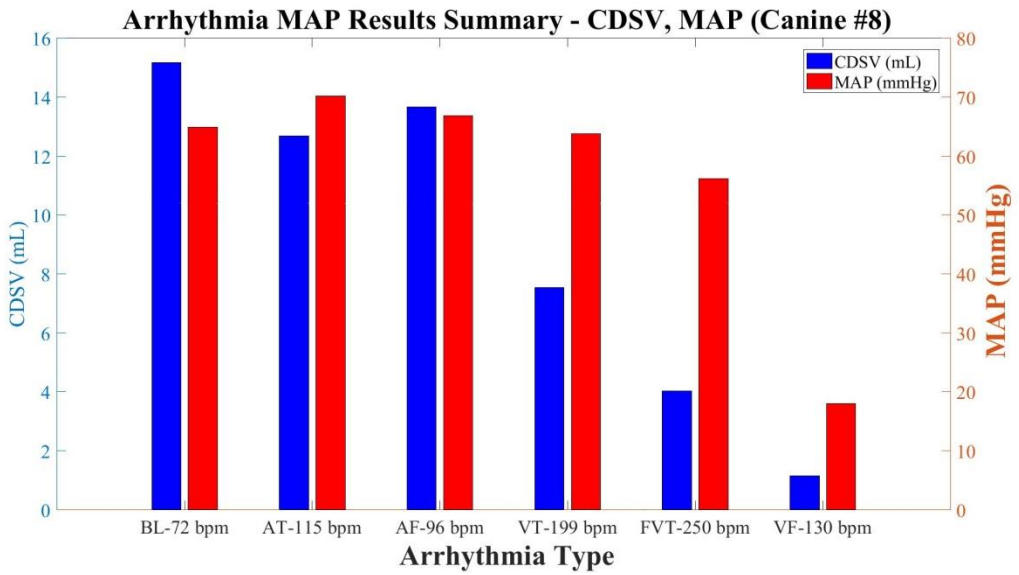

Figure 57. Canine #8 CHF Arrhythmia CDSV and MAP Results

Simularly to the previous section, each subjects MAP data was normalized as a percentage of baseline. The normalization was necessary because of inter-subject variations in baseline MAP measurements. The baseline normalized MAP data for all 8 subjects is provided in Figure 58.

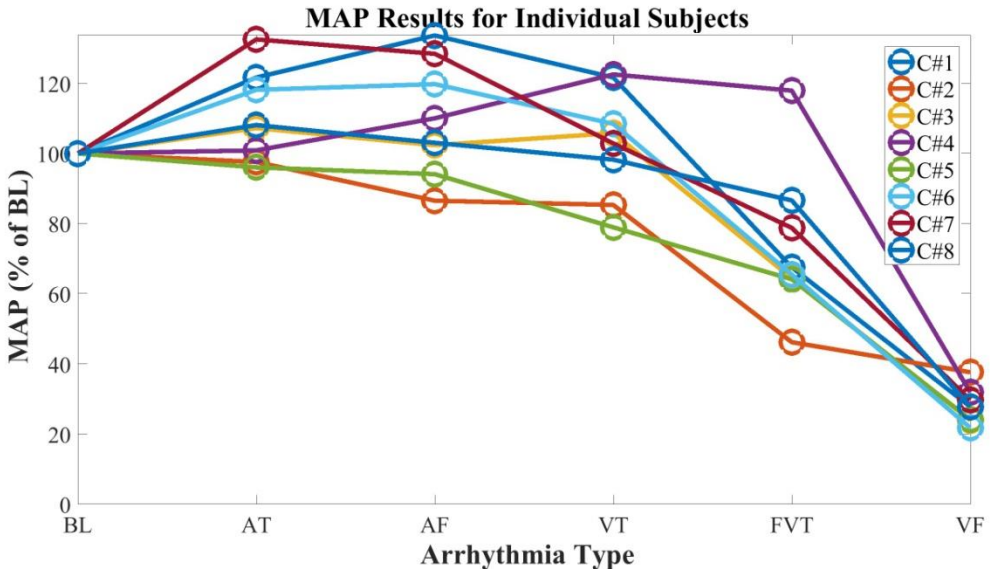

Figure 58. Baseline Normalized CHF Arrhythmia MAP Results

The aggregate results were then calculated by averaging the percentage of baseline measurements for all 8 subjects. In the aggregate results, CDSV had a strong positive correlation with MAP ($R^2 = 0.83$). The aggregate results are provided in Figure 59. Error bars are provided for ± 1 standard deviation.

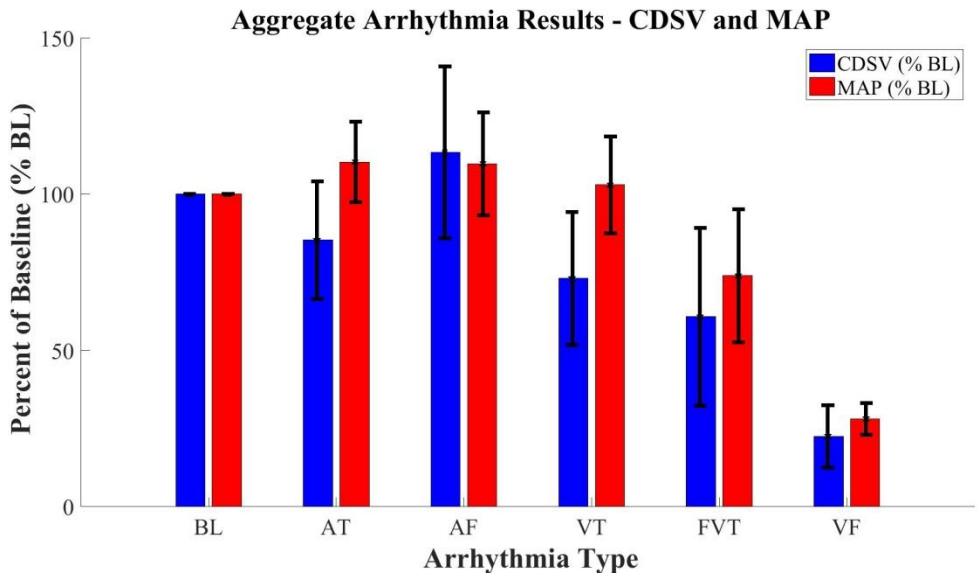

Figure 59. Aggregate CHF Arrhythmia CDSV and MAP Results

The ADSV/CDSV results were evaluated against LVOT VTI SV and arterial PP for each subject. CDSV, on average, had a strong positive correlation between LVOT VTI SV ($R^2 = 0.73 \pm 0.21$) and arterial PP ($R^2 = 0.84 \pm 0.14$). ADSV, on average, had a strong positive correlation between LVOT VTI SV ($R^2 = 0.62 \pm 0.19$) and arterial PP ($R^2 = 0.71 \pm 0.19$). Since CDSV significantly outperformed ADSV when compared to the SV ground truths of LVOT VTI SV and PP, all subsequent analysis is only reported for the CDSV results. CDSV was then evaluated for its ability to determine the hemodynamic stability of subjects during arrhythmias. The ground truth for hemodynamic stability was determined using MAP. In a set of N=40 arrhythmias, CDSV correctly classified the hemodynamic state for N=33 of the 40 arrhythmias. The hemodynamic classification information from CDSV was then used to improve the arrhythmia diagnoses of commercial ICD arrhythmia discrimination algorithms. For the St. Jude Medical ICD, N=12 of 40

arrhythmia classifications were improved by the CDSV hemodynamic classification information. For the Medtronic ICD, N=13 of 40 arrhythmia classifications were improved by the CDSV hemodynamic classification information.

In conclusion, CDSV was found to have significantly higher correlation with LVOT VTI SV and PP when compared to the ADSV method. The CDSV method strongly correlates with LVOT VTI SV and arterial PP in CHF canine subjects. The method provides a means to directly determine hemodynamic stability during atrial and ventricular arrhythmias. CDSV can be utilized as an additional ICD discriminator that withholds therapies based on hemodynamic stability. The CDSV discriminator can be used to reduce the number of inappropriate therapies during AF. Additionally, the discriminator can be used to establish distinct therapy zones for hemodynamically unstable VTs and hemodynamically stable VTs. In the stable VT zone, ICD shocks can be withheld in favor of less aggressive therapies such as anti-tachycardia pacing that decrease morbidity and mortality in patients. The addition of the CDSV hemodynamic discriminator has the potential to significantly improve the configuration and delivery of ICD therapies.

4.4. DISCUSSION

4.4.1. Motion Artifact

Intraventricular admittance measurements track changes in blood volume when an ideal electrode configuration is used. However, the tripolar RV lead configuration has the potential to track both blood volume and lead motion due to the non-uniform spatial sensitivity of the induced electric field [14]. To confirm that the RV lead configuration is primarily sensitive to blood volume and not lead motion, a post-mortem experiment was performed on N=6 canine subjects, whereby subjects were physically oscillated in a

sequence of rates and forces (slow soft, slow fast, hard slow, hard fast). The CDSV signal generated by the post-mortem motion experiment was 19.00 % ± 8.00 % of baseline. Considering the CDSV fibrillation threshold is 40 % of baseline, the motion contribution to the CDSV signal is tolerable.

4.4.2. Tricuspid Valve Regurgitation

Tricuspid valve regurgitation (TR) is a source of error in the ADSV/CDSV method. The ADSV/CDSV measurement is made in the RV of the heart and during normal cardiac function RV SV and LV SV are equivalent. In patients that exhibit TR, RV SV and LV SV are not necessarily equivalent. The improper function of the tricuspid valve allows blood to flow backwards during systole resulting in a loss of forward RV stroke volume. However, ADSV/CDSV detects both the forward and reverse stroke volume and increases in the presence of TR.

In this study, two sources of TR were identified. The first source is caused by fibrosis of the tricuspid valve, which results from chronic lead implantation [39]. Fibrotic tissue and tricuspid valve thickening were observed at necropsy for several of the subjects. The second source was a result of the DCM CHF model [40] with a loss of leaflet coaptation.

To quantify the degree of TR in subjects 2D-TTE was used. TR was semi-quantitatively measured using the proximal isovelocity surface area (PISA) method [41]. N=3 CHF arrhythmia subjects were evaluated for TR. 2 subjects exhibited a PISA radius from 0.6 cm - 0.9 cm which is consistent with moderate levels of TR. 1 subject had a PISA radius > 0.9 cm which indicates a severe level of TR. In the patient with severe levels of

TR, CDSV was found to overestimate LVOT VTI SV. Even in the presence of TR CDSV was able to track the hemodynamic parameters of PP and LVOT VTI SV.

5. Chapter 5: Hemodynamic Based ICD Discrimination Algorithm

5.1. MOTIVATION

In general, commercial ICD arrhythmia discrimination algorithms are largely rate based. While ICDs do contain several discriminators that are used to determine if the arrhythmia originates in the atrium or the ventricle, once the arrhythmia has been identified to originate in the ventricle the ICD shocking algorithms operate in a rate-based manner. Rate-based ICD shocking algorithms are most effective when tailored to the specific arrhythmias of a patient. While low rate VTs are not always hemodynamically unstable, the generalization cannot be applied to all patients. The same is true for hemodynamically stable high rate VTs. ICDs do enable physicians with the ability to configure rate thresholds for patients, but the correct settings can be hard to configure optimally on an individual basis and can only be fully utilized when the arrhythmia rate is known. However, many of these arrhythmias are hemodynamically stable, and if they could be treated with antitachycardia pacing (ATP)rather than defibrillation, there would be improved patient outcomes [20].

No matter how an ICD is configured, one can expect there to be misclassifications. The same statement can be made about CDSV hemodynamic classifications. It is reasonable to expect an algorithm that combines ICD IEGM classifications with CDSV hemodynamic classifications to perform better than either can do alone.

5.2. METHODS

5.2.1. ICD IEGM Playback

A benchtop system was built to “play back” IEGMs recorded during arrhythmias onto commercial ICDs (St. Jude CD2357-40C and Medtronic D264DRM). Three detection zones were programmed at 170-200 BPM for ventricular tachycardia monitoring, 200-240

BPM for ventricular tachycardia therapy, and >240 BPM for ventricular fibrillation therapy. Programmed rate settings were selected in consultation with three electrophysiologists and comply with recommended settings reported in clinical trials [17E][17H][42]. All available atrial discriminators were turned on per nominal settings and morphology templates were acquired using baseline IEGM recordings. Each thirty second recording was allowed to cycle for at least three minutes, or until the first therapy was delivered.

5.2.2. Hemodynamic Stability Assessment

The CDSV measurements for each subject during AT, AF, VT, FVT, and VF were classified as hemodynamically stable, hemodynamically unstable, or ventricular fibrillation. The ground truth for classification was based on MAP. Typically, a MAP <60 mmHg is used to define hemodynamic instability. For these subjects, baseline MAP was considerably low (66 ± 10 mmHg), so hemodynamic instability was defined as MAP <55 mmHg.

The CDSV classification problem was setup as a diagnostic test with 3 outcomes (hemodynamically stable, hemodynamically unstable, and ventricular fibrillation). Ventricular fibrillation is an important subclass of the hemodynamically unstable class due to its lethality. For this reason, it was included as a separate class of the diagnostic test. The optimal classification thresholds for the CDSV measurement were found using a receiver operator curve (ROC) [38]. The optimal CDSV thresholds for the 3 classifications were selected from the ROC by choosing the optimal point that contained no incorrectly withheld therapies (false negatives). This behavior is an important safety consideration as it ensures that the discrimination algorithm will be less likely to inappropriately withhold a therapy based on CDSV hemodynamic information.

5.3. RESULTS

5.3.1. Commercial ICD Discrimination Results

The Medtronic ICD correctly classified N=29 of 40 arrhythmias and the St. Jude ICD correctly classified N=31 of 40 arrhythmias. The St. Jude Medical playback results are provided in Table 7 and the Medtronic playback results are provided in Table 8. AF in Canine #4 was likely incorrectly classified because the rate was 240 BPM on average. Both misclassifications of AT by the Medtronic ICD were also due to high rates of 207 BPM (Canine #4) and 214 BPM (Canine #6), which were much higher on average compared to the AT rates induced in other subjects and were both above the VT threshold (200 BPM). Both devices also incorrectly classified all FVTs as VF. All FVTs were induced at a rate of 250 BPM, which exceeded the VF threshold (240 BPM). It should be noted that the medical community does not normally consider FVTs classified as VF a misclassification. ICDs are designed to classify all ventricular arrhythmias with rates above the fibrillation threshold (240 BPM) as VF.

5.3.1.1. St. Jude Medical ICD

Table 7. St. Jude Medical Therapy Performance

ST JUDE					
Subject	**AT**	**AF**	**VT**	**FVT**	**VF**
Canine 1	None	SVT	VT	VF	VF
Canine 2	None	None	VT	VF	VF
Canine 3	SVT	SVT	VT	VF	VF
Canine 4	SVT	VF	VT	VF	VF
Canine 5	SVT	None	VT	VF	VF
Canine 6	SVT	SVT	VT	VF	VF
Canine 7	SVT	None	VT	VF	VF
Canine 8	None	None	VT	VF	VF

Misclassifications are highlighted in red.

5.3.1.2. Medtronic ICD

Table 8. Medtronic ICD Arrhythmia Discrimination Results

MEDTRONIC					
Subject	**AT**	**AF**	**VT**	**FVT**	**VF**
Canine 1	None	SVT-AF	VT	VF	VF
Canine 2	None	None	VT	VF	VF
Canine 3	VT-Monitor	AT/AF	VT	VF	VF
Canine 4	VT	VF	VT	VF	VF
Canine 5	VT-Monitor	AT/AF	VT	VF	VF
Canine 6	VT	AT/AF	VT	VF	VF
Canine 7	VT-Monitor	AT/AF	VT	VF	VF
Canine 8	None	AT/AF	VT	VF	VF

Misclassifications are highlighted in red.

5.3.2. CDSV Hemodynamic Classification Performance

To accommodate hemodynamic classification using CDSV, the patients baseline MAP (MAP_{BL}) and baseline CDSV ($CDSV_{BL}$) measurements were utilized. These baseline measurements were used to determine the CDSV classification thresholds on a patient by patient basis. A patient who has a 60-mmHg MAP_{BL} would have an CDSV unstable classification threshold of 55/60 = 91.6%. A patient who has a 90-mmHg MAP_{BL} would have an CDSV unstable classification threshold of 55/90 = 61.1%. The general solution for the unstable classification threshold of a patient is $(CDSV / CDSV_{BL}) < 55/MAP_{BL}$. A separate CDSV VF classification threshold was defined as $(CDSV/CDSV_{BL}) < 25/MAP_{BL}$. The motivation behind this methodology is to account for the fact that a

patient with a more stable baseline blood pressure should be able to tolerate a larger drop in CDSV before being classified as hemodynamically unstable. In practice, the patients MAP_{BL} could be measured at the time of implant and the unstable MAP threshold of 55 mmHg could be adjusted by the physician based on patient characteristics such as health or high blood pressure. Using the above definitions, the CDSV measurements were able to correctly classify the hemodynamic state for N=33 of 40 arrhythmias and the results are provided in Table 9. Misclassifications were observed during AT, VT, and FVT. None of the misclassification resulted in an inappropriately withheld therapy (false negative). These misclassifications were likely the result of inter-subject variations in the relationship between MAP and SV. Since the ground truth for hemodynamic stability was based on MAP and not LVOT VTI SV the classification performance relies on an inherent correlation between SV and MAP.

Table 9. CDSV Hemodynamic Classification Results

	AT		AF		VT		FVT		VF	
Subject	**CDSV**	**MAP**	**CDSV**	**MAP**	**CDSV**	**MAP**	**CDSV**	**MAP**	**CDSV**	**MAP**
Canine 1	S	S	S	S	U	S	U	U	VF	U
Canine 2	U	U	U	U	U	U	U	U	VF	U
Canine 3	S	S	S	S	S	S	U	U	VF	U
Canine 4	U	S	S	S	S	S	S	S	VF	U
Canine 5	S	S	S	S	U	U	U	U	VF	U
Canine 6	S	S	S	S	U	S	U	U	VF	U
Canine 7	U	S	S	S	U	S	S	S	VF	U
Canine 8	S	S	S	S	U	S	VF	S	VF	U

Misclassifications are highlighted in red.

5.3.3. Combined Discrimination Algorithm

No matter how an ICD is configured, one can expect there to be misclassifications. The same statement can be made about CDSV hemodynamic classifications. It is reasonable to expect an algorithm that combines ICD IEGM classifications with CDSV hemodynamic classifications to perform better than either can do alone. Here is an example of how the two can be combined.

The primary purpose of the algorithm is to enable physicians with the ability to configure different therapies for hemodynamically unstable and hemodynamically stable ventricular tachycardias. The algorithm also improves the classification performance during atrial fibrillation and atrial tachycardia. The combined algorithm contains 3 therapy zones: stable VT, unstable VT, and VF. The zones are identified using a combination of the ICD IEGM classifications and the CDSV hemodynamic classifications. A summary of these classifications is provided in Table 10 and a block diagram outlining the decision tree for the algorithm is provided in Figure 60.

Table 10. ICD IEGM, CDSV Hemodynamic, and Combined Classifications

Classification Name	Classification Condition	Classification Description
ICD IEGM Classifications		
AF	ICD Atrial Discriminator	Atrial Fibrillation
AT	ICD Atrial Discriminator	Atrial Tachycardia
SVT	ICD Atrial Discriminator	Supraventricular Tachycardia
VT	RV Rate [200-240] BPM	Ventricular Tachycardia
VF	RV Rate >240 BPM	Ventricular Fibrillation
CDSV Hemodynamic Classifications		
STABLE	$(CDSV_U/CDSV_{BL}) \geq (55/MAP_{BL})$	Hemodynamically Stable
UNSTABLE	$(CDSV_U/CDSV_{BL}) < (55/MAP_{BL})$	Hemodynamically Unstable
VF	$(CDSV_{VF}/CDSV_{BL}) < (25/MAP_{BL})$	Severe Hemodynamic Instability
Combined ICD and CDSV Hemodynamic Classifications		
AF	ICD Atrial Discriminator	Atrial Fibrillation
AT	ICD Atrial Discriminator	Atrial Tachycardia
SVT	ICD Atrial Discriminator	Supraventricular Tachycardia
ST-VT	CDSV: STABLE, ICD: VT	Hemodynamically Stable VT
U-VT	CDSV: UNSTABLE ICD: VT	Hemodynamically Unstable VT
VF	CDSV: VF	Severe Hemodynamic Instability

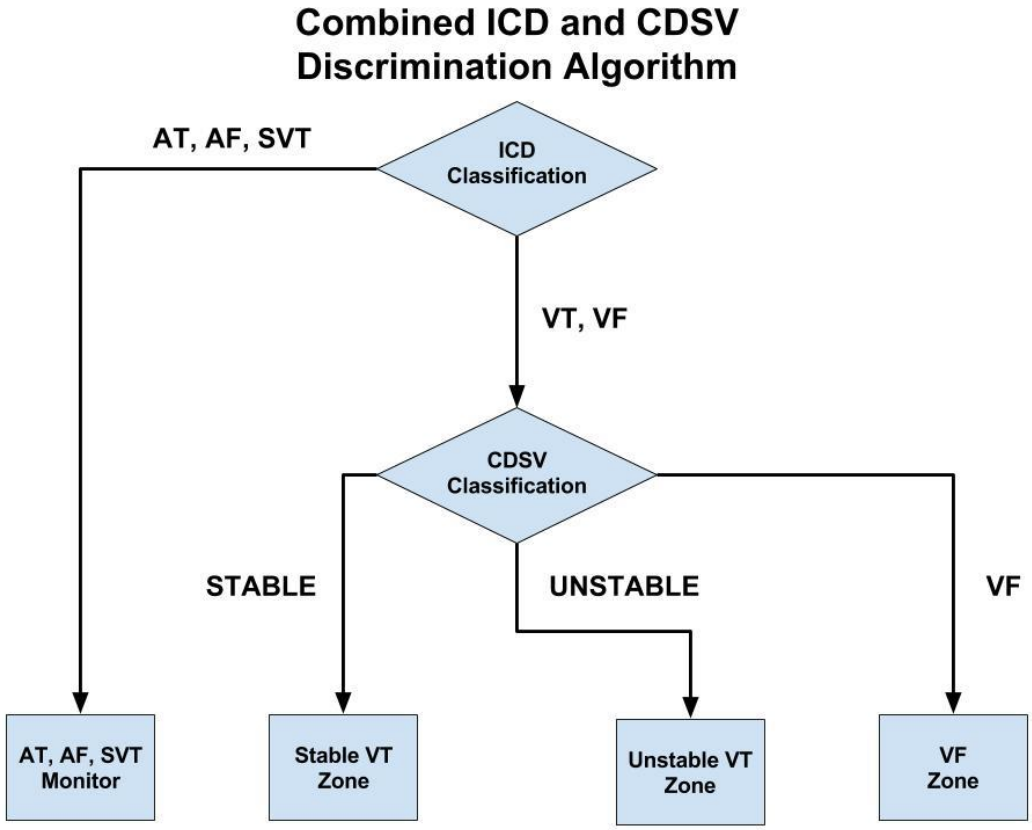

Figure 60. Combined ICD and CDSV Therapy Algorithm

An improvement to classification performance was defined as any classification that would allow for a less aggressive set of therapies to be used. The therapy classifications in ascending order of aggressiveness are assumed to be as follows: stable VT, unstable VT, and VF. None of the classifications resulted in a worse delivery of therapies when compared to the ICD IEGM only algorithms of SJM and Medtronic. For the SJM ICD, the combined discrimination algorithm improved the classification performance for N=10 of 40 arrhythmias. Only one of these improvements was for an AF arrhythmia that was incorrectly classified as VF. This was because the dataset for this study was limited and

only one such misclassification was observed. However, VT and FVT classifications were also improved. 2 VT classification were improved to stable VT. 2 FVT classifications were improved from VF to stable VT. 5 FVT classification were improved from VF to unstable VT. A complete summary of these results is provided in Table 11. For the Medtronic ICD, the combined discrimination algorithm improved the classification performance for N=11 of 40 arrhythmias. The improvements for the Medtronic ICD were identical to the SJM ICD with the addition of one improvement for an AT misclassified as VT. A complete summary of these results is provided in Table 12.

Table 11. Combined SJM and CDSV Therapy Performance

	AT		AF		VT		FVT		VF	
Subject	**S+C**	**MAP**	**S+C**	**MAP**	**S+C**	**MAP**	**S+C**	**MAP**	**S+C**	**MAP**
Canine 1	None	S	SVT	S	U-VT	S	U-VT	U	VF	U
Canine 2	None	U	None	U	U-VT	U	U-VT	U	VF	U
Canine 3	SVT	S	SVT	S	ST-VT	S	U-VT	U	VF	U
Canine 4	SVT	S	ST-VT	S	ST-VT	S	S-VT	S	VF	U
Canine 5	SVT	S	None	S	U-VT	U	U-VT	U	VF	U
Canine 6	SVT	S	SVT	S	U-VT	S	U-VT	U	VF	U
Canine 7	SVT	S	None	S	U-VT	S	S-VT	S	VF	U
Canine 8	None	S	None	S	U-VT	S	VF	S	VF	U

Classifications that were improved using the CDSV hemodynamic information are highlighted in green. Classifications that could have been improved by CDSV, but were not properly classified by CDSV when compared to hemodynamic ground truth are highlighted in blue. The blue classifications result in the same delivery of therapies as an ICD only discriminator algorithm. AT indicates atrial tachycardia, AF indicates atrial fibrillation, VT indicates ventricular tachycardia, FVT indicates fast ventricular tachycardia, VF indicates ventricular fibrillation, S+C indicates a combined SJM CDSV results column, MAP indicates a mean arterial pressure results column, SVT indicates supraventricular tachycardia, S indicates a stable MAP, ST-VT indicates a stable ventricular tachycardia, and U-VT indicates an unstable ventricular tachycardia.

Table 12. Combined Medtronic and CDSV Therapy Performance

	AT		AF		VT		FVT		VF	
Subject	**M+C**	**MAP**	**M+C**	**MAP**	**M+C**	**MAP**	**M+C**	**MAP**	**M+C**	**MAP**
Canine 1	None	S	SVT-AF	S	U-VT	S	U-VT	U	VF	U
Canine 2	None	U	None	U	U-VT	U	U-VT	U	VF	U
Canine 3	VT-M	S	AT/AF	S	ST-VT	S	U-VT	U	VF	U
Canine 4	U-VT	S	ST-VT	S	ST-VT	S	S-VT	S	VF	U
Canine 5	VT-M	S	AT/AF	S	U-VT	U	U-VT	U	VF	U
Canine 6	ST-VT	S	AT/AF	S	U-VT	S	U-VT	U	VF	U
Canine 7	VT-M	S	AT/AF	S	U-VT	S	S-VT	S	VF	U
Canine 8	None	S	AT/AF	S	U-VT	S	VF	S	VF	U

Classifications that were improved using the CDSV hemodynamic information are highlighted in green. Classifications that could have been improved by CDSV, but were not properly classified by CDSV when compared to hemodynamic ground truth are highlighted in blue. The blue classifications result in the same delivery of therapies as an ICD only discriminator algorithm. AT indicates atrial tachycardia, AF indicates atrial fibrillation, VT indicates ventricular tachycardia, FVT indicates fast ventricular tachycardia, VF indicates ventricular fibrillation, M+C indicates a combined Medtronic and CDSV results column, MAP indicates a mean arterial pressure results column, VT-M indicates ventricular tachycardia monitoring, AT/AF indicates atrial tachycardia/atrial fibrillation, SVT-AF indicates supraventricular tachycardia/atrial fibrillation, S indicates a stable MAP, ST-VT indicates an stable ventricular tachycardia, and U-VT indicates an unstable ventricular tachycardia.

5.4. DISCUSSION

With the combined ICD and CDSV discrimination algorithm therapies can be configured to be less aggressive as the arrhythmia becomes less life threatening, i.e., it is hemodynamically stable. For example, antitachycardia pacing (ATP) can be programmed as a first therapy in the stable VT zone before subjecting the patient to an ICD shock. Alternatively, the stable VT zone could be configured as a monitor zone. The addition of CDSV hemodynamic information would enable additional arrhythmia zones that allow physicians to better control the delivery of therapies to patients. Using the combined ICD and CDSV discrimination algorithm the following arrhythmia zones can be configured:

stable VT, unstable VT, and VF. Therapies for each of the zones could be configured to reduce the shock burden to patients.

5.4.1. ICD Misclassifications

Both the Medtronic and St. Jude Medical (SJM) ICDs had expected classification performance given state of the art in IEGM discriminator capabilities. Atrial arrhythmias with rates above the VT and VF thresholds are the most likely arrhythmias to be misclassified. The Medtronic ICD misclassified 2 high rate ATs as VT. Both the Medtronic and SJM ICD misclassified a high rate AF as VF. The experimental results showed MAP remained stable during high rate atrial arrhythmias. In patients, these types of misclassifications result in the inappropriate delivery of ICD shocks, specifically in the case of AF/VF misclassifications. The resolution of AF/VF misclassifications is an important area of improvement in ICD technology.

5.4.2. CDSV Misclassifications

CDSV misclassifications were observed in 17.5% of the analyzed arrhythmias. All CDSV misclassifications in this dataset resulted in a more aggressive therapy. Hence, the misclassifications never resulted in an inappropriately withheld therapy, which is considered to be significantly more dangerous than an inappropriately delivered therapy. With a 17.5% false classification rate the need for improvement in the CDSV method is apparent. However, in the presented combination IEGM and ICD discrimination algorithm, the CDSV classifications never resulted in a less effective delivery of therapies and an improvement in 32.5% of delivered therapies when compared to IEGM-alone based arrhythmia discrimination algorithms.

5.4.3. Improved VT Therapies

The combined ICD and CDSV discrimination algorithm improved the delivery of therapies for 75% of the VT and FVT arrhythmias. In the set of improved therapies, 2 of the improvements came from reclassifying VF as stable VT. 5 of the improvements came from reclassifying VT as Stable VT. 3 of the improvement came from reclassifying VF as unstable VT. The reclassification of VF to stable VT has the potential to significantly improve the delivery of therapies. Similarly, reclassifying VT as stable VT has the potential to improve the delivery of therapies. However, it is unclear if patients will ever have high rate stable VT. The rapid RV pacing induced DCM CHF model reconditioned the cardiac physiology of the subjects in this study to an elevated HR. It is possible that the stable high rate VTs observed during VT and FVT were the result of the DCM CHF model.

5.4.4. Improved AF Therapies

The AF/VF misclassification that occurred was reclassified as a stable arrhythmia using the combo ICD and CDSV discrimination algorithm. This is an obvious way that the CDSV information can be used to improve ICD arrhythmia discrimination algorithms.

5.4.5. Inappropriately Withheld Therapies

In this dataset, the CDSV classification thresholds for Unstable VT and VF were optimized to not cause any inappropriately withheld therapies (false negatives). However, this dataset was only composed of 8 subjects and in a larger clinical dataset it is possible that a threshold that meets these conditions would not be identified. The introduction of additional false negatives into ICD arrhythmia discrimination algorithms is something that must be studied with a significantly larger data set. It is possible that the misclassification of an unstable VT as stable VT is tolerable in a small subset of the patient population. However, the misclassification of VF as stable VT is unacceptable and would result in the

unintended death of a patient. At this point, this type of misclassification is highly unlikely. A larger clinical dataset must be used to better evaluate the likelihood of CDSV misclassifications which result in inappropriately withheld therapies.

6. Chapter 6: Conclusion and Future Work

6.1. FUTURE WORK

In general, the CHF arrhythmia study successfully evaluated the use of admittance hemodynamic measurements to improve ICD arrhythmia discrimination algorithms. However, several areas for improvement remain.

The pacing catheter that was used to simulate atrial and ventricular arrhythmias is a potential source of error in the admittance measurement. For the RV tripolar admittance vector, the use of the catheter in the atrium is tolerable. However, the use of the pacing catheter in the ventricle should be replaced with an epicardial pacing system. In practice, an epicardial pacing system can be introduced between the ribs using a specialized delivery system. The introduction of the system will cause a loss of negative pressure in the pleural space, which may affect respiration and the respiratory component of the admittance signal. However, it is believed that this affect will be more desirable when compared to the effect of the pacing catheter in the RV.

The evaluation of tricuspid valve regurgitation (TR) is in important variable to monitor during all experiments. The intraventricular admittance measurement is unable to differentiate between forward and reverse stroke volume (SV). Since TR directly effects reverse SV it is an important experimental variable to quantify. The chronic implantation of leads as well as the DCM CHF model were found to cause significant levels of TR in the subjects used for this study. Unfortunately, TR was only evaluated in N=3 of 8 subjects since it was not identified as a confounding experimental variable until late in the study. Going forward, the evaluation of TR during all experiments should be required.

This study was originally designed assuming that the induction of sustained natural arrhythmias would be possible. The DCM CHF model was supposed to make the canine hearts arrhythmogenic. In actuality, the only natural arrhythmias that resulted from the

DCM CHF model were the VFs that occurred as a result of cardiogenic shock and caused premature mortality during the CHF arrhythmia protocol. Fortunately, the study was preemptively modified for the simulation of AT, AF, VT, and FVT arrhythmias under the assumption that the DCM CHF model would not make the hearts arrhythmogenic in the intended way.

All ethical researchers who work with animal subjects endeavor to perform studies and collect meaningful data while minimizing discomfort to subjects. In protocols performed under sedation, this goal is generally met. In the case of the rapid RV pacing induced DCM CHF model, it is difficult to convince one's self that the subjects live comfortably under overdrive pacing at 220 BPM for 4 weeks. For this reason, this part of the protocol should always be evaluated with the highest level of scientific scrutiny. In the original study, the DCM CHF model was supposed to enable the reliable induction of sustained arrhythmias. This was not the case, and the only remaining justification for the model is the fact that most patients who have ICDs have some form of CHF. Going forward, I would encourage a full scientific review around the justification and use of the DCM CHF model.

Only one subject exhibited a high rate AF that resulted in a VF misclassification. In future studies, the induction of this type of arrhythmia should be emphasized. In this study, the use of pharmaceuticals was limited in order to reduce the number of variables affecting experimental results. Dobutamine was used during the CHF arrhythmia protocol to prevent cardiogenic shock. However, no pharmaceuticals were intentionally used to induce arrhythmias. The lack of high rate AF in subjects was the result of atrioventricular (AV) node block. The AV node acts to protect the ventricle from high rate atrial arrhythmias. Atropine is one drug that can be used to reduce the ability of the AV node to

prevent rapid atrial arrhythmias from conducting to the ventricle. However, atropine is an antagonist of the muscarinic receptors of the parasympathetic nervous system and its ability to reduce AV node block beyond the VF conduction threshold (240 BPM) may be limited. Alternatively, Isoproterenol acts as an agonist of the beta receptors of the sympathetic nervous system and may also be used to prevent heart block. The subject that exhibited high rate AF was unintentionally administered a large dose Dobutamine drip at a rate of 12 mL/hr, which may have aided in the induction of high rate AF. Like Isoproterenol, Dobutamine acts in part as a beta-1 agonist of the sympathetic nervous system. The AV node contains both M-2 muscarinic receptors and Beta-1 adrenergic receptors. Drugs which act as antagonists of M-2 muscarinic receptors or agonists of Beta-1 adrenergic receptors should be considered for the purpose of inducing high rate AF. Unfortunately, such drugs will also have a significant effect on cardiac performance and to a greater extent the circulatory system. These effects will likely be inconsistent across subjects and introduce an additional set of inter-subject variables into the experimental setup.

In this study, the Cardiovol system that was used was a "multi-vector" admittance measurement system. The RV tripolar vector is one of the intraventricular admittance measurements that were collected during the experiment. Using the 2 electrodes of the atrial pacing lead, 3 electrodes of the ventricular shocking lead, and the 4 electrodes of the coronary sinus lead a variety of admittance vectors can be collected using different electrode sets. Alternative vectors or combinations of vectors may improve the admittance SV measurement. I expect future research from the research group to evaluate the use of multi-vector admittance measurements to monitor cardiac hemodynamics.

Future studies should continue to evaluate the difference between the ADSV and CDSV methods. Previous studies have proven the effectiveness of the admittance method [4-16]. However, many of these studies were performed in a murine model using a tetra-polar conductance catheter. It is possible that the tri-polar admittance configuration, when applied to a large animal model, is less effective than previous studies have shown. Continued investigation must be used to further evaluate these findings.

6.2. CONCLUSION

CDSV was found to have significantly higher correlation with LVOT VTI SV and PP when compared to the ADSV method in the CHF arrhythmia study. The CDSV method strongly correlates with LVOT VTI SV and arterial PP in CHF canine subjects. The method provides a means to directly determine hemodynamic stability during atrial and ventricular arrhythmias. CDSV can be utilized as an additional ICD discriminator that withholds therapies on the basis of hemodynamic stability. The CDSV discriminator can be used to reduce the number of inappropriate therapies during AF. Additionally, the discriminator can be used to establish distinct therapy zones for hemodynamically unstable VTs and hemodynamically stable VTs. In the stable VT zone, ICD shocks can be withheld in favor of less aggressive therapies such as anti-tachycardia pacing that decrease morbidity and mortality in patients. The addition of the CDSV hemodynamic discriminator has the potential to significantly improve the configuration and delivery of ICD therapies.

Appendix A: Complete Lead Implant Protocol

Lead Implant Procedure

Summary

Procedure 1 (Lead Implant) – Week 0:

Aseptic procedure general anesthesia required,
Baseline Imaging - 2D TTE,
Implant leads (RA,RV,CS),
Confirm lead placement with standard methods (pacing/fluoro),
Abridged RA pacing protocol,
Reposition leads as necessary,
Implant leads in subcutaneous pocket right neck

Detailed

This protocol will be performed on canines placed under general anesthesia and prepared for aseptic surgical procedures.

Preparation & Anesthesia (LAR staff):

1. A percutaneous catheter is placed in peripheral vein (cephalic) for induction and fluid administration.
2. Induction with 2-6 mg/kg Propofol IV (given to effect) followed by placement of an appropriately sized endotracheal tube.
3. Anesthesia is then maintained on 1-4% Isoflurane in 100% Oxygen at 1-3 liters/min.
4. Animal is clipped/shaved for the surgical procedure and then moved to surgical table.
5. Animal is placed on top of warmer on surgical table followed by placement of temperature, heart rate, respiratory rate, EtCO2 and ECG monitors.
6. LRS fluids are infused through the cephalic catheter at 10ml/kg/hr for the first hour then decreased to 3-5ml/kg/hr for the continuation of the surgery. Preoperative analgesics and antibiotics are given.
7. Place patient on table on RIGHT side down
8. Take baseline echo measurements
9. Turn patient on table on LEFT side down
10. Place urinary catheter to make sure the animal can relieve itself. This is important to keep the heart rate low, especially in long studies.
11. Surgical sites are aseptically prepped with 3 alternating scrubs of betadine and alcohol.

Procedure:

12. Perform jugular cutdown and place tearaway vascular sheaths in the right jugular vein.

13. Place three pacemaker/ICD leads in the heart by passing them through the sheaths under fluoroscopy guidance. This includes a RA lead, a RV lead and a LV lead.
14. Make CardioVol/ECG measurements in order to confirm lead placement.
    1.1. Abridged RA Pacing procedure (Cardiovol 1.0)
        1.1.1. Establish paced baseline (PBL) generally ~100 BPM.
        1.1.2. Establish max rate w/o AV node block rate generally 140-180 BPM.
        1.1.3. Pace from the RA lead in the follow order pbl, max, pbl, max.
            1.1.3.1. At each rate allow for 30 seconds stable pacing.
            1.1.3.2. Collect 30 seconds of CardioVol/ECG w/ respirator.
            1.1.3.3. Collect VTI/Cardiovol/ECG data w/o respirator (End expiration).
15. Analyze data.
16. Reposition leads as necessary. Repeat step 9 until successful lead placement.
17. Repeat step 9 for Cardiovol 2.0 instrument
18. Remove tearaway sheaths.
19. Create a subcutaneous pocket on the right neck and implant the leads.
20. Discontinue anesthesia and recover the animal.

Appendix B: Complete Pacemaker Implant Protocol

Pacemaker Implant Arrhythmia Procedure
Summary

Procedure 2 (Pacemaker Implant) – Week 4:

Aseptic procedure general anesthesia required,
Baseline Imaging - 2D TTE,
Ensite Patch Placement,
Introduce Arterial Pressure Catheter
Introduce Pacing catheter,
Explant leads,
Attach Cardiovol to leads,
Attach Ensite to leads
Place pacing catheter in RA
Collect baseline, paced baseline, Atach, and Afib data
Place pacing catheter in RV
Collect baseline,vp 120 BPM, Vp 170 BPM, vtac 200 BPM, and vtac 250 BPM
Implant leads and pacemaker in subcutaneous pocket right neck
Remove pacing catheter,
Remove Arterial Pressure Catheter
Recover patient

Detailed

This protocol will be performed on canines placed under general anesthesia in a sterile preparation.

Preparation & Anesthesia (LAR staff):

1. A percutaneous catheter is placed in peripheral vein (cephalic) for induction and fluid administration.
2. Induction with 2-6 mg/kg Propofol IV (given to effect) followed by placement of an appropriately sized endotracheal tube.
3. Anesthesia is then maintained on 1-4% Isoflurane in 100% Oxygen at 1-3 liters/min.
4. Shave animal appropriately for Ensite Patches
5. Animal is clipped/shaved for the surgical procedure and then moved to surgical table.
6. Animal is placed on top of warmer on surgical table followed by placement of temperature, heart rate, respiratory rate, EtCO2 and ECG monitors.
7. LRS fluids are infused through the cephalic catheter at 10ml/kg/hr for the first hour then decreased to 3-5ml/kg/hr for the continuation of the surgery. Preoperative analgesics and antibiotics are given.
8. Place patient on table on RIGHT side down
9. Take baseline echo measurements
10. Turn patient to LEFT side down

11. Place urinary catheter to make sure the animal can relieve itself. This is important to keep the heart rate low, especially in long studies.
12. If blood pH < 7.38 or SBP < 70 mmHg start dobutamine drip
    12.1. 2-20 mcg/kg/min IV; titrate to desired effect; not to exceed 40
    12.2. Once stable allow up to 30 minutes before starting protocol
13. Place Ensite Patches

Procedure:

14. Verify lead placement using fluoroscopy
15. Place percutaneous pressure catheter in peripheral artery (femoral or radial).
16. Place 7F sheath in peripheral vein access (femoral or radial).
17. Remove pacemaker and explant leads.
18. Place pacing catheter in RA under fluoroscopy
19. Cardiovol 1.0 Calibration (Optional)
    19.1. Attach Cardiovol 1.0 to leads,
    19.2. Test Cardiovol 1.0
    19.3. Place pacing catheter
    19.4. Test RA pacing
    19.5. Establish paced baseline (PBL) generally 120 BPM
    19.6. Perform Cardiovol 1.0 vector calibration w/ RA pacing 120 BPM
20. Replace Cardiovol 1.0 w/ Cardiovol 2.0
21. Test Cardiovol 2.0
22. Test for Cardiovol 2.0 pacing interference w/ RA pacing 120 BPM
23. Reposition as necessary.
24. Data collection definition
    24.1. At each rate allow for 30 seconds stable pacing.
    24.2. Collect 30 seconds of CardioVol/ECG/Pressure w/ respirator.
    24.3. Collect VTI/Cardiovol/ECG/Pressure data w/o respirator (End expiration).
    24.4. Power off cardiovol 2.0
    24.5. Collect 30 seconds of Ensite and Pressure w/ respirator
    24.6. Collect TR view 2D-TTE (When Requested)
    24.7. This data collection process shall be repeated for all datasets
25. Perform x3 Simpsons calibration w/ RA pacing 120 BPM
26. Establish max rate before AV node block (Atach) generally 140-180 BPM
27. Take baseline 0 data (TR Requested)
28. Abridged RA Pacing procedure - Atach
    28.1. Pace from the pacing catheter in the follow order pbl, Atach, pbl, Atach (TR Requested).
    28.2. Collect data at each rate
29. Take baseline 1 data
30. Afib Pacing Procedure
    30.1. Using the stimulator attempt to induce natural Afib pace up to 600 BPM for ~5 minutes

30.2. If natural Afib is not induced use randomized pacing pattern to simulate Afib
30.3. Take 2 sets of Afib data (TR Requested for Second Afib)
31. Reposition pacing catheter to the RV under fluoroscopy
32. Test for Cardiovol 2.0 pacing interference w/ RV pacing 120 BPM
33. Reposition as necessary.
34. Take baseline 2 data (TR Requested).
35. Collect V pace 120 BPM data
35.1. RV pacing 120 BPM
36. Collect V pace 170 BPM data
36.1. RV pacing 170 BPM
37. Collect Vtach 0 data
37.1. RV pacing 200 BPM (TR Requested)
38. Collect Vtach 1 data
38.1. RV pacing 250 BPM (TR Requested)
39. Collect end baseline (TR Requested)
40. Disconnect cardiovol and Ensite from leads
41. Attach pacemaker
42. Test lead impedances and ECG using the SJM Interrogator
43. Implant leads and pacemaker in subcutaneous pocket right neck.
44. Remove pressure catheter.
45. Remove RV pacing catheter.
46. Final Image fluoroscopy
47. Discontinue anesthesia and recover the animal.

Appendix C: Complete Overdrive Pacing Protocol

Overdrive Pacing Protocol

Summary

Overdrive Pacing Protocol – Weeks 5-9:

Baseline Imaging - 2D TTE,
Pacing rate 150 BPM (2 days)
Pacing rate 170 BPM (5 days)
Imaging - 2D TTE
Pacing rate 220BPM (4 weeks)
Imaging - 2D TTE
Imaging - 2D TTE
Imaging - 2D TTE
Imaging - 2D TTE

Detailed

This protocol will be performed using the St. Jude Interrogator.

Detailed Protocol:

1. Perform 2D TTE Imaging protocol
    1.1. If pacemaker is programmed on, turn pacing off and allow 5-10 minutes for heart rate to stabilize
    1.2. Place animal in standing position for the entire imaging protocol
    1.3. Acquire the following views. At least 3 images are taken for each view:
        1.3.1. View: Parasternal Short Axis
            1.3.1.1. Analysis: Left ventricular dimensions, EF, FS
        1.3.2. View: Parasternal Short Axis M-Mode
            1.3.2.1. Analysis: Left ventricular dimensions, EF, FS
        1.3.3. View: Parasternal Long Axis
            1.3.3.1. Analysis: Left ventricular dimensions, EF, FS, LVOT diameter
        1.3.4. View: Apical 4 Chamber
            1.3.4.1. Analysis: EDV, ESV, EF, SV
        1.3.5. View: Apical 4 Chamber LVOT Pulse Wave Doppler
            1.3.5.1. Analysis: LVOT VTI, LVOT SV
2. Program pacemaker
    2.1. After obtaining echo views, program pacemaker in the VOO setting at the desired rate
    2.2. Check 2D TTE EKG trace to verify rate capture

Appendix D: Complete CHF Arrhythmia Protocol

Arrhythmia Procedure
Summary
Procedure 3 (Week 10 Arrhythmia Procedure) – Week 10:

Stop overdrive pacing 30 minutes before,
Nonsterile procedure general anesthesia required,
Baseline Imaging - 2D TTE,
Ensite Patch Placement,
Introduce arterial pressure catheter,
Introduce RV pacing catheter,
Place ICD subcutaneously upper left thorax
Remove pacemaker and explant leads
Attach Switch Box to scarred in leads
Attach ICD, Cardiovol, to Switch Box,
Place pacing catheter in RA
Collect baseline, paced baseline, Atach, and Afib data
Move pacing catheter to the RV
Collect Vtach, and Vfib data
Euthanize Patient

Detailed
This protocol will be performed on canines placed under general anesthesia in a non-sterile preparation
.
Preparation & Anesthesia (LAR staff):

1. A percutaneous catheter is placed in peripheral vein (cephalic) for induction and fluid administration.
2. Induction with 2-6 mg/kg Propofol IV (given to effect) followed by placement of an appropriately sized endotracheal tube.
3. Anesthesia is then maintained on 1-4% Isoflurane in 100% Oxygen at 1-3 liters/min.
4. Animal is clipped/shaved for the surgical procedure and then moved to surgical table.
5. Animal is placed on top of warmer on surgical table followed by placement of temperature, heart rate, respiratory rate, EtCO2 and ECG monitors.
6. LRS fluids are infused through the cephalic catheter at 10ml/kg/hr for the first hour then decreased to 3-5ml/kg/hr for the continuation of the surgery. Preoperative analgesics and antibiotics are given.
7. Place patient on table on RIGHT side down
8. Take baseline echo measurements
9. Turn patient to LEFT side down
10. Place urinary catheter to make sure the animal can relieve itself. This is important to keep the heart rate low, especially in long studies.
11. If blood pH < 7.38 or SBP < 70 mmHg start dobutamine drip
    11.1. 2-20 mcg/kg/min IV; titrate to desired effect; not to exceed 40

11.2. Once stable allow up to 30 minutes before starting protocol
12. Place Ensite Patches.

Procedure:
13. Verify lead placement using fluoroscopy
14. Turn patient to RIGHT side down
15. Place percutaneous pressure catheter in peripheral artery (femoral or radial).
16. Place 7F sheath in peripheral vein access (femoral or radial).
17. Place ICD subcutaneously in upper left thorax w/ extra leads outside of body.
18. Turn patient to LEFT side down.
19. Remove pacemaker and explant leads.
20. Attach Switch Box to scarred in leads
21. Attach ICD to switch box
    21.1. Connect ICD in isolation using switch box
    21.2. Test ICD ECG/Impedances
22. Attach Ensite to switch box
23. Cardiovol 1.0 Calibration (Optional)
    23.1. Cardiovol 1.0 to Switch Box,
    23.2. Connect Cardiovol 1.0 in isolation using switch box
    23.3. Test Cardiovol 1.0
    23.4. Place pacing catheter in RA under fluoroscopy
    23.5. Test RA pacing
    23.6. Establish paced baseline (PBL) generally 120 BPM
    23.7. Perform Cardiovol 1.0 vector calibration w/ RA pacing PBL
24. Replace Cardiovol 1.0 w/ Cardiovol 2.0
25. Test Cardiovol 2.0
26. Test for Cardiovol 2.0 pacing interference w/ RA pacing PBL
27. Reposition as necessary.
28. Data collection definition
    28.1. At each rate allow for 30 seconds stable pacing.
    28.2. Collect 30 seconds of CardioVol/ECG/Pressure w/ respirator.
    28.3. Collect VTI/Cardiovol/ECG/Pressure data w/o respirator (End expiration).
    28.4. Power off Cardiovol 2.0
    28.5. Collect 30 seconds of Ensite and Pressure w/ respirator
    28.6. Collect TR view 2D-TTE (When Requested)
    28.7. This data collection process shall be repeated for all datasets
29. Perform x3 Simpsons calibration at Paced Baseline
30. Establish max rate before AV node block (Atach) generally 140-220 BPM
31. Take baseline 0 data (TR Requested)
32. Abridged RA Pacing procedure - Atach
    32.1. Pace from the RA lead in the follow order pbl, Atach, pbl, Atach (TR Requested).
    32.2. Collect data at each rate

33. Take baseline 1 data
34. Afib Pacing Procedure
    34.1. Using the stimulator attempt to induce natural Afib pace up to 600 BPM for ~5 minutes
    34.2. If natural Afib is not induced use randomized pacing pattern to simulate Afib
    34.3. Take 2 sets of Afib data (TR Requested for Second Afib)
35. Reposition pacing catheter to the RV under fluoroscopy
36. Test for Cardiovol 2.0 pacing interference w/ RV pacing PBL
37. Reposition as necessary.
38. Take baseline 2 data (TR Requested)
39. Collect Ventricular pacing 120 BPM data
40. Collect Ventricular pacing 170 BPM data
41. Collect Vtach 0 data
    41.1. RV pacing 200 BPM (TR Requested)
42. Collect Vtach 1 data
    42.1. RV pacing 250 BPM (TR Requested)
43. Collect Vfib data
    43.1. Connect ICD in isolation using switch box
    43.2. Disconnect pressure catheter
    43.3. Enable ICD therapies
    43.4. Deliver DC fibber
    43.5. Disable ICD therapies
    43.6. Immediately connect pressure
    43.7. Immediately connect Cardiovol 2.0 in isolation
    43.8. Collect Vfib data
    43.9. Monitor external ECG for Vfib
    43.10. Continue recording for no more than 15 seconds
    43.11. Connect ICD in isolation using switch box
    43.12. Disconnect pressure catheter
    43.13. Administer manual cardioversion therapy
    43.14. Monitor heart rate and recovery from Vfib
    43.15. Emergency VOO pacing 100 BPM if necessary
    43.16. Prolonged Cardiac Arrest Algorithm (Optional)
        43.16.1. If Vfib sustained shock x2
        43.16.2. CPR 1 minute
        43.16.3. If Vfib sustained shock x3
        43.16.4. Epinephrine 0.5mg-1mg
        43.16.5. CPR 1 minute
        43.16.6. If Vfib shock x3
        43.16.7. CPR 1 minute...
44. Repeat the previous step two more times
45. Euthanize Patient.

Appendix E: Cardiovol Circuit Diagram

System Block Diagram:

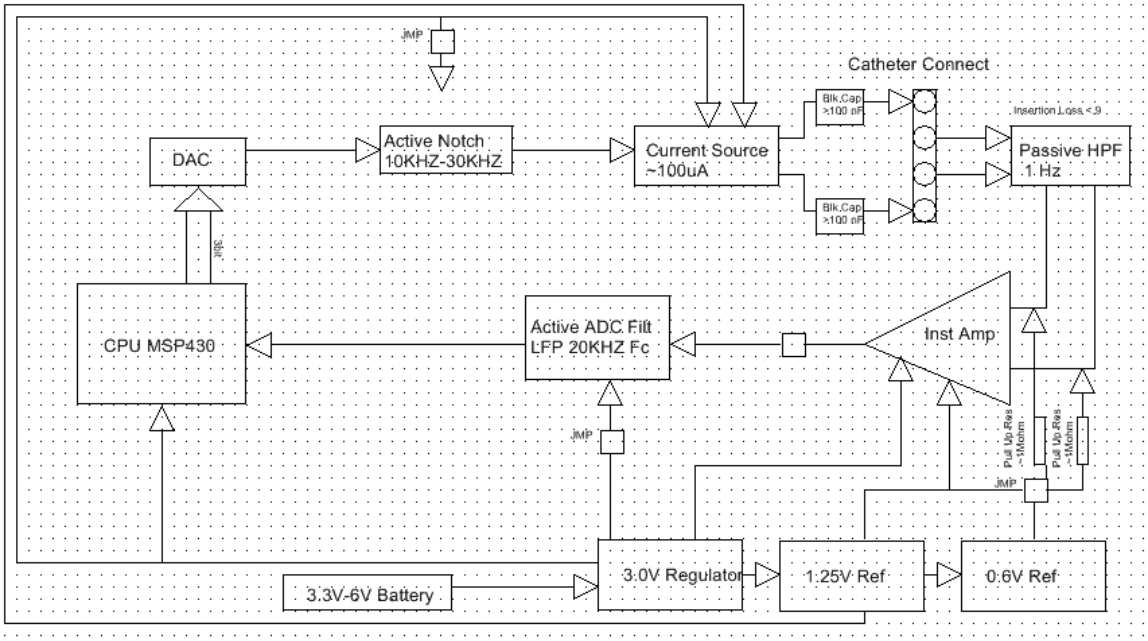

Current Source Output and Voltage Sense Input:

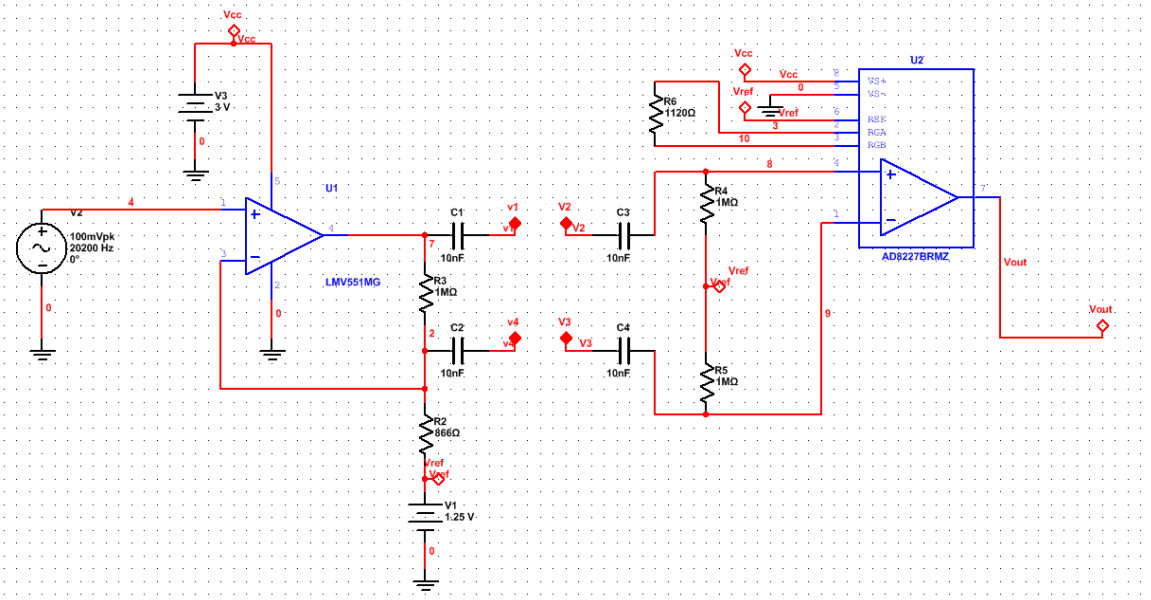

References

[1] J. Mishkin, et. al., "Appropriate evaluation and treatment of heart failure patients after implantable cardioverter-defibrillator discharge: time to go beyond the initial shock." *Journal of the American College of Cardiology*, vol. 54(22), pp. 1993-2000, 2009.

[2] S. F. Sears, et al., "Quality of life and psychological functioning of ICD patients," *Heart*, vol. 87(5), 2002.

[3] M. D. Feldman, et al., "Validation of a mouse conductance system to determine LV volume: comparison to echocardiography and crystals.," *American Journal of Physiology*, vol. 279(4), pp. 698-707, 2000.

[4] A. T. Kottam, *Measurement of electrical admittance to study the onset and progression of myocardial ischemia* [Dissertation]. Austin: The University of Texas, 2006.

[5] J. E. Porterfield, et al., "Dynamic correction for parallel conductance, GP, and gain factor, alpha, in invasive murine left ventricular volume measurements," *Journal of Applied Physiology*, vol. 107(6), pp.1693-703, 2009.

[6] J. E. Porterfield, et al., "Left ventricular epicardial admittance measurement for detection of acute LV dilation," *Journal of Applied Physiology*, vol. 110(3), pp. 799-806, 2009.

[7] J. E. Porterfield, et al., "Numerical models of the volume response function of conductance catheters: the effect of multiple unused electrodes," *Applied Computational Electromagnetics Society Journal*, 2008.

[8] K. Raghavan K, et al., "A bio-telemetric device for measurement of left ventricular pressure-volume loops using the admittance technique in conscious, ambulatory rats," *Physiological Measurement*, vol. 32(6), pp. 701-15, 2011.

[9] K. Raghavan K, et al., "Design of a wireless telemetric backpack device for real-time in vivo measurement of pressure-volume loops in conscious ambulatory rats," *Proceedings IEEE Engineering in Medicine and Biology Society (IEEE EMBS),* pp. 993-996, 2008

[10] K. Raghavan, et al., "Electrical conductivity and permittivity of murine myocardium," *IEEE Transactions in Biomedical Engineering*, vol. 56(8), pp. 2044-53, 2009.

[11] K. Raghavan, et al., "Design of instrumentation and data-acquisition system for complex admittance measurement," *Biomedical Sciences Instrumentation*, vol. 40, pp. 453-457, 2004.

[12] M. Reyes, et al., "Impact of physiological variables and genetic background on myocardial frequency-resistivity relations in the intact beating murine heart," *American Journal of Physiolgy*, vol. 291(4), pp. 1659-1669, 2006.

[13] C. L. Wei, et al., "Calibration capacity of the conductance-to-volume conversion equations for the mouse conductance catheter measurement system," *IEEE Transactions on Biomedical Engineering*, vol. 56(6), pp. 1627-1634, 2009.

[14] E. Larson, et al., "Analysis of the spatial sensitivity of conductance / admittance catheter ventricular volume estimation," *IEEE Transactions on Biomedical Engineering,* vol. 60(8), pp. 2316-2324 [cover of journal], 2013.

[15]C. L. Wei CL, et al., "Volume catheter parallel conductance varies between end-systole and end-diastole," *IEEE Transactions on Biomedical Engineering*, vol. 54(8), pp. 1480-1489, 2007.

[16] E. Larson, et al., "Admittance to detect alterations in left ventricular stroke volume," *Heart Rhythm Society*, vol 11(11), pp. 2075-2083, 2014.

[17] J. C. Daubert, et al., "Cardiac resynchronization therapy in combination with implantable cardioverter-defibrillator," *Europace*, vol. 11(Suppl 5), pp. v87-v92, 2009.

[17A] B. Johannes, et al., "Inappropriate Implantable Cardioverter-Defibrillator Shocks: Incidence, Predictors, and Impact on Mortality," *Journal of the American College of Cardiology*, vol. 57(5), pp. 556-562, 2011.

[17B] L. Bruce, et al., "Strategic Programming of Detection and Therapy Parameters in Implantable Cardioverter-Defibrillators Reduces Shocks in Primary Prevention Patients: Results from the PREPARE (Primary Prevention Parameters Evaluation) Study," *Journal of the American College of Cardiology*, vol. 52(7), Issue 7, pp. 541-550, 2008.

[17C] A. Auricchio, et al., "Low inappropriate shock rates in patients with single- and dual/triple-chamber implantable cardioverter-defibrillators using a novel suite of detection algorithms: PainFree SST trial primary results," *Heart Rhythm*, vol. 12(5), pp. 926-936, 2015.

[17D] M. Gasparini, et al., Long Detection Programming in Single-Chamber Defibrillators Reduces Unnecessary Therapies and Mortality: The ADVANCE III Trial," *Journal of the American College of* Cardiology: Clinical Electrophysiology, 2017.

[17E] Moss, et al., "Reduction in inappropriate therapy and mortality through ICD programming," *New England Journal of Medicine*, vol. 367(24), pp. 2275-2283, 2012.

[17F] Yee, et al., "Initial clinical experience with a new automated antitachycardia pacing algorithm: feasibility and safety in an ambulatory patient cohort," *Circulation: Arrhythmia and Electrophysiology*, vol. 10(9), e004823, 2017.

[17G] Wathen, et al., "Prospective randomized multicenter trial of empirical antitachycardia pacing versus shocks for spontaneous rapid ventricular tachycardia in patients with implantable cardioverter-defibrillators," *Circulation*, vol. 110(17), pp. 2591-2596, 2004.

[17H] B. L. Wilkoff, et al., "Strategic programming of detection and therapy parameters in implantable cardioverter-defibrillators reduces shocks in primary prevention patients: results from the PREPARE (Primary Prevention Parameters Evaluation) study," *Journal of the American College of Cardiology*, vol. 52(7), pp. 541-550, 2008.

[17I] A. Auricchio, A., et. al., "Low inappropriate shock rates in patients with single-and dual/triple-chamber implantable cardioverter-defibrillators using a novel suite of detection algorithms: PainFree SST trial primary results," *Heart Rhythm*, vol. 12(5), pp. 926-936, 2015.

[18] D. J. Whellan, et al., "Development of a method to risk stratify patients with heart failure for 30-day readmission using implantable device diagnostics," *The American Journal of Cardiology*, vol. 111(1), pp. 79–84, 2013.

[19] G. B. Forleo, et al., "Device monitoring of heart failure in cardiac resynchronization therapy device recipients: a single-center experience with a novel multivector impedance monitoring system," *Journal of cardiovascular medicine*, vol. 14(10), pp. 726–732, 2013.

[20] D. E. Haines, et al., "Validation of a defibrillation lead ventricular volume measurement compared to three-dimensional echocardiography," *Heart Rhythm*, vol. 14(10), pp. 1515 – 1522, 2017.

[21] R. Pallas-Areny, R., et al., "Bioelectric impedance measurements using synchronous sampling," *IEEE Transactions on Biomedical Engineering*, vol. 40(8), pp. 824-829, 1993.

[22] C. S. Koukourlis, et al., "Differential synchronous demodulation for electrical impedance tomography," *Clinical Physics and Physiological Measurement*, vol. 13(A), pp. 31, 1992.

[23] E. R. Larson, *Admittance measurement for assessment of cardiac hemodynamics in clinical and research applications* [Dissertation]. Austin: The University of Texas, 2006.

[24] J. W. Valvano, et al., J. W., Feldman, M. D., Porterfield, J., Pearce, J. A., Larson, E., Shuhatovich, L., ... & Cetrulo, R., U.S. Patent No. 9,295,404. Washington, DC: U.S. Patent and Trademark Office, 2016.

[25] P. S. Shevchenko, et al., "Polyphase sliding goertzel demodulator for continuous phase frequency modulated signals," *IEEE Transactions on Applied Superconductivity*, vol. 19(3), pp. 570-573, 2009.

[26] D. Schwingshackl, D., et al., "Universal tone detection based on the Goertzel algorithm. In Circuits and Systems*," 49th IEEE International Midwest Symposium*, vol. 1, pp. 410-413, August 2006.

[27] J. W. Cooley, et al., "Historical notes on the fast Fourier transform," *Proceedings of the IEEE*, vol. 55(10), pp. 1675-1677, 1967.

[28] Y. Wang, et al., "Time-Frequency Analysis of Non-Stationary Biological Signals with Sparse Linear Regression Based Fourier Linear Combiner," *Sensors*, vol. 17(6), pp. 1386, 2017.

[29] D. Stupin, et al., "Adaptive Filtering for Impedance/Admittance Spectroscopy Noise Immunity Enhancement: Comparison with Fourier Transform," *arXiv* (preprint), arXiv:1701.06503, 2017.

[30] F. J. Harris, "On the use of windows for harmonic analysis with the discrete Fourier transform," *Proceedings of the IEEE*, vol. 66(1), pp. 51-83, 1978.

[31] R. Dubey, et al., "Vibration signature analysis using variable Tukey window: A case study on Bearing Fault Data" *Proceedings from IEEE Industrial Instrumentation and Control (ICIC)*, pp. 540-544, May 2015.

[32] S. M. Al-Khatib, et al., "Trends in use of implantable cardioverter-defibrillator therapy among patients hospitalized for heart failure," *Circulation*, vol. 125(9), pp. 1094-1101, 2012.

[33] J. A. Dixon, et al., "Large animal models of heart failure," *Circulation: Heart Failure*, vol. 2(3), pp. 262-271, 2009.

[34] J. A. Boon, *Veterinary echocardiography*. John Wiley & Sons, 2011.

[35] N. Hanna, et al., "Differences in atrial versus ventricular remodeling in dogs with ventricular tachypacing-induced congestive heart failure*," Cardiovascular research*, vol. 63(2), pp. 236-244, 2004.

[36] K. Shinagawa, et al., "Dynamic nature of atrial fibrillation substrate during development and reversal of heart failure in dogs," *Circulation*, vol. 105(22), pp. 2672-2678, 2002.

[37] R. Bighamian, et al., "Relationship between stroke volume and pulse pressure during blood volume perturbation: a mathematical analysis," *BioMed research international*, vol. 2014, 2014.

[38] K. Hajian-Tilaki, et al., "Receiver operating characteristic (ROC) curve analysis for medical diagnostic test evaluation," *Caspian journal of internal medicine*, vol. 4(2), pp. 627, 2013.

[39] J. H. Lee, et al., "Permanent Pacemaker Lead Induced Severe Tricuspid Regurgitation in Patient Undergoing Multiple Valve Surgery," *The Korean journal of thoracic and cardiovascular surgery*, vol. 48(2), pp. 129, 2015.

[40] S. A. Dickerman, et al., "Mitral and tricuspid valve regurgitation in dilated cardiomyopathy," *The American journal of cardiology*, vol. 63(9), pp. 629-631, 1989.

[41] P. Lancellotti, et al., "European Association of Echocardiography recommendations for the assessment of valvular regurgitation. Part 2: mitral and tricuspid regurgitation (native valve disease)," *European Journal of Echocardiography*, vol. 11(4), pp. 307-332, 2010.

[42] B. L. Wilkoff, et al., "A comparison of empiric to physician-tailored programming of implantable cardioverter-defibrillators: results from the prospective randomized multicenter EMPIRIC trial," *Journal of the American College of Cardiology*, vol. 48(2), 330-339, 2006.

Vita

Lucas Martin Holt was born in Pleasanton, CA. In high school he attended Plano East Senior High in Plano, TX. He completed his B.S.E.E. at the University of Texas at Austin (UT Austin) in December of 2012. He then continued his education at the same university. During that same time Lucas began pursuing an industry career path. He started working at International Biomedical in the summer of 2013 as an embedded systems intern working on neonatal infant care products. He continued working for International Biomedical part-time for the extent of his graduate studies. After the completion of his M.S.E. in May of 2014, Lucas began working on his PhD at UT Austin as a research assistant for an NIH R01 grant under the direction of Dr. Marc Feldman (MD) and Dr. Jonathan Valvano (PhD).

Email address: lucas.hlt@gmail.com

This dissertation was typed by the author.